مخبرالهندسة
الميكانيكية
والتطوير
LGMD

THESIS

To obtain the degree of

DOCTOR

Speciality : Clean and renewable energy

Presented by

SARMOUK Mohammed Dhiya-eddine

Experimental and numerical development of a hybrid solar/gas heating system

Defended on July 12, 2021 in front of a jury composed of :

Djamel BOUKHETALA	**Professeur**	**ENP**	**Chairman**
Arezki SMAILI	**Professeur**	**ENP**	**Supervisor**
Hachimi FELLOUAH	**Professeur agrégé**	**U.Sherbrooke**	**Co-supervisor**
Salah LARBI	**Professeur**	**ENP**	**Examiner**
Smaïl SEMAOUI	**MRA**	**CDER**	**Examiner**
Younes CHIBA	**MCA**	**U.Médéa**	**Examiner**

République Algérienne Démocratique et Populaire
Ministère de l'Enseignement Supérieur et de la Recherche Scientifique

École Nationale Polytechnique
Département de Génie mécanique
Laboratoire Génie Mécanique et Développement

مخبر الهندسة
الميكانيكية
والتطوير
LGMD

THESIS

To obtain the degree of

DOCTOR

Speciality : Clean and renewable energy

Presented by

SARMOUK Mohammed Dhiya-eddine

Experimental and numerical development of a hybrid solar/gas heating system

Defended on July 12, 2021 in front of a jury composed of :

Djamel BOUKHETALA	**Professeur**	**ENP**	**Chairman**
Arezki SMAILI	**Professeur**	**ENP**	**Supervisor**
Hachimi FELLOUAH	**Professeur agrégé**	**U.Sherbrooke**	**Co-supervisor**
Salah LARBI	**Professeur**	**ENP**	**Examiner**
Smaïl SEMAOUI	**MRA**	**CDER**	**Examiner**
Younes CHIBA	**MCA**	**U.Médéa**	**Examiner**

République Algérienne Démocratique et Populaire
Ministère de l'Enseignement Supérieur et de la Recherche Scientifique

École Nationale Polytechnique
Département de Génie mécanique
Laboratoire Génie Mécanique et Développement

مخبر الهندسة
الميكانيكية
والتطوير
LGMD

Thèse de Doctorat

en vue d'obtention du grade de

DOCTEUR

En Génie mécanique
Spécialité : Énergies propres et renouvelables

Présentée par

SARMOUK Mohammed Dhiya-eddine

Experimental and numerical development of a hybrid solar/gas heating system

Soutenue le 12 Juillet 2021 devant le jury constitué de :

Président	Djamel BOUKHETALA	Professeur	ENP
Directeur	Arezki SMAILI	Professeur	ENP
Co-directeur	Hachimi FELLOUAH	Professeur agrégé	U.Sherbrooke
Examinateur	Salah LARBI	Professeur	ENP
Examinateur	Smaïl SEMAOUI	MRA	CDER
Examinateur	Younes CHIBA	MCA	U.Médéa

ملخص

الهدف الرئيسي من هذه الأطروحة هو فهم وصياغة العلاقة بين أداء النظام الهجين ومعايير التصميم، من أجل دمج أنظمة الطاقة الشمسية الهجينة في تصميم المباني الموفرة للطاقة. لذلك تم اعتماد الاستخدام المشترك للمحاكاة العددية وتصميم التجارب (DoE) ونهج التحسين لهذا الغرض. بالإضافة إلى ذلك، فإن الاستخدام المشترك للمحاكاة العددية وتقنية DoE يجعل من الممكن تطوير علاقات النمذجة الوصفية بين متغيرات الاستجابة، هنا الكسر الشمسي (SF)، نسبة توفير الطاقة الأولية (PESR)، والتكلفة المرتفعة للحرارة (LCOH) ومعايير التصميم. تُستخدم هذه النماذج الوصفية، أولاً ، لإجراء تحليل الحساسية ، وثانيًا ، لتحسين تصميم أنظمة الطاقة الشمسية الهجينة. ثم يتم النظر في نهج وظيفة الاستحسان والخوارزميات الجينية من أجل تحسين جميع معلمات SF وPESR و LCOH في وقت واحد. يتم تطبيق الطريقة المقترحة في حالة حقيقية، وهي منصة تجريبية تم تطويرها لاحتياجات هذه الدراسة. تم الحصول على التصميم الأمثل 78.46٪ ، 44.87٪ و DA / 7.7 kWh لكل من SF، PESR و LCOH على التوالي. تشير النتائج التي تم الحصول عليها إلى أن التصميم الأمثل يمكن تحقيقه باستخدام النهج المقترح الذي يمثل طريقة بسيطة وسريعة لتحسين معايير تصميم الطاقة الشمسية الهجينة.

الكلمات المفتاحية : الطاقة الهجينة الشمسية / الغازية ، تصميم التجارب ، المحاكاة العددية ، دراسة الحساسية ، التحسين متعدد الأهداف ، توفير الطاقة ، الربحية الاقتصادية.

Résumé

L'objectif principal de cette thèse est de comprendre et de formuler la relation entre la performance du système hybride et les paramètres de conception, afin d'intégrer les systèmes solaires hybrides dans la conception de bâtiments économes en énergie. L'utilisation combinée de simulations numériques, de techniques de plans d'expériences (DoE) et d'une approche d'optimisation est donc adoptée dans ce but. De plus, l'utilisation combinée des simulations numériques et de la technique DoE permet de développer des relations de méta-modélisation entre les variables de réponse, ici la fraction solaire (SF), le ratio d'économie d'énergie primaire (PESR), le coût actualisé de la chaleur (LCOH) et les paramètres de conception. Ces méta-modèles sont utilisés, premièrement, pour effectuer une analyse de sensibilité, et deuxièmement, pour optimiser la conception des systèmes solaires hybrides. L'approche de la fonction de désirabilité et les algorithmes génétiques sont ensuite considérés afin d'optimiser simultanément l'ensemble des paramètres SF, PESR et LCOH. La méthode proposée est appliquée dans un cas réel, une plateforme expérimentale qui a été développée pour les besoins de cette étude. Une conception optimale a été obtenue 78.46%, 44.87% et 7.7 DA/kWh pour le SF, PESR et LCOH respectivement. Les résultats obtenus indiquent que la conception optimale est réalisable en utilisant l'approche proposée qui représente une méthode simple et rapide pour optimiser les paramètres de conception du solaire hybride.

Mot clés : Hybride solaire/gaz, Plans d'expériences, Simulations numériques, Etude de sensibilité, Optimisation multiobjective, Economie d'énergie, Rentabilité économique.

Abstract

The main purpose of this thesis is to understand and formulate the relationship between the hybrid system performance and design parameters, in order to integrate hybrid solar systems in the design of energy efficient buildings. The combined use of numerical simulations, Design of Experiments (DoE) technique and an optimization approach is thus adopted for this aim. Moreover, the combined use of numerical simulations and DoE technique allows the development of meta-modeling relationships between response variable, here solar fraction (SF), primary energy savings ratio (PESR), levelized cost of heat (LCOH) and design parameters. These meta-models are used, first, to perform a sensitivity analysis, and second, to optimize the design of hybrid solar systems. The desirability function approach and genetic algorithms are then considered in order to simultaneously optimize all of SF, PESR and LCOH. The proposed method is applied in a real case study, an experimental platform that has been developed for the purpose of this study. An optimal design was obtained 78.46%, 44.87% and 7.7 DA/kWh for the SF, PESR and LCOH respectively. The obtained results indicated that optimal design is achievable using the proposed approach which represents a simple and fast method to optimize hybrid solar design parameters.

Keywords: Hybrid solar/gas, Design of experiments, Numerical simulation, Sensitivity analysis, Multiobjective optimization, Energy savings, Cost effectiveness.

Acknowledgments

Completing my Ph.D. has been one of the most significant academic challenges that I ever had to face, but provided me a remarkable experience! Accomplishing this academic challenge would not have been possible without many people, not only for their contributions to scientific knowledge, but also for my personal benefit from the privilege of working alongside them during this journey. These lines are dedicated to all of you.

I would like to thank the president of the jury: Djamel BOUKHETALA for his interest in my research work. I would like also to offer my special thanks to Salah LARBI, Smaïl SEMAOUI and Younes CHIBA for accepting to review this dissertation.

First of all, I would like to express my deepest appreciation to my thesis supervisors, Arezki SMAILI and Hachimi FELLOUAH. I am grateful to them for their guidance, encouragement and critical appraisal of my thesis and for their availability during the different steps of our research project. I am fully indebted to my supervisor Abdelatif MERABTINE for creating me a new chance, welcoming me as a Ph.D. student. I have always felt privileged to be working with you. I thank Abdelatif for his continuous support, advice, encouragement, patience, enthusiasm, and for being always beside me, teaching me the importance of critical thinking and inspiring me to work multi-disciplinary. This thesis would not have been possible without your unwavering support either on academic or personal issues, critiques, questions and remarkable patience.

I would like to thank Abdelkrim LAHLAH of the LGMD laboratory, for the technical support especially during the implementation of the installation. Thanks are also due to DJAH Houssem eddine for his help devoted to performing experimental measurements.

I would like to thank my lab mates for their continued support. I would like also to offer my special gratitude to the EPF's (école d'ingénieur-e-s, Troyes) members and colleagues, I am thankful towards Mohammed Ali BOUAZIZ and Julien KAUFFMAN for their technical support and scientific advice. This thesis would not be accomplished without your valuable help.

Thanks are also due to the Directorate-General for Scientific Research and Technological Development (DGSRDT) for their financial support that I otherwise would not have been able to develop my scientific discoveries.

Last but not least, I would like to express my deepest gratitude to my family and friends. This dissertation would not have been possible without their warm love, continued patience, and endless support.

Table of contents

Chapter 1 : Literature review

Chapter 2 : Design framework and research methodology

Chapter 3 : Experimental development of a Hybrid Solar/Gas Heating System

Chapter 4 : Hybrid solar gas heating system Mono-source analysis

Chapter 5 : Hybrid solar gas heating system Multi-sources analysis

List of Figures

Liste of Tables

List of Symbols

Abbreviations

ANOVA	Analysis of variance
ASHP	Air Source Heat Pump
ASHRAE	American Society of Heating, Refrigerating and Air-Conditioning Engineers
CCHP	Combined Cooling, Heating and Power
CDERR	Carbon Dioxide Emission Reduction Rate
CFD	Computational Fluid Dynamics
COP	Coefficient of performance
CVRMSE	Coefficient of Variation of the Root Mean Square Error
DoE	Design of Experiments
ETC	Evacuated tube collector
EU	European Union
FPC	Flat plate collector
GA	Genetic Algorithm
GHG	Greenhouse Gas
GSA	Global Sensitivity Analysis
HSGHS	Hybrid Solar Gas Heating System
HVAC	Heating, Ventilation and Air Conditioning
IEA	International Energy Agency
LCOH	Levelized Cost Of Heat
LHV	Low Heating Value
LINMAP	Linear programming technique for multidimensional analysis of preference
LSA	Local Sensitivity Analysis
MILP	Mixed Integer Linear Programming
MOBO	Multi-Objective Building Optimization
NSGA II	Non-dominated Sorting Genetic Algorithm
OFAT	One Factor At a Time
PESR	Primary Energy Saving Ratio
PSO	Particle Sworm Optimization
PV	Photovoltaic
PVT	Photovoltaic/Thermal
SA	Sensitivity Analysis
SAGSHP	Solar Assisted Ground Source Heat Pump
SF	Solar Fraction
SHC	Solar Heating and Cooling programme
SHS	Solar Heating System

SWH	Solar Water Heater	
SWHS	Solar Water Heating System	
TPES	Total Primary Energy Supply	
WSHP	Water Source Heat Pump	

Nomenclature

a_1	1st order heat loss coefficient	[W/m².K]
a_2	2nd order heat loss coefficient	[W/m².K²]
A_c	Collector area	[m²]
C_p	Specific heat	[kJ.kg^{-1}.K^{-1}]
d	Desirability	[-]
F'	Efficiency factor	[-]
F_R	Heat removal factor	[-]
I	Solar radiation	[W/m²]
k	Thermal conductivity of the fluid	[W/m.K]
L	Lower limit	[-]
$\dot{m}$	Mass flow rate	[kg.s^{-1}]
Q/S	Normalized flow rate	[kg.s^{-1}.m²]
Q_a	Available solar radiation	[W]
Q_{loss}	Heat losses	[W]
Q_u	Useful power	[W]
S	Collector area	[m²]
T	Target limit	[-]
T_	Temperature	[°C]
U	Upper limit	[-]
U_L	Heat loss coefficient	[W/m².K]
V/S	Volume to area ratio	[m3/m²]
Y	Response variable	[-]

Greek letters

α	Collector slope	
ρ	Reflectance	
θ	Angle	
η	Efficiency	
η_0	Intercept efficiency	
β	Coefficient	

Subscript

a	Absorber	
avg	Average	
b	Beam	
bottom	Bottom node of the tank	
c,in	Collector inlet	
c,out	Collector outlet	
d	Diffuse	
edges	Edge nodes of the tank	
env	Environment temperature for tank losses	
ext	Exterior	
g	Ground	

supply	Supplied water to radiators
t	Total
top	Top node of the tank
z	Zenith

Introduction

Motivation and Background

The necessity of reducing energy resource consumption and moving towards energy transition is a widely accepted fact, since the population growth and industrialization bring the problems of depleting resources, climate change and environmental pollution [1]. In light of the increasing trend of urbanization, cities account for 70% of total energy consumption and energy-related greenhouse gas (GHG) emissions [2]. According to the European Environment Agency, the residential-commercial sector represents 40% of the total final energy consumption [3]. This concern has led to the development of different strategies, concepts, policies, standards and regulations that aim to promote sustainable development in the building, such as low energy consumption buildings and zero energy buildings [4]. These concepts are based on improving the building envelope, and using high-efficiency equipment as well as renewable energy resources [5], [6]. Fortunately, stakeholders across the world show an increasing willingness to enhance the energy efficiency in different sectors. This is mainly due to two reasons: the greater awareness of the detrimental environment issues, on the one hand, and economic reasons driven by the cost's constant rising of non-renewable energy sources on the other hand [7]. The introduction of renewable energy resources through incentive and constraining programs of energy efficiency, has led to improvement over the years in the energy demand in the building sector.

Among all the renewable sources, solar energy has attracted considerable attention as the promising alternative for heat demand and hot water production in many sectors. Apparently, solar thermal technologies can meet a substantial amount of heat demand namely in the building sector. On a building scale, however, solar thermal systems face strong competition from solar photovoltaic systems, heat pumps and gas boiler mainly in the Algerian context. Indeed, with the increasing arrival of the electric devices in the residences, the photovoltaic solar systems seem quite useful. In addition, the heat pump market is growing due to the energy efficiency of this type of system and its ease of installation. Nevertheless, their use further increases the use of electricity in the building. It is therefore more appropriate to use thermal sources than electrical sources for heat production in the building.

These solar thermal systems when integrated to existing heating systems can become even more competitive [8]. In that view, the solar hybrid systems have been the focus of many research studies. Several studies considered the integration of solar heating systems with heat pumps. The International Energy Agency (IEA) has had special interest in such hybrid

technology. Particularly, Task 44 of IEA (Solar Heating and Cooling, SHC, programme) investigated different combinations of solar thermal systems and heat pumps technologies[9].

In recent years, hybrid solar thermal systems are becoming more popular for heat production in public, commercial and industrial buildings. However, the hybridization in solar heating systems certainly leads to changes in the energetic performances due to the difference in characteristics between solar energy and the other source. Hence, poorly designed hybrid systems hugely affect the energy performance as well as economic profitability. For this reason, researchers in energy and building domain are tending toward integrating new optimization techniques and methodologies that takes into consideration the hybridization and the changes in operation conditions to optimize the overall performance of the systems. This shift towards hybridization and optimization process leads to further requirements of adequate monitoring devices and optimization techniques. In addition, the majority of the proposed approaches are based on artificial intelligence, thus implementing them in the early stage of building design leads to more complexity in the design process. Therefore, a better comprehension of thermal performance and integration of hybrid thermal systems in buildings, especially in the very early phases, could be an essential step towards achieving a trade-off between energy-savings, thermal comfort and economic profitability.

Objectives and research question

The objective of this research work is to develop a hybrid solar heating system and to formulate the relationships between thermal performance, energy savings and the system design parameters, through a comprehensive evaluation of the system, in order to improve the design of hybrid solar heating systems and their integration in energy efficient buildings. The specific objectives intended through this formulation are:

- First, to develop an experimental test unit of a hybrid solar/gas heating system and evaluate its performance.
- Second, to develop a numerical model of the installation to provide a realistic and accurate predictions of energy performance and to assess in the optimization process.
- Third, to understand the relationship between the system performance and the design parameters in order to achieve optimal design.

The review of the literature at the beginning of the thesis allowed us to formulate the questions outlined below:

Q.1: Is it possible to design a hybrid solar heating system so that a trade-off between energy savings, thermal performance and energy cost is fulfilled?

In the aim of reducing energy consumption, designers tend to increase the storage size or the solar field, this act could improve the thermal performance of the hybrid heating system. However. The thermal performance is not the sole objective, economical aspect is of high importance, thus investing in solar collectors or storage tanks lead to additional costs in detriment of higher performance. Therefore, the optimization of the performance of the hybrid solar thermal systems through exhaustive assessment may represent an important step towards achieving a trade-off between the energy and economic aspects.

Q.2: How to integrate the thermal performance in the design of hybrid solar systems?

Thermal performance can vary dramatically between different designs. This variation is due to the difference in solar systems' related parameters, as well as building design which lead to variations in the performance. Formulating the relationship between thermal performance and related parameters is thus an important step towards integrating system thermal performance in the design of solar heating systems.

Research outcomes

In this work, we adopt a research methodology to formulate the relationship between the solar fraction (SF), the primary energy savings (PESR), the levelized cost of heat and the design parameters, namely, collectors' area, storage volume and flow rate. The methodology is based on the combined use of numerical simulations, Design of Experiments (DoE) technique and desirability function approach or Genetic Algorithm (GA). Numerical simulation helps in extending the investigations with low additional costs and less time. In addition, it facilitates the assessment of new control strategies since no additional costs are added for the installations and experimentations. Moreover, the combined use of numerical simulations and DoE technique leads to the development of meta-models for the prediction of thermal performance and energy costs. These meta-models are then used to perform a sensitivity analysis in order to identify the critical parameters affecting the solar fraction, energy savings and levelized cost of heat. Finally, the obtained meta-models are used to determine a set of optimal solutions using the desirability function approach for single objective optimization or GA for multi-objective optimization.

The proposed method is applied to a real case study, an experimental test unit of a hybrid solar/gas heating system built-up in the "École Nationale Polytechnique El-Harrach", Algiers, Algeria. The unit is instrumented and monitored. First, a numerical model using a modular

simulation environment TRNSYS [10] is developed. The numerical model is then validated via experimental measurements collected from the unit monitoring system using only the solar source. The validated model is then used to assess the system performance in the deemed case study. In addition, model was considered to further enhance and optimize the system design parameters. For the analysis, the developed and validated numerical model is used. DoE technique is then employed to determine the critical parameters affecting solar fraction, energy savings and levelized cost of heat, as well as to develop meta-modeling relationships between design factors and objective functions. The developed meta-models are then used to determine a set of optimal solutions by performing an optimization of the solar fraction at first for solar mode only based on the desirability function approach [11], then a multi-objective optimization of SF, PESR and LCOH for a hybrid operation mode based on GA through MATLAB [12]. Furthermore, a control strategy is implemented in the developed model to investigate the energy saving potential. The sensitivity of the different objective function is evaluated using the DoE approach. A generalized framework for hybrid solar systems optimization process is proposed.

Thesis structure

In order to achieve the overall purpose of this research study, the thesis is composed of five chapters as well as an introduction and general conclusions and perspectives, described as follows:

- **Introduction** summaries the motivation and background of this research work, its objective and outcomes.
- **Chapter 1** demonstrates a comprehensive literature review followed by identifying some research gaps.
- **Chapter 2** details the design framework and the adopted research methodology.
- **Chapter 3** describes the hybrid solar/gas heating system as well as the monitoring system and collected data. In addition, the chapter presents the performance analysis of the experimental unit.
- **Chapter 4** designates the development of the solar heating system model and its validation. The chapter demonstrates the functioning of the system in solar mode only. The model is then used to extend the investigation in combination with DoE for the purpose of a sensitivity study and optimization based on the desirability function approach.
- **Chapter 5** details the functioning of the system in the hybrid mode through a sensitivity analysis to develop metamodeling relationships between each of the objective functions (SF, PESR and LCOH) and design parameters. These metamodels are then used to

conduct a multi-objective optimization based on GA implemented in MATLAB and to determine the Pareto front of the optimal solutions.

- **General conclusions and perspectives** summarize the main findings of the present research work demonstrated in this dissertation and outline the potential for future investigations in this field.

Chapter 1

Literature review

1.1. Energy and environment context

The shortage of fossil fuels is expected to lead to a significant increase in their cost in the future. In order to undertake measures to reduce consumption and achieve greater efficiency in energy systems, it is necessary to target the sectors of activity that consume the most energy. With this in mind, Figure I- 2 provides a graphic representation of the distribution of final energy consumption by sector worldwide from 1990 to 2018 [13]. By final energy, we mean the energy recovered at the end of the energy transformation chain, directly used by the consumer.

According to the International Energy Agency (IEA) organization [13], world total primary energy supply (TPES) has increased by almost 2 times between 1990 and 2018 from nearly 8766 Mtoe (Million Tons of Oil Equivalent) in 1990 to 14279 Mtoe in 2018 (Figure I- 1). In 2018, fossil fuels (coal, natural gas and oil) accounted for 81 % of the TPES. Oil remains the largest energy source at a global level, accounting for 31.5% of global needs, followed by coal 26.9% and natural gas 22.8%. These statistics show the strong global dependence on fossil fuels even though they are responsible for a dangerous climatic change for the planet. Furthermore, supply of these resources is subject to high uncertainties and can be disturbed very quickly by natural events (the exhaustion of oil in 50 years) or technical (industrial disaster), but also geopolitics (political instability in the Middle East region for example).
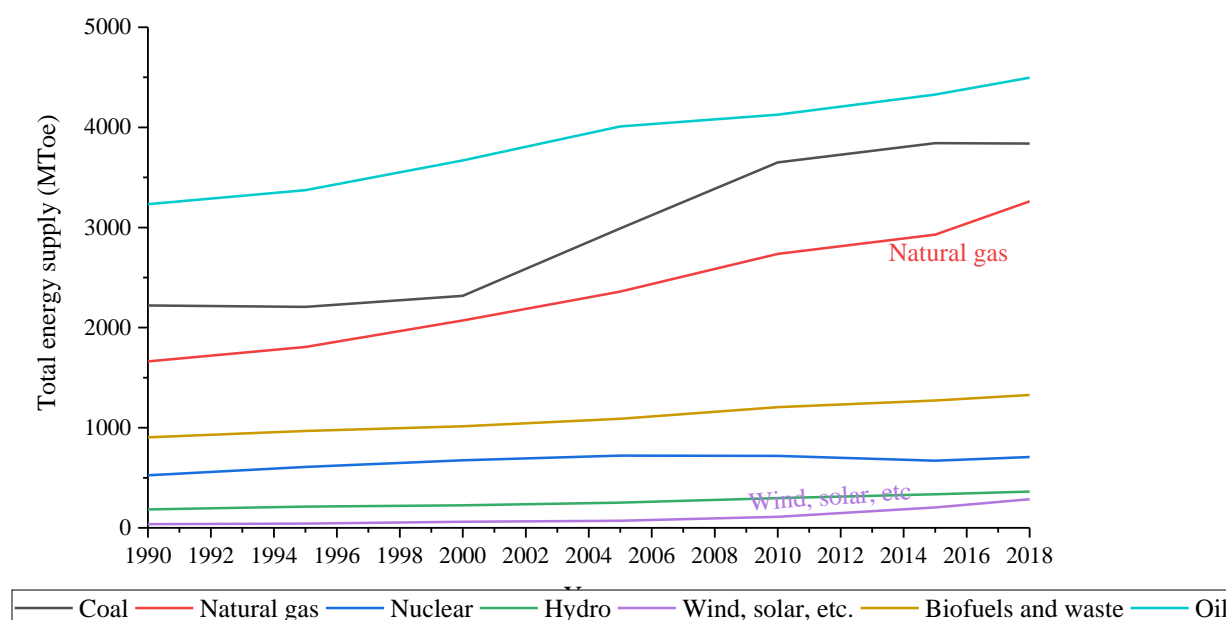
Figure I- 1: Total annual energy supply by source 1990-2018 [13].

1.2. Building sector

The total end-use energy consumption presented in Figure I- 2 shows that industrial and transport sectors are the most energy consuming sectors followed by the residential sector which represents around 30% of the total energy consumption with a noticeable decrease in recent years. In fact, progress towards sustainable buildings is advancing, but improvements are still not keeping up with a growing buildings sector and rising demand for energy services. In addition, the building sector is also responsible for 19% of greenhouse gas emissions worldwide [14]. It is ranked ahead of the transport sector (14%), the energy sector (11%) and the waste treatment sector (3%). Industry remains the most emitting sector of greenhouse gas (29%) followed by the Land Use, Land Use Change and Forestry (LULUCF) sector which is responsible for 24%.
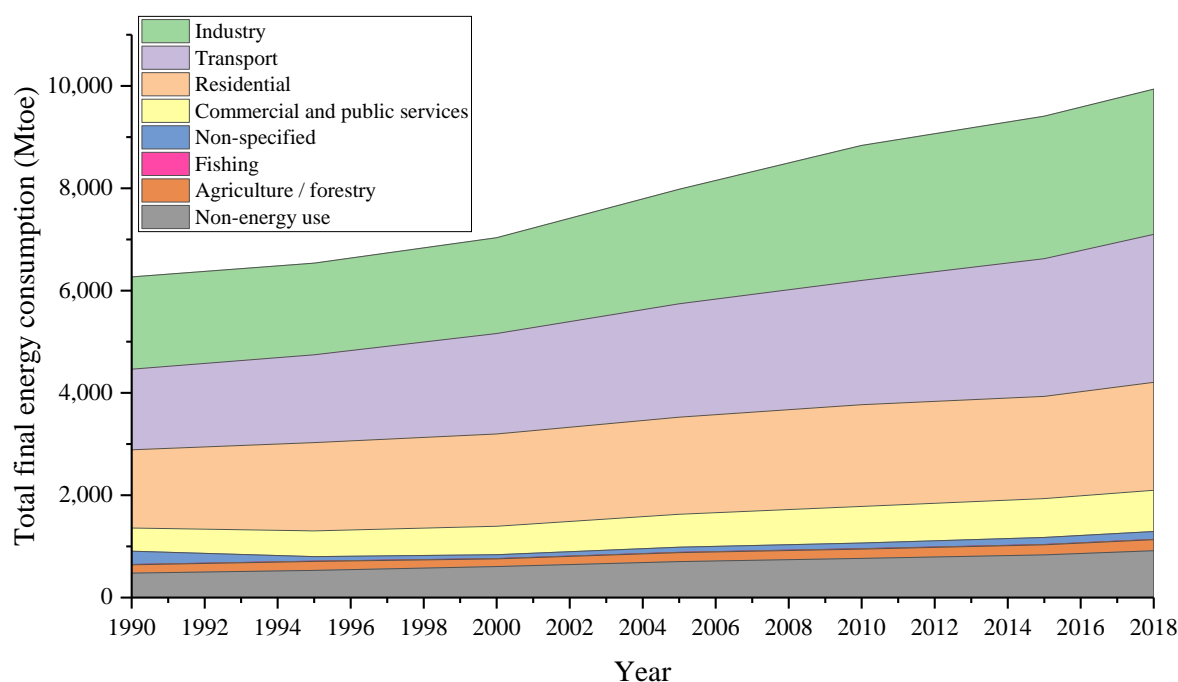
Figure I- 2:Total annual final energy consumption by sector 1990-2018 [13].

The breakdown of final energy consumption by end-use in the building sector is demonstrated in Figure I- 3. In 2018, heat/cool demand and hot water production account for about 52% of the total energy use in buildings [15]. Space heating and water heating denote 14% and 13% respectively in buildings and the remaining total energy use is distributed among all other end-uses. However, these percentages may hugely differ from one region to another, for example in EU-28 energy use in the residential sector is mainly consumed by space heating (68.4%) followed by lighting and appliances (14.1%) [16].

In recent years, a number of standards and regulations that aim to promote sustainable development in the building sector have been established worldwide. For instance, Algerian authorities have established the so-called Thermal Regulation, which defines performance standards of buildings. This regulation is an ambitious step towards promoting green buildings. A special attention is required in the selection of the "elements" constituting the building, such as reducing heat loss by improving the thermal insulation of the envelope [17], [18], minimize thermal bridges, choose a system of ventilation that limits heat loss through air exchange, etc.
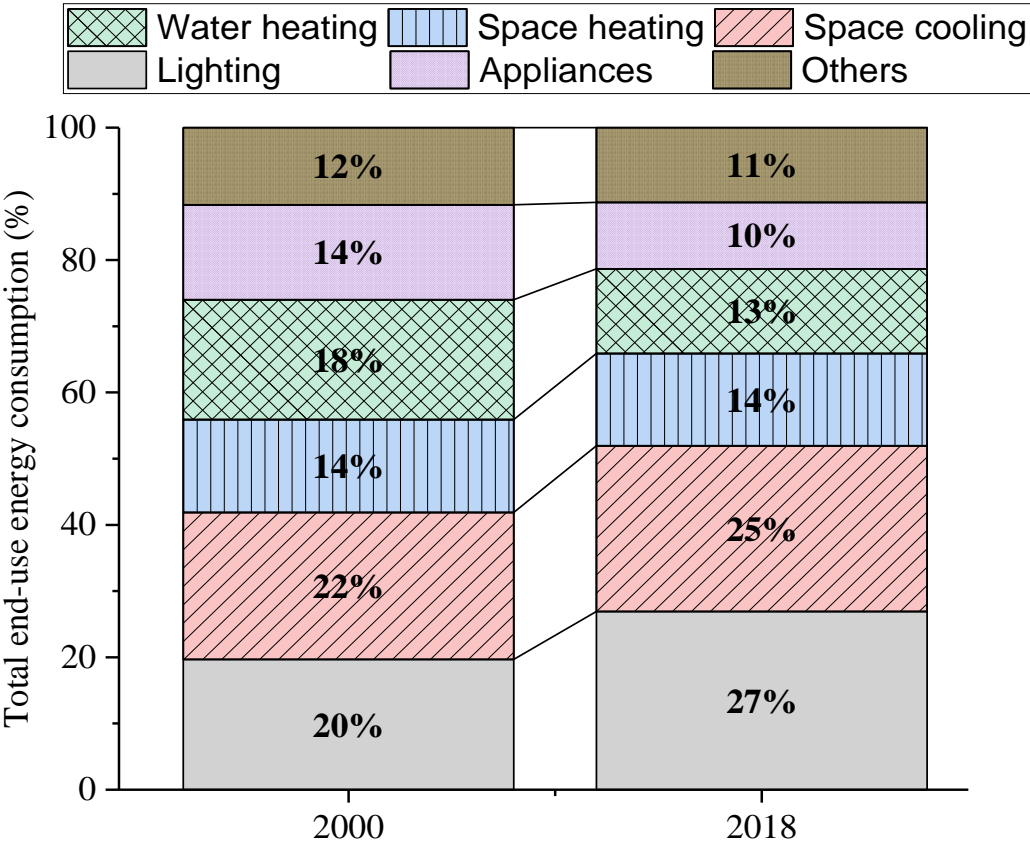
Figure I- 3:Final building energy consumption in the world between 2000 and 2018.

In addition, energy-savings could also be achieved by substituting conventional energy equipment systems with energy efficient equipment. Such as the use of condensation boilers for heating [19], solar thermal panels for the production of the domestic hot water [20], [21], dual flow ventilation systems with high efficiency heat recovery system [22] or using the Canadian wells. These choices represent promising alternatives that aim at helping designers and engineers to attain energy-efficient buildings. Therefore, promoting energy-efficient buildings requires the integration of improved building elements as well as energy efficient systems.

On the other hand, the primary objective of buildings must be to provide a comfortable environment for the people, since they spend 80-90% of the day indoors [23]. Moreover, inappropriate indoor thermal comfort leads to lower work efficiency, higher possibilities of personal errors, and indirect effect on the energy consumption of the buildings [24]. Therefore, the improvement of the energy performance of buildings must take into account the integration of renewable technologies alongside energy-savings measures, and as a result, it is necessary to design energy-efficient solar systems so that a trade-off between energy-savings and occupants' thermal comfort is fulfilled. The following section presents a review of the solar thermal application employed for space heating and/or hot water production.

1.3. Solar thermal applications in building sector

Solar hot water has been utilized for several applications in the building sector. Until 1930, hot water for space heating and domestic purposes were mainly engaged by the coal fired boilers [25]. Solar water heater (SWH) become a commercial product in the early 1960s. During the last decades, the utilization of solar energy technologies in the sector and has grown significantly. Solar heating systems (SHS) provide thermal energy for both space heat and domestic hot water needs, they present viable alternatives for reducing primary energy consumption [26]. Several solar water heaters have been designed and to meet the requirement of different applications and local climatic conditions.
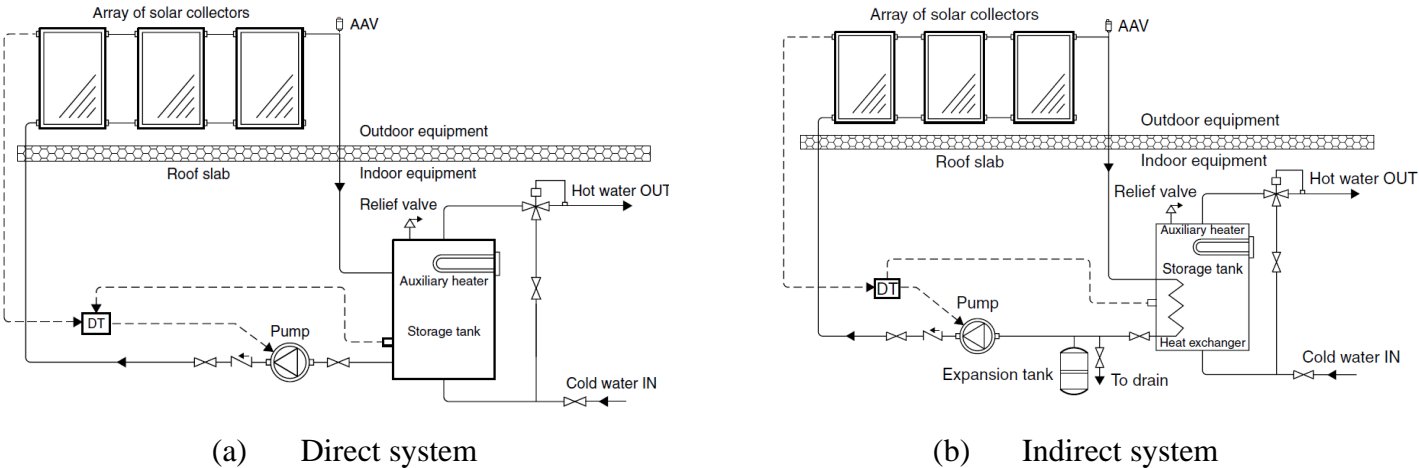
Figure I- 4: Solar water heaters (a) Direct system (b) Indirect system.

These systems are usually classified into direct and indirect systems (

Figure I- 4) depending on the nature of heat transfer through the working fluid. In direct system, heated water in the collector is in direct contact with end-use water. In indirect system, the heating fluid passes through an exchanger to heat water. Similarly, depending on the

25

circulation of heating fluid SWH can be grouped into either: active circulation system or passive circulation system. Active systems utilize a pump to effect forced circulation to the heating fluid, see

Figure I- 4. On the other hand, passive systems rely on thermosyphon effect in which the density difference induces the natural circulation of the fluid [27].

1.4. Solar heating system component designs

A typical SWH consists of a collector, storage tank and a heat medium fluid. Also, other accessory such as incorporated piping, heat exchanger and pumps. The thermal performance of a SWH is improved by optimizing the design and configuration of the collector, the absorber design which is aimed to increase the solar heat harnessing. The major drawback of the solar energy is its intermittence, this issue is minimized by storing the harvested solar thermal energy using thermal energy storage materials. The different thermal performance improvement of SWH is illustrated in Figure I- 5 Significant studies on the design modification of the main components are reported below in the perspective subsections [28].
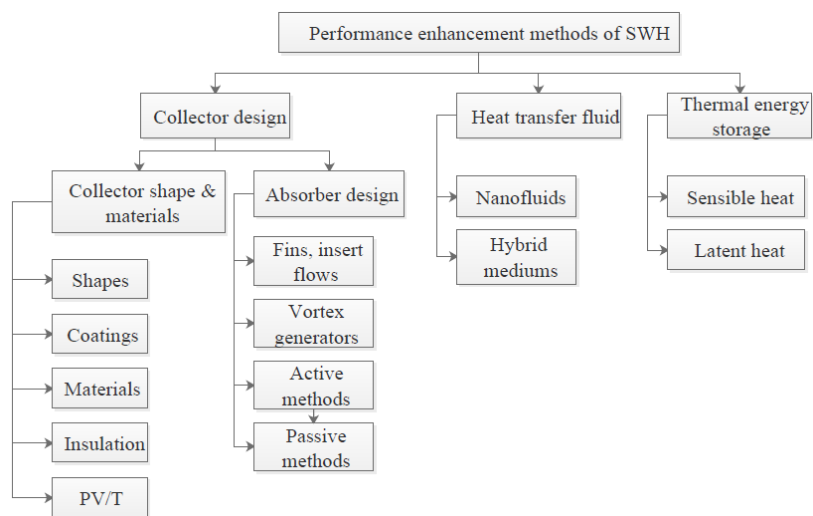
Figure I- 5: Different methods of improving SWH [28].

1.4.1. Solar collectors

A solar collector is a heating device that harnesses the solar energy and converts it to useful heat which is transferred to the heating fluid circulating through the collector. The design parameters such as heat removal factor (F_R) and efficiency factor (F') were developed by Hottle and Whiller which it reduced significantly the empiricism associated in the design of a solar collector. The efficiency of a solar water heater depends mainly on the effectiveness of the solar

collector, and thus numerous researches have been focused in enhancing the performance of the collectors.

1.4.1.1 Flat-plate collectors (FPC)

A flat-plat collector (FPC) represents the heart of a SWH, it is commonly used for harvesting solar thermal energy at low ambient temperatures. It consists of: an absorber plate selectively coated, heating fluid to extract heat from the absorber plate, tubes for the flow of heating fluid, a transparent cover to increase greenhouse effect and reduces top heat-losses, a heat insulating support to minimize heat losses, and a protective casing to ensure that the components are free from moisture and dust.

Several studies have focused on design and development of FPC. The configuration of the collectors is of major importance regarding its thermal performance [29]. The parallel-tube design is a widely used configuration, in which risers (tubes) are integrated to the absorber plate. Hottle and Whillier [30] were the first to evaluate the performance of parallel-tube collectors. Some of the disadvantages of this configuration were: non-uniformity of temperature distribution over the absorber surface and heat loss increase caused by temperature augmentation in low flow rate conditions. Therefore, the serpentine tube design was introduced to overcome these issues. It was mainly designed to compensate the low flow rate conditions; the design allows the total mass flow rate to circulate through the tube, which increases the heat transfer coefficient [29].

The core component of a FPC is the absorber, its thermal performance depends on the design parameters as well as the material properties. Numerous designs have been proposed in recent years analyzing different geometries and materials of the absorber component [31]–[35]. Collectors' efficiency can be further improved by incorporating appropriate transparent insulation materials. Glass is the most commonly used in glazed solar collectors because of its low cost and high solar transmittance 90% [25], [36], [37]. Different types of reflectors were also integrated in the FPC design for improvement purposes and demonstrated better performances in terms of solar gains [38], which spots the light on the next technology.

1.4.1.2 Evacuated tube collectors (ETC)

Evacuated tube collectors (ETC) have been available in markets for more than 20 years. Though they present better performance compared to FPC in producing high temperatures, they are not competitive because of their high initial costs. An ETC consists of : evacuated tubes (double glass seal) minimizing the heat losses, copper heat pipes for their high thermal

conductivity and aluminum reflectors and casing to ensure durability and integrity of the structure to the system.

At present, ETC have become a key feature in solar thermal utilization, as they present higher efficiencies and less heat loss issues when compared to FPCs. The absorber shape is one of the important design factors. For instance, Kim and Seo compared four different designs of the absorber tube: finned tube, U-tube welded on copper plate, U-tube welded inside a rectangular duct and U-tube welded inside circular fin. The results showed that the latter presented the best performance among all [39].

The required output temperature determines the type of collector to be employed [40]. FPC type is widely used in water and space heating applications due to their operating temperatures [30-80] °C relatively low compared to other solar collector types, and it has better performance in warm climates while ETC type ensures higher performance in cold and cloudy conditions [27], [41].

1.4.2. Storage tank

The storage tank is a key component of any SWH system. It plays an important role in dictating the performance of the system. A storage tank is typically used to store the harvested solar thermal energy supplying hot water at the desirable temperature to final use [42].

One of the main issues experienced with storage tanks is thermal losses due to the effect of mixing cold and hot water. Hereby, several designs have been proposed to favorize thermal stratification which seems essential to minimize the mixing effect and thereby maximize the harvesting of energy from the collector [43]. Several theoretical and experimental studies have been conducted to evaluate stratified storage tanks. Different geometrical factors have been considered, such as orientation, vertical or horizontal tanks, wall thickness, material of the tank and height to the diameter ratio. Operational conditions were also studied, mainly temperature difference between outlets and inlets of the storage tank, the flow rate into and out of the tank [44].

1.5. Solar thermal systems design methods

To ensure the reliability of the Solar Water Heating System (SWHS), it is necessary to consider how to design such a system in an economic and efficient manner, as well as to analyze its performance. In literature, a multitude of design approaches has been proposed such as experimental testing, correlation, and simulation-based methods.

a) Experimental methods

Many research studies tackled the design of thermal systems from an experimental point of view, for instance, Ayompe and Duffy [45] experimentally analyzed the thermal performance of a SWHS with 3 m² heat pipe ETC. They thoroughly evaluated different energy performance indices, collected, and delivered energy, supply pipe losses, SF, collector, and system efficiencies. They concluded that the development of a better control strategy would improve the system's performance. Shi et al. [46] conducted experiments on SWHS with ETC and FPC in two different cities in China. They studied their dynamic thermal performance and compared the two considered systems from an economic and environmental point of view. Singh et al. [47] fabricated a SWHS using an improved design of a FPC to enhance its efficiency, then they compared its efficiency with normal FPC. They concluded that the fabricated FPC is highly dependent on the mass flow rate and the wind velocity. In addition, IEA Solar Heating and Cooling (SHC) is a well-known program that has been developing projects (Tasks) studying various aspects of solar heating and cooling.

b) Correlation-based methods

Among the correlation-based methods, the f-chart method [48] and [49] is commonly used, it is based on correlations of a large number of detailed simulations. Solar Utilizability methods [50] which depend on the determination of critical radiation levels for solar collectors and ϕf-chart method [51]. However, as a limitation, the correlation-based methods cannot provide information on system dynamics compared to the simulation-based methods.

c) Simulation-based methods

The simulation-based methods have the ability to provide a significant data related to solar heating system indicators in transient conditions allowing designers to simulate several climatic and technical-economic scenarios. Several researchers worked on the development of numerical models and experimental validation to analyze the solar systems using different collectors [52], [53] also combined solar systems with different energy sources [54], [55].

Validated numerical models might serve as a good tool for the analysis of solar systems, the prediction of their behavior as well as the improvement and optimization of their design parameters. Deng et al. [56] investigated a SWHS combined with a low-temperature air source heat pump via economic analysis and system optimization design. The TRNSYS developed model was validated with experiments on a pilot project under cold climate conditions. A sensitivity analysis was conducted to identify the minimum tank required temperature, the tank volume, and the control of the solar collecting system. The existing building was then compared

to a typical rural house to investigate the effect of the insulation of the building on the SF and average heat load index. Bahria et al. [57] conducted a parametric study on a solar system providing heat, cool, and domestic hot water by comparing two types of constructions in different Algerian climates. The simulation model was compared to IEA Task 38 results [58]. They reported that increasing the thermal insulation showed improvement regarding the inside building temperature; 4 to 5 °C for winter. Optimum collector areas and tilt angles were deduced to maximize SF favoring the cooling production for regions with a hot climate. In the same trend, Mehdaoui et al. [59] established an experimental prototype of a SHS to supply heat to a room via a radiant floor. The TRNSYS model was then validated. A set of optimum parameters was determined, providing the maximum SF.

1.6. Advances in solar thermal systems

The instability and intermittence of solar radiation limit the feasibility and economic performances of solar systems for satisfying the continuous energy demands. Thus, the hybrid technologies of solar energy combining another fuel or more energies become attractive options to both effectively utilize solar energy and eliminate its limitations [60].

Several studies considered the integration of solar heating systems with heat pumps. The International Energy Agency (IEA) has had special interest in such hybrid technology. Particularly, Task 44 of IEA SHC investigated different combinations of solar thermal systems and heat pumps technologies [9].

In literature, various hybrid solar systems have been proposed and investigated. Such as, hybrid PVT for combined heating, cooling and power generation [61], [62], solar collector and ground source heat pump [63], combined solar collector-geothermal heat pump systems [64] or hybrid solar/biomass heating system [65]. Significant interest has been shown to solar and ground/air heat pump technologies because of the high COP in air source heat pumps, moreover, ground source heat pumps have lower operation costs. For instance, a pilot project of air source heat pump combined with a solar water heater was established and its economic analysis was investigated in Beijing [56], then the system design was optimized using validated TRNSYS model. Huang et al. [66] carried out experimental and theoretical investigations on a solar assisted ground source heat pump for both heating and cooling. They validated a TRNSYS model then used it to identify an optimal solution based on a parametrical investigation. They found that adding domestic hot water load not only ensures thermal balance of the ground but reduces the primary energy consumption, and the system proved an increase of 9.4% in the COP. Bellos et al. performed in their study [67] an energetic and financial comparison of

different solar heating systems, Air Source Heat Pump (ASHP) coupled with Photovoltaic (PV) panels against water source heat pump coupled with Photovoltaic/Thermal (PVT), PV or flat plat collectors, they concluded that for higher electricity prices PVT system coupled to Water Source Heat Pump (WSHP) present the most environmental friendly and financially attractive solution for space heating.

The hybridization in solar heating systems certainly leads to changes in the energetic and economic performances due to the difference in characteristics between solar energy and the other source. Many efforts have been made to discuss the systems performances from different point of views including energetic [68], [69], economic [70], [71], environmental impacts [72], operation strategies [73] and system configurations [26], [67]. Therefore, the optimization methodologies have been used to optimize system configurations and operation strategies to improve the performances of hybrid solar heating systems.

1.7. Solar hybrid systems optimization methods

Recent studies focused on the optimization of the solar heating system components, design parameters, and operation strategies, in order to achieve better thermal performance while preserving the user's comfort and to be cost-effective [74]–[76]. Huang et al. [66] developed a TRNSYS model of a solar assisted ground source heat pump (SAGSHP) and validated it against experimental data. The model was then used to minimize the renovation cost and to achieve the best cost performance ratio. The results showed that adding a domestic hot water system to the SAGSHP increase the COP of the system by 9.4 % and reduce the overall operating cost by 16%. Araùjo et al. [77] used a genetic algorithm to optimize the control parameters of the fluid flow which maximize the SF, both proportional and on-off control strategies were studied. They reported that the SF using the proportional control exceeded by 50% the SF values using the on-off control in most practical cases.

Optimization of hybrid solar systems have been carried out in numerous research studies to guarantee certain quality and reliability of these systems, the goal is often to maximize the energetic performance of such systems [78]–[80] minimize their total cost of the ecological impact regarding GHG emissions [81]–[83]. Single objective optimization is a widely used approach, usually handled by genetic algorithm (GA) [84], mixed integer linear programming (MILP) [85] or commercial optimization programs such as GenOpt [86]. However, there is usually more than one objective to be optimized, which is described as a multi-objective optimization problem. Many researchers considered multi-objective optimization for hybrid solar heating systems using different techniques. Evolutionary algorithms attracted significant

interest. For example, Ren et al. [87] optimized the configuration of a hybrid combined cooling, heating and power (CCHP) system, using non-dominated sorting genetic algorithm II (NSGA II) based on primary energy saving ratio (PESR), carbon dioxide emission reduction rate (CDERR) and annual saving cost (ACSR) as evaluation criterion for the optimization of the system's performance. Bany Mousa et al. [88] compared a side-by-side configuration of PV panels with Fresnel solar thermal collectors, to identify the best mix distribution through single and multi-objective simulation from economic, technical and environmental perspectives. The authors used TRNSYS package with GenOpt based on particle sworm optimization (PSO) approach for single objective optimization GA inside MATLAB linked to TRNSYS for multi-objective optimization. They found that a mix distribution of the two technologies improved the levelized cost of energy, the solar fraction and reduced the environmental payback period. Shah et al. [89] in their study considered minimizing the total life cycle cost and the cost of GHGE, they combined TRNSYS to Multi-Objective Building Optimization (MOBO) using Non-Sorting Genetic Algorithm II (NSGA II), in order to optimize the design variables of a seasonal solar thermal energy storage system in six cold climate locations. When others develop their own algorithms or use hybrid approaches. However, these techniques are time-consuming especially when coupled to dynamic simulation programs [90], and requires high number of generations to approximate the pareto front [91] compelling the designer to find a balance between optimization time and accuracy of optimal results [87].

1.8. Discussion and research gaps

Although most of the studies conducted parametric and sensitivity analyses to investigate the effect of certain parameters on different performance metrics and to improve the process of the solar thermal systems, the followed approaches were based on the one factor at a time (OFAT) method, which considers one variable factor when holding the rest of the factors at fixed values and conceals the interaction between the factors. However, the thermal behavior of a SWHS is a complex problem since it involves several interrelated parameters. Variations in these parameters affect the SWHS performance and some of them might not be considered without other parameters. Thus, many concerns, related to the way that one can follow to conduct a sensitivity study leading to the optimization of the SWHS performance, should be tackled. Among them, how does the interaction between design parameters influences the SWHS performance? To what extent the sensitivity study could be an asset to the optimization of the SWHS performance?

Among the tools that are intended to address these issues is the Design of Experiment (DoE) method. DoE method is a formal structured technique designed to address complex problems

where a response might be affected by more than one variable and the variables might interact with each other. DoE uses an optimum number of experiments to provide rigor answers about system behavior and allows the detection of the presence of interaction between variables and their quantification [92]–[94]. To the authors' best knowledge, this technique has not been employed yet in the solar thermal applications for prediction or optimization concerns. It appears there are few published studies dealing with sensitivity analysis, by taking the interaction between single parameters and optimization with regards to the thermal solar applications [95]–[97]. None of these studies concerned north African climatic context characterized by a harsh solar potential with either a moderate or cold weather conditions.

The design of experiments (DoE) method can reduce the number of experiments or simulations to an optimum number [94]. DoE methods have been used to assess the performance of solar systems, calise et al. [96] carried out a study to maximize the primary energy savings by defining optimal set of operating conditions using TRNSYS program for dynamic simulations and full factorial design to reduce the number of simulations and study the effects of the various design parameters on the PESR. In another work, the authors implemented a computer-based DoE and performed a sensitivity analysis in a thermo-economic optimization of a solar trigeneration system [95]. Recently, Kalogirou et al. [98] developed and validated a new TRNSYS type for thermosiphon thermal collectors, they investigated the influence of the design and operating parameters on the economic and energy performance of the developed model using DoE. These techniques have been limited to studying variables' effects, sensitivity studies or single objective optimization[99]. Yet, they offer the possibility of establishing analytical models also called metamodels, which may be exploited to conduct multi-objective optimization.

The multi-objective optimization provides a set of optimal solutions called Pareto front, which is represented by non-dominated superior solutions, where the objective functions are confronted to each other's. For example, Starke et al. [74] presented a methodology to evaluate the compromise between the annualized life cycle cost (ALCC) and thermal comfort for swimming pools, by optimizing the configuration of a solar-assisted heat pump. In a pareto front, each solution can be chosen as optimal solution depending on the designer's preference. Thereby, numerous decision-making methods and approaches have been proposed in literature, which can be implemented to define a relative compromise optimal solution. Namely three famous and robust decision-making techniques, LINMAP, TOPSIS and Shannon's Entropy. For instance, Cao et al. [100] used the three techniques to select a final optimal solution where the COP and the collector efficiency were the objective functions. Li et al. [75] adopted the

LINMAP method to find a tradeoff between primary energy consumption and levelized annual cost of a hybrid solar system for air-conditioning and space heating application. These techniques were also compared in other fields [101] and their suitability varied from one case to another depending on the deviation index. The LINMAP method was selected in this paper for decision-making

The literature review conducted in this chapter, and the above analysis of research gaps, were used as a basis for constructing our research approach. The latter is to be presented in the next chapter in detail.

Chapter 2

Design framework and research methodology

2.1. Dynamic energy modelling

The dynamic analysis solar thermal system integrated to buildings using computer modeling simulation methods requires powerful tools for evaluation of the systems' performance, the effect of building envelope design and control strategies. In the recent years, the use of these tools is increasing by all professions elaborated in the design of buildings. This increase is correlated to two main reasons; the first is that the dynamic energy simulation tools become more advanced, integrated and easy to use. The second is that, the dynamic simulations allow designers and engineers to take early decisions that help in improving system performance, reducing its costs and saving time [102].

Energy modeling in buildings is based on so-called physical techniques, which are based on the solving of equations describing the physical behavior of the heat transfer.

2.1.1. Physical models

Physical modeling techniques are used to model and evaluate the thermal performance of different building types, including models for different aspects such as HVAC systems, hygro-thermal effects, occupants' behavior, etc. They can be divided into three main categories: Computational Fluid Dynamics (CFD), zonal, and multi-zone/nodal methods. Each method has its own principle, application field, advantages and drawbacks, thus the choice of the physical model depends principally on the problem under investigation. Table II- 1 summarizes the specificity of each technique. A detailed description of each approach and a review of their applications in the buildings modeling is presented in [103].

The CFD method is indisputably the most detailed and comprehensive method, it allows the fine description of each mechanism occurring in the building system. However, this approach requires significant computational resources and is highly complex, so that it requires highly skilled laborers. A huge number of CFD software are available such as FLUENT and COMSOL Multiphysics. Their application fields are very large and not always specific to building simulation [103].

The zonal approach represents a simplification of first degree of the CFD method. It divides the building into different zones and each zone into different cells. It solves the physical equations of each zone instead of each mesh element. The zonal approach is less comprehensive and accurate than the CFD approach but represents a faster way that gives good results related to the indoor environment parameters.

Table II- 1:Summary of the specificity of each physical technique [103].

Physical technique	Specificity of each technique	Application field	Advantages	Drawbacks
CFD method	One cell=a control volume (3-D); Local state variables	Contaminant distribution; Indoor air quality; HVAC systems	Detailed description of the fluid flows occurring inside the building; Large volume zones	Huge computation time; Complexity of the model implementation
Zonal method	One cell=a division of a room (2-D); Local state variables	Indoor thermal comfort; Artificial and natural ventilation	Spatial and time distribution of local state variables (temperature, concentration, pressure, airflow) in a large volume	Large computation time Requirement of a detailed description of the flow field and flow profiles
Nodal method	One cell=a room (1-D); Uniform state variables	Determination of the total energy consumption/ the average of the indoor temperature/the cooling or heating load; Time evolution of the global energy consumption/ the space-averaged indoor temperature	Multiple zone buildings. Reasonable computation time; Easier implementation	Difficulty to study large volume systems Unable to study local effects as heat or pollutant source

The multi-zone or nodal approach is probably the simplest method compared to the zonal and CFD techniques. It assumes that each building zone is a homogeneous volume with uniform state variables. In addition, this technique simplifies the physical problem by linearizing the equations, when it is possible. This results in significantly reducing the technical complexity of the problem and thus the computation time. Thus, the advantage of nodal approach is its ability to compute simulations for large periods with minimum computation time. The most popular software that uses the nodal approach for building simulations are TRNSYS, EnergyPlus, IDA-ICE, and ESP-r.

Based on the aforementioned discussion and information provided in Table II- 1 one can deduce that the nodal technique is most useful among others for the study of the current system. Since in this work, the modelling process focuses on thermal loads and energy consumptions and the detailed analysis resulting from the CFD approach is unnecessary.

Furthermore, the use of dynamic energy simulations can result in valuable benefits. For example, parametric and sensitivity studies that aim at evaluating the influence of altering system parameters can be simply examined using simulation software, rather than changing the parameters of the actual system, which lead to additional costs.

It is obvious that simulation tools have gained a huge acceptance and are now approved as the best practice to demonstrate the real life scenarios [104]. However, the complex dynamic principles of the real systems require realistic simulations, rather than simple estimation coupled with uncertainties due to the transition from the real life to simulations [104]. These uncertainties may lead to disclosing the accuracy of the model, thus affecting the validity of the outcomes.

2.1.2. Uncertainty in building thermal performance modeling

Several factors contribute to the uncertainty of the building simulation models. For instance, the simulation software itself, software user's knowledge or simulation skills may be sources of uncertainty. In addition, the input parameters such as weather data and thermo-physical properties, since these parameters are always expressed under a certain part of uncertainties [103] . This could be correlated to the lack of detailed information related to the occupant behavior, equipment scenario, sub-metering instruments, and the complete as-built drawings, which could help in developing a detailed and accurate model. The stochastic nature of occupant behavior often leads to the largest source of uncertainty in the building simulation, in addition to its large influence on energy consumption [105], [106]. And also, incomplete and fragmented weather data used for the creation of real weather files could lead to some uncertainties in the collected data and thus in the simulation results [106].

2.2. Sensitivity analysis

Sensitivity analysis (SA) was considered and often defined as a local measure of the effect of a given input on a given output [107]. It is a valuable approach that can be used to identify the key parameters influencing solar system performance for both observational and energy simulation studies [108]. In the recent years, SA has been extensively used to discover the characteristics of building thermal performance [108], [109], a literature review of the

application and used methods of SA in building thermal performance analysis is presented in [108].

There are numerous techniques to employ SA in building performance studies. These techniques are commonly grouped into local and global methods [110]. The local sensitivity analysis (LSA) is performed in a similar means to the differential analysis, where the uncertainty of outputs is evaluated by a slight increase in the value of one input variable. However, in the global sensitivity analysis (GSA), the influences of all of input variables are estimated on the uncertainty of outputs.

GSA techniques evaluate the variations of the output resulting from one input variable by varying all other parameters over their variation range at the same time [107], [111]. Thus, GSA methods measure the interaction of factors and provide robust sensitivity measures. It is considered more reliable than the LSA, but it requires higher computational time compared to LSA. The GSA includes regression, screening-based, variance-based, and meta-modeling methods. The characteristics of the mentioned methods are summarized in Table II- 2.

Table II- 2: Comparison of sensitivity analysis methods used in building performance analysis [108].

Method	Characteristics
Local	Explore a reduced space of the input factor around a base case; low computational cost; simple to implement; easy to interpret; not consider interactions between inputs; no self-verification
Regression	SRC and t-value, suitable for linear models; SRRC, suitable for non-linear but monotonic models; moderate computational cost for energy models; fast to compute; easy to implement and understand; high SRC means more important of the variable
Screen	Suitable for a larger number of inputs and computationally intensive models; model-free approach; qualitative measure to rank factors; no self-verification; not suitable for uncertainty analysis
ANOVA	Decompose the variance of the model output for every input; model-free approach; consider both main and interactions effects; quantitative measures; high computational cost; FAST is not suitable for discrete distributions
Meta-model	Suitable for complex and computationally intensive models; quantify output variance due to different inputs; the accuracy dependent on the meta-model

2.3. Model boundary conditions and validation

Since simulation tools are widely used to model solar systems in order to predict their thermal behavior, the prediction capability of these models is an influential factor in order to reflect the reliability of the results. These models must be suitable and provide significant contributions to reflect the ambiguity effects associated to the building design parameters, construction quality, building uses and climatic conditions; therefore, the validation of the developed model is essential. Indeed, to predict the thermal behavior of the whole system, all the contributing factors must be adequately defined in the model in order to outcome truthful results. Weather data is one of the main factors that contribute to the quantification of thermal behavior of the solar systems.

2.3.1. Weather data

Typical Meteorological Year (TMY), a year of hourly weather data collected from a dataset of several preceding years so that it exemplifies a typical annual data for a specified location, is recommended to be used in the building simulations [112]. However, extreme weather events are not included in the TMY data files, since these files are intended to best represent the building operation and performance when exposed to normal weather conditions. Also, TMY data files are not suitable for the validation of the building models, since they represent a typical prototype, but not the real data during a particular time. Thus, for validation, actual weather data occurring during the monitoring of the real building is recommended, so that the response of the model and that of the real building are matched during a specified period. This yields to best tuning the building model by comparing actual and predicted parameters profiles using the same input factors, hence diminishing the uncertainty related to weather parameters.

Nevertheless, the real weather data should not be used for long term evaluations, since they only provide definite results for the location and over the studied period. Therefore, after the model validation is accomplished, the real weather data must be replaced by the TMY data file of the specified location to carry out simulations. So that the desired investigations using the building model could be performed, the objectives of the study could be achieved, and the obtained results will be more representative. Noting that, the implementation of real weather data depends on the used simulation software.

2.3.2. Validation methodology

To validate a developed model, several resulting parameters, called predicted or simulated results, should be compared to real measured data from the real system. This comparison should be performed by the application of metrics that aim at quantifying the discrepancies between predicted and actual data.

A comprehensive documentation for the calibration and validation of building thermal models was published by ASHRAE in 2002. This document, known as ASHRAE Guidline-14 (G-14) [113], is extensively used for the validation of models using energy data. Specifically, the document recommends the use of the so-called coefficient of variation of the root mean square error (CVRMSE) to evaluate the validity of the developed model. CV(RMSE) measures the variability of the errors between measured and simulated values. It gives an indication of the model's ability to predict the overall load shape that is reflected in the data [113]. It is expressed as follows:

$$CV(RMSE) = \frac{1}{\overline{m}}\sqrt{\frac{\sum_{i=1}^{n}(m_i - s_i)^2}{n}} \times 100(\%) \qquad \text{(II. 1)}$$

Where $\overline{m}, m_i, s_i$ and n represent the mean of the measured values, the individual measured values, the individual simulated values, and the number of measured data.

2.4. Research Methodology

As previously discussed, in this research work the focus will be on developing a hybrid solar heating system analyzing its thermal performance. Then, to deriving and reformulate the design of the hybrid system to achieve satisfactory results. Therefore, a suitable and adequate approach to predict the actual behavior of the system is required. Here, we adopted the energy simulation approach because of its capability to provide adequate results with less time and cost. So, the first step will be selecting a simulation environment for modeling purposes. After modeling the system, design variables must be selected for the evaluation. Since the main intention of this research work is to enhance the performance of the system while being economically efficient, the well-known thermal indicators, SF and PESR and economic indicator, LCOH are used for the evaluation. The sensitivity analysis represents a worth approach for the comprehensive evaluation of the system performance because it enables understanding the relationship between the studied variable and the design parameters. In this study, the use of meta-modeling approach based on the DoE technique is adopted, because it allows the designer to derive mathematical formulation, noted as meta-models, between the studied variable and design parameters.

Indeed, the final step will be adopting an optimization approach that simultaneously optimizes thermal and economic performance. Figure II- 1 shows the graphical representation of the proposed research methodology. The adopted simulation environment is presented in the next section, followed by a brief definition of the DoE technique, the determination and validation of the meta-models, and the used optimization processes, successively.
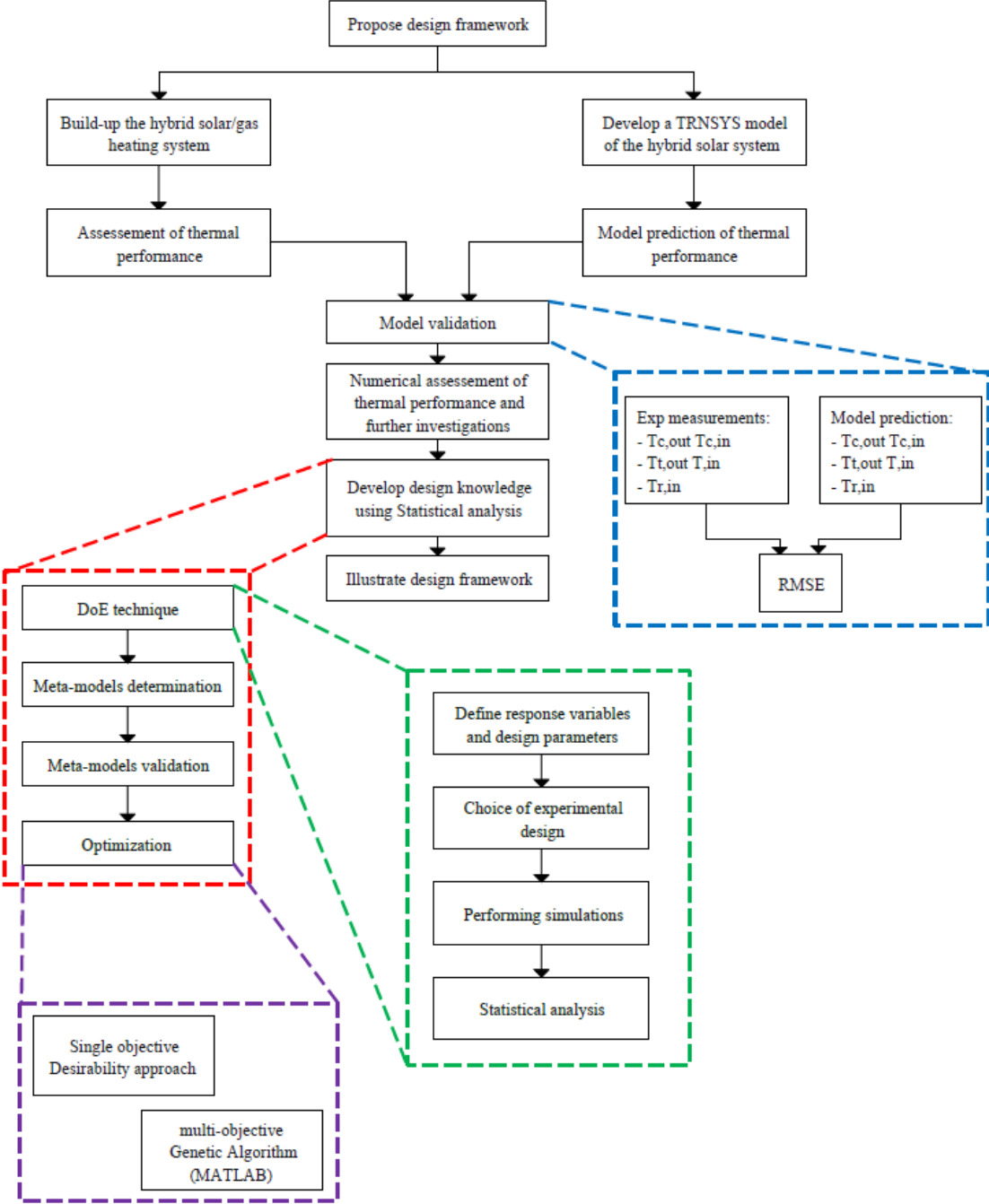
Figure II- 1: Research methodology.

2.4.1. TRNSYS for energy simulation

The numerical modeling and simulations were performed using TRNSYS, which is an algebraic and differential equation solver in which components are connected graphically in the simulation studio. In building simulations, all HVAC components are solved simultaneously with the building envelope thermal balance and the air network at each time step. The simulation results are based on the individual component simulation performances which can be selected from the simulation studio. It is suitable for the simulation of complicated systems. Users can easily accomplish the desired system control strategies by writing the logical programming or use simple equations thanks to TRNSYS open-source code. TRNSYS also includes the program TRNEdit, which is an all-in-one editor for reading and writing TRNSYS input and output files. TRNEdit can also perform parametric TRNSYS simulations and plot data from the TRNSYS simulation output [114]. TRNSYS was developed to simulate plant systems and therefore has a huge component library. and TRNSYS offer a GUI to the 3D tool Google SketchUp.

2.4.2. Design of experiments (DoE)

The DoE technique is a statistical method used to approximate the mathematical relationship between different factors affecting several response variables, and most often one response variable. It could be used to simplify parametric studies by reducing significantly the required number of experiments or simulations [5]. The obtained mathematical models, also known as meta-models, could be used instead of numerical simulation tools to simplify and accelerate the parametric studies to find optimal solutions and to analyze the effect of each factor on the response variable and the interaction between factors. In order to implement a DoE technique, the following procedure is recommended [94]:

1. Recognition and statement of the problem.

2. Selection of the response variable.

3. Choice of factors, levels, and ranges.

4. Choice of experimental design.

5. Performing the experiment.

6. Statistical analysis of the data.

7. Conclusions and recommendations.

The Analysis of Variance (ANOVA) in combination with Fisher's statistical test (P-value < 0.05) could be used to test the significance of the model along with model terms. The

significance of a factor or its effect is determined based on its P-value, which is an important parameter used to identify statistically significant factors influencing the response variable. If the P-value of a factor or its effect was less than 0.05, it is considered as significant [115]. Contrarily, factors with P-value greater than 0.05, are deemed as not significant [115]. Additionally, graphical illustrations, such as the Pareto plots of standardized effects and the Normal plots of standardized effects, could be used to identify the significant terms using graphical analysis.

2.4.3. Meta-modeling and determination of meta-models' coefficients

One of the main objectives of the DoE technique it to pursue a suitable mathematical model, called "meta-model" or "model of the model", that approximate the response variable as a function of predefined factors. The most common meta-models are the first-order linear model (Equation (II. 2)), the linear model with interaction terms (Equation (II. 3)), the pure quadratic model (Equation (II. 4) and the complete quadratic model (Equation (II. 5)) expressed as follows [94]:

$$Y_i = C_0 + \sum_{i=1}^{n} C_i X_i + \epsilon \tag{II. 2}$$

$$Y_i = C_0 + \sum_{i=1}^{n} C_i X_i + \sum_{i=1}^{n-1} \sum_{j=1+1}^{n} C_{ij} X_i X_j + \epsilon \tag{II. 3}$$

$$Y_i = C_0 + \sum_{i=1}^{n} C_{ii} X_i^2 + \epsilon \tag{II. 4}$$

$$Y_i = C_0 + \sum_{i=1}^{n} C_i X_i + \sum_{i=1}^{n-1} \sum_{j=1+1}^{n} C_{ij} X_i X_j + \sum_{i=1}^{n} C_{ii} X_i^2 + \epsilon \tag{II. 5}$$

where Y_i is the predicted response variable, X_i and X_j are the independent coded factors, $X_i X_j$ represents the two-factor interaction, C_0 and C_i represents the regression coefficients for intercept and linear terms, C_{ij} is the coefficients for interaction terms, C_{ii} is the coefficient of the quadratic terms, and ϵ is a random error term that accounts for the experimental error. Indeed, the transition from dimensional to coded factors must be made by applying the following formulation:

$$X_i = \frac{x_i - (x_{i,high} + x_{i,low})/2}{(x_{i,high} - x_{i,low})/2} \tag{II. 6}$$

44

where X_i is the coded value of the variable xi ranging between -1 and +1, $x_{i,low}$ and $x_{i,high}$ are the values of the variable at low and high levels, respectively. Simple matrix multiplication could be used to determine the coefficients of the meta-model. Firstly, the meta-model is expressed in matrix notation as:

$$[Y] = [X] \cdot [A] + [e] \qquad \text{(II. 7)}$$

Where $[Y]$ is a vector consisting of the response observations, $[X]$ is design matrix of the considered factors, $[A]$ is the vector of regression coefficients (C_0, C_i, C_{ij}, C_{ii}), and $[e]$ is the residual vector. Then, the least squares method is used to calculate the coefficients vector $[A]$ as follows:

$$[A] = ([X]^t \cdot [X])^{-1} \cdot [X]^t \cdot [Y] \qquad \text{(II. 8)}$$

After obtaining a meta-model that best describes the relationship between the response variable and the factors, its validity is vital to reflect the adequacy of the performed sensitivity analysis as well as apply an optimization procedure.

2.4.4. Validation of the obtained meta-models

The model adequacy, and as a result the adequacy of the performed analysis, can be done easily by graphical analysis of residuals [94]. The residual (e_i) is defined as the difference between the actual observation (y_i) and the corresponding fitted value($\hat{y}_i$):

$$e_i = y_i - \hat{y}_i \qquad \text{(II. 9)}$$

If the model is accurate, the residuals should be "structure-less"; in particular, they should be unrelated to any other variable including the predicted response. A simple check is to plot the residuals versus the fitted values. This plot should not reveal any obvious pattern (in other words, there should be no relationship between the size of the residuals and the fitted values, such as tendency for negative or positive residuals to occur with low, intermediate or high fitted values.). In addition, a very useful method is "The Normality Assumption", which is to construct a normal probability plot of the residuals. If the underlying error distribution is normal, this plot will resemble a straight line, and thus confirming the validity of the model.

Moreover, computer programs for supporting DoE display some other useful information. The coefficient of determination ($R2$) is loosely interpreted as the proportion of the variability in the data "explained" by the ANOVA model. It ranges between zero and one, with larger values being more desirable. The "adjusted-$R2$" is a variation of the ordinary $R2$ that reflects

the number of factors in the model. It can be a useful statistic for more complex experiments with several design factors when we wish to evaluate the impact of increasing or decreasing the number of model terms.

Up to this point, we have explained the use of DoE technique in order to identify the significant factors affecting a deemed response variable and the determination of regression meta-model as well as the validation processes to check the adequacy of the obtained results. The obtained meta-model could be used to find a desirable result, such as maximizing or minimizing the response variable. However, in many cases the term "desirable" is a function of more than one response. For instance, to achieve a trade-off between energy-savings and levelized cost of heat a simultaneous optimization procedure is needed to minimize the cost as well as maintain the energy-savings or SF in a desired range. a simultaneous optimization procedure is needed to find a compromise solution.

2.4.5. Optimization methods

Simultaneous consideration of multiple responses involves first building an appropriate mathematical model for each response and then trying to find a set of operating conditions, design factors, which in some sense optimizes all responses or at least keeps them in desired ranges.

A relatively straightforward approach is to overlay the contour plots for each response, then determine the appropriate conditions by examining visually the contour plot [116]. However, this approach works well when there are only few factors, because the contour plot is two-dimensional that means n-2 of the design factors must be held constant to construct the graph. The determination of these factors requires a lot of trial and error [116], which implies that the use of a formal optimization method is of practical interest.

In this consequence, the simultaneous optimization technique, known as the desirability function approach, represents a useful approach to optimization of multiple responses. The desirability function approach proposed by Harrington [117] and then modified and popularized by Derringer and Suich [11] aims to simultaneously optimize multiple equations. Its basic idea is to convert a multiple response problem into a single one by converting each response y_i into an individual desirability function d_i that varies over the range [0, 1], where d_i=1 if the response y_i is at its target or desirable value, and d_i=0 if the response is outside a desired range. The individual desirability functions have different formulations depending on the desired objective (maximize, minimize or target value). If the objective is a maximum, a minimum or a target value, the desirability functions are written, respectively, by the following equations:

$$d_i^{max} = \begin{cases} 0 & \text{if} & y_i < L \\ \left(\dfrac{y_i - L}{T - L}\right)^r & \text{if} & L \leq y_i \leq T \\ 1 & \text{if} & y_i > T \end{cases} \tag{II. 10}$$

$$d_i^{min} = \begin{cases} 0 & \text{if} & y_i > U \\ \left(\dfrac{U - y_i}{U - T}\right)^r & \text{if} & T \leq y_i \leq U \\ 1 & \text{if} & y_i < T \end{cases} \tag{II. 11}$$

$$d_i^{\text{target}} = \begin{cases} 0 & \text{if} & y_i < L \\ \left(\dfrac{y_i - L}{T - L}\right)^{r_1} & \text{if} & L \leq y_i \leq T \\ \left(\dfrac{U - y_i}{U - T}\right)^{r_2} & \text{if} & T \leq y_i \leq U \\ 1 & \text{if} & y_i > U \end{cases} \tag{II. 12}$$

(L), (T) and (U) are successively the lower, the target and the upper limits, r_i is a weighting parameter used to determine how important it is for the response to be close to the desired objective.

Afterward, the individual desirability functions are combined in the so-called global desirability function (D) as expressed in Equation (2.16). Lastly, the algorithm should search for the set of input factors to maximize the overall desirability function D [118].

2.4.6. Pareto front

When a problem involves more than one objective function that are to be maximized or minimzed, it is called a multiobjective optimization problem, the answer to that problem is a set of solutions that defines the best tradeoff between competing objectives. In the single-objective optimization problem, the superiority of a solution over other solutions is easily determined by comparing their objective function values. In multi-objective optimization problems, the goodness of a solution is determined by the dominance. To find or to approximate the set of non-dominated solutions and make a selection among them is the main topic of multiobjective optimization and multicriterion decision making [119]. This set of solution is called Pareto front, see Figure II- 2. The general formula of multiobjective optimization is :

$$\begin{aligned} min/max \quad & f_m(\boldsymbol{x}), \quad && m = 1,2,\cdots,M \\ \text{subject to} \quad & g_j(x) \geq 0, \quad && j = 1,2,\cdots,J \\ & h_k(\boldsymbol{x}) = 0, \quad && k = 1,2,\cdots,K \end{aligned} \tag{II. 13}$$

$$x_i^{(L)} \leq x_i \leq x_i^{(U)}, \quad i = 1,2,\cdots,n$$

The concept of Pareto dominance is of fundamental importance to multiobjective optimization, as it allows to compare two or more objective vectors in a precise sense. There are several different multiobjective optimization evolutionary algorithms that helps to define or approximate the pareto front. For instance, Non-dominated Sorting Genetic Algorithm II (NSGA II) classifies the solutions into several mutually exclusive equivalent non-dominated sets. "Paretosearch" algorithm is based on the NSGA II and available in MATLAB. It uses pattern search on a set of points to search iteratively for nondominated points. The pattern search satisfies all bounds and linear constraints at each iteration. Theoretically, the algorithm converges to points near the true Pareto front.
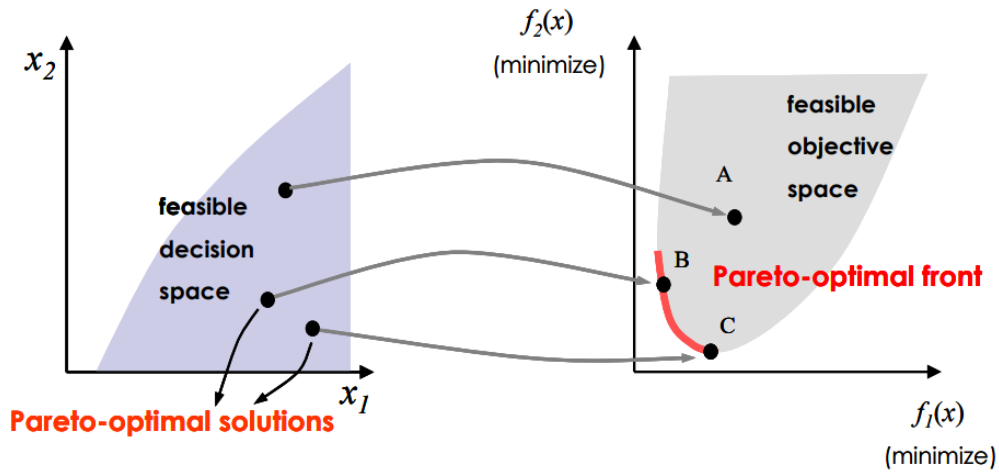
Figure II- 2 : Graphical depiction of pareto optimal solutions.

2.5. Conclusion

In this chapter, we summarized the design framework towards the optimization of the solar heating system. Every step requires actions and activities to be performed, for this we introduced the prediction models proposed in the literature and adopted the required tools to perform our investigations. Finally, we proposed a research methodology that aims to evaluate the influence of the different parameters on the system performances and to formulate relationships between them to assess the optimization process.

As indicated above, a case study is required for the modeling and investigations. A detailed description of the characteristics of the considered system is presented in the following chapter. Next, a computer simulation model using TRNSYS is then developed. Comparing model

predictions with objective measurements enables the validation of the model. Numerical simulations are then performed using the validated model to assess thermal performance of the system and to conduct the multiobjective optimization.

Chapter 3

Experimental development of a Hybrid Solar/Gas Heating System

3.1. Introduction

With the development of solar heating systems, a large amount of heat demand is ensured by these technologies. Their performance, however, depends on several factors. Notably, the climatic conditions, their configuration, the end-use energy consumption profile. In the past few years, several studies on the use of solar heating systems in buildings were performed. In north African climate, Mehdaoui et al. [59] investigated the energetic and thermal performance of a solar heating system used to prevail air-heating needs, based upon a validated numerical model they predicted annual solar fraction of 78%. Bahria et al. [57] conducted a parametric study in different regions in Algeria for different building envelops. The solar fraction for heating varied between 24% and 35%. The experimental setups, however, provide thorough details on the performance of such systems. In that view, a hybrid solar gas/heating system, which is the case study in the current work, is built up in Algiers, Algeria.

As previously discussed, a case study should represent an informative and useful part of the research work to reflect the reliability and credibility of the obtained results. In this chapter, the developed system is described in detail from the design stage up to the instrumentation of the unit, the monitoring and how data is collected. Experimental measurements are then presented and used for further experimental investigation. The aim of that investigation is to characterize the thermal collectors in terms of their dynamic and steady-state behavior and to provide reliable data for further modeling of the system.

3.2. Description of the experimental setup

3.2.1. Context of the experiment

A hybrid solar gas heating system (HSGHS) was built-up in the "École Nationale Polytechnique" located in the city of El-harrach (36.72N; 3.15E), Algiers, Algeria. A Mediterranean city characterized by a relatively huge amount of solar energy even in winter. The system is intended to provide heat to an office at a setpoint temperature of 21°C. The office has an area of 50 m² (10m x 5m x 4m), and it is located on the ground floor of a two-story non-insulated building, as shown in Figure III- 1. The northern wall is the only wall exposed to outside weather conditions; its orientation disfavors the solar gain. Only the deemed office (shown up in red) is equipped with a heating system in the building, thus, its internal walls are adjacent to none heated zones.
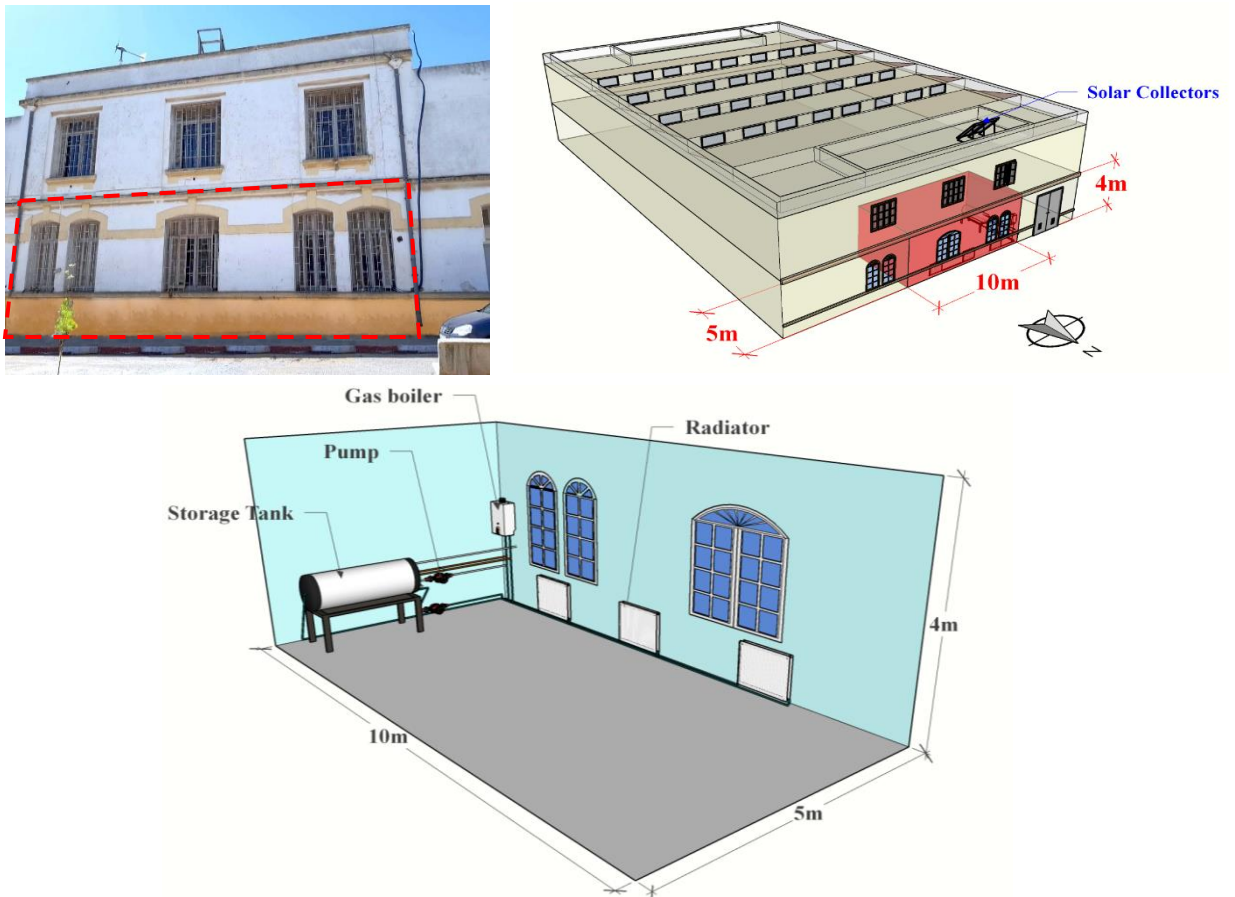
Figure III- 1:3D view of the building and the HSGHS.

3.2.2. Building specifications

The building has an ancient construction (1925), the internal walls of the building consist of three layers, inner and outer layers 20 mm of gypsum plaster separated by hollow brick masonry with a thickness of 150 mm having a U-value of 1.715 W/m².K. The external wall is made of 500 mm reinforced concrete, the outer layer made of cement mortar 20 mm and the inner layer 20 mm of gypsum plaster. Its U-value is 1.924 W/m².K. The windows of the office are single glazing windows with a U-value of 5.69 W/m².K. From the building specifications, we can observe that the building envelope has week insulation and thus important heat losses. Table III- 1 summarizes the building envelope specifications.

Table III- 1: Building envelope specifications.

Surface Types	Structure	U-value (W/m².K)
Internal walls	20 mm gypsum plaster (inner) + 150 mm hollow brick masonry + 20 mm gypsum plaster (outer)	1.715
External wall	20 mm gypsum plaster + 500 mm reinforced concrete + 20 mm cement mortar	1.924
Ceiling	25 mm + 250 mm concrete slab C600	0.759
Window	Single glazing 6 mm	5.69

3.2.3. System Description and Design Intent

In this thesis, the system configuration presented in Figure III- 2 is of particular interest and is referred to as the Hybrid solar gas heating system (HSGHS). The system is comprised of the following major components:

- Solar collectors
- Hot water storage tank
- Gas boiler
- Serpentine heat exchanger
- Radiators
- Two hot water circulating pumps

The HSGHS comprises two main features for the heat production, a gas boiler "Saunier Duval" and an array of solar thermal collectors "Giordano". The solar panels are connected directly to the storage tank, while the gas boiler is connected to the storage tank by means of an immersed serpentine heat exchanger. In the solar loop, the harvested solar energy from solar collectors is transferred towards the storage tank to heat the water within the tank by means of the circulating pump P1. The gas boiler interferes whenever the solar part is unable to meet the required temperature inside the tank, which depends on the control strategy selected scenario. For the distribution loop, the heat is diffused into the office through hydronic radiators connected in parallel. The radiators are distributed as illustrated in Figure III- 1 on the northern wall subject to the external weather conditions. For the security of the system, the collectors' array and the storage tank are equipped with relief valves to evacuate vapor if higher temperatures are reached. Additionally, an expansion tank is installed on the return pipe from

the radiators towards the storage tank to maintain relative pressure, 1.5 bar, throughout the system.
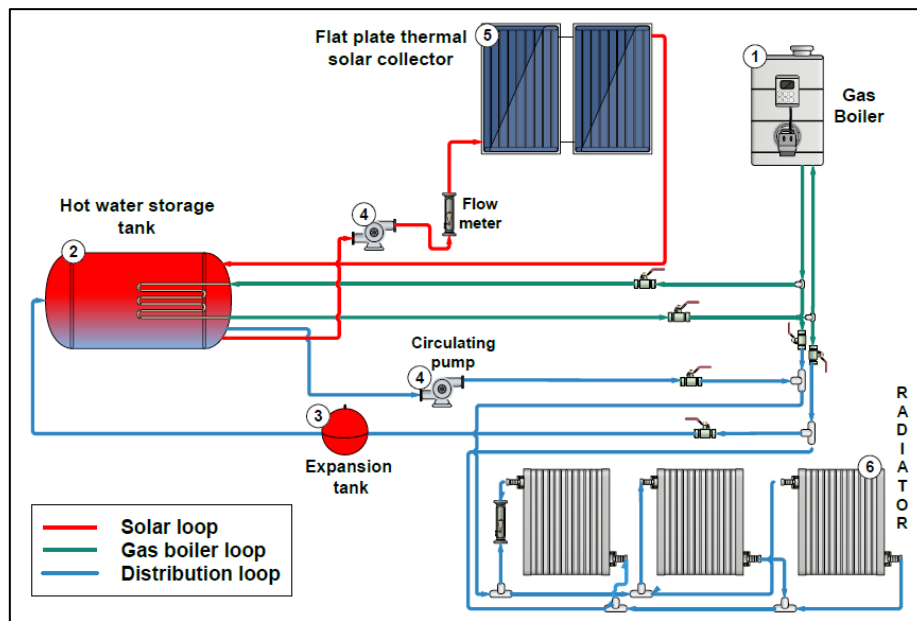
Figure III- 2: Hydraulic scheme of the HSGHS.

3.2.4. Experimental test unit

The experimental test unit described herein, see Figure III- 3, has been built up from the very beginning to accommodate the experimental investigation of the HSGHS. The experimental testing apparatus consists of a closed-loop direct solar system, represented schematically in Figure III- 2. The collectors are installed on a south oriented frame with 37° inclination angle, close to location latitude. This angle ensures a maximum energy collection over the entire year in Algiers. The solar collectors installed on the building's roof are depicted in Figure III- 3 (b). A 187 L storage tank allows the system to operate in a closed loop, thus collecting energy during the day. The inlet port from the collector is located at the top, the outlet ports towards the collectors and the radiators are located at the bottom and the inlet port from the radiator is located at the center. The storage tank was initially installed on a mono-bloc water heater; therefore, the disposition of the ports was limited and thus discourages the mixing inside the tank. The storage tank was modified to be able to achieve the hybridization by conceiving a serpentine heat exchanger and installing it at the tank's level. Water is circulated in the collector loop with a three-speed circulation pump (model Salmson NXL 13-25P) and in the distribution loop with a similar pump (model Grundfos UPS 25-60). The main components within the building are illustrated in Figure III- 3 (a). Table III- 2, summarizes the main components of the system and their models.
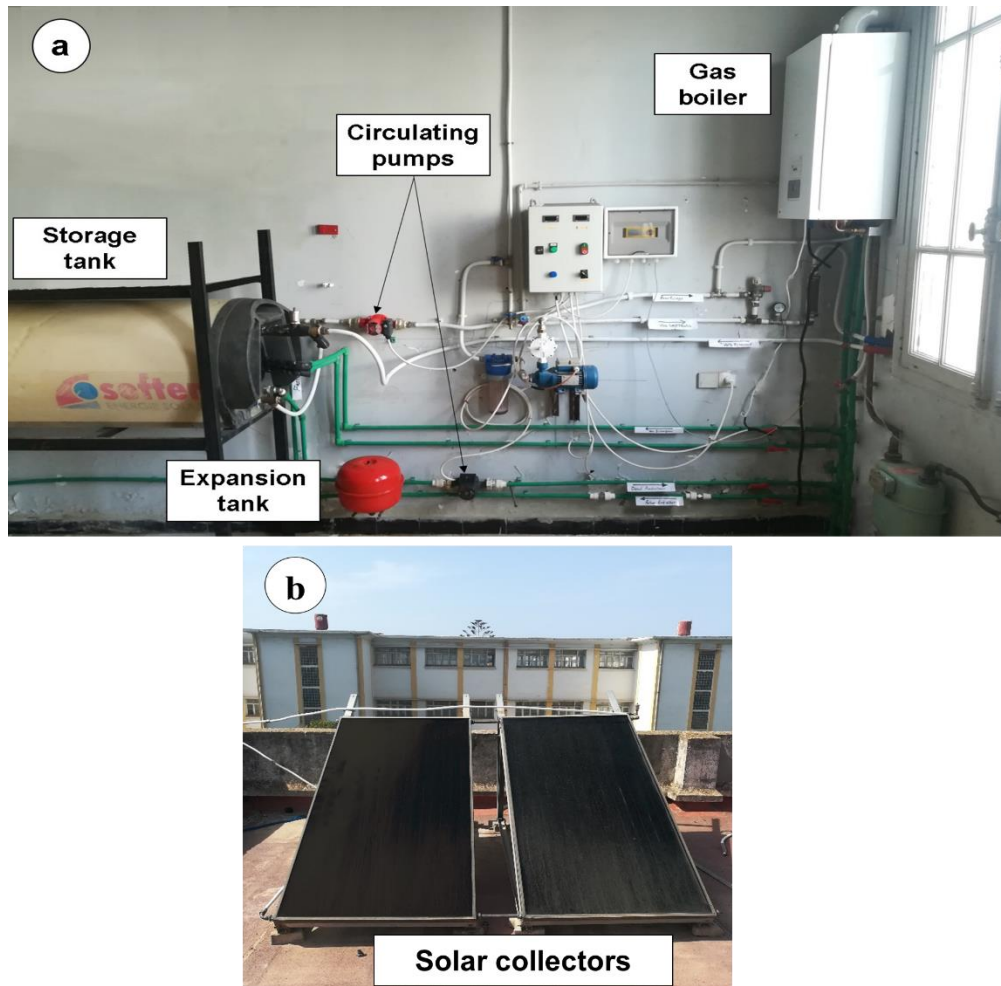
Figure III- 3: Experimental setup of the HSGHS.

Table III- 2: Main components of the HSGHS.

Equipment	Make and Model	Size
Solar collectors	GIORDANO C8/11.SU	2 m²
Storage tank	GIORDANO KSH 200 SH	187 L
Gas boiler	Saunier Duval F25	24 kW
Circulation pump	Salmson NXL 13-25P	45 W
Circulation pump	Grundfos UPS 25-60	60 W

3.2.4.1 Solar collectors

Two flat plate solar collectors, Model GIORDANO C8/11.SU, are mounted in series configuration on the building's roof, Table III- 3 describes the specifications of the collector. The solar collector consists of a box composed of a frame in pre-painted galvanized steel sheet and an aluminum sheet bottom integral with the insulation, see Figure III- 4. This box is equipped successively, from the bottom to the surface:

- a polyurethane insulation and glass wool sheet.
- an absorber with a grill shape copper tubes laser-welded on an aluminum sheet coated with a selective treatment "MIROTHERM". Absorptivity α = 0.95+/-0.01 and emissivity ε = 0.05 +/- 0.02.
- a transparent cover made of tempered glass with a low iron content.
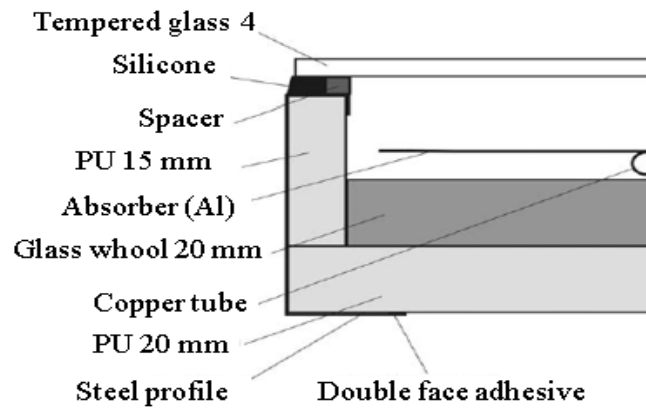
Figure III- 4: Structure of the C8/11.SU collector.

Table III- 3: Solar collector's sepecifications.

Collector Model	C8/11.SU
Gross area (m²)	2.1
Aperture area (m²)	2.0
Absorber area (m²)	1.97
Max service pressure (bars)	6
Gross dimensions: l x w x h (mm)	2002 x 1050 x 75

The thermal characteristics of the collector as per the manufacturer and according to EN12975-2 following the requirements for collector certifications, are summarized in Table III- 4.

Table III- 4 : Thermal characteristics of the solar collector.

Tests done according to the standard EN 12975-2	
Flow rate (l/h.m²)	72
Intercept efficiency η_0 (dimensionless)	0.73
1st order heat loss coefficient a_1 (W/m².K)	4.003
2nd order heat loss coefficient a_2 (W/m².K²)	0.015
Conventional stagnation temperature T_{stg} (°C)	126

3.2.4.2 Storage tank

The storage tank, Model KSH 200, has a nominal capacity of 187 L. the tank's interior diameter is 450 mm; it consists of a cylindrical body closed by two convex bottoms. The assembly of the elements of the tank is made by TIG welding without filler metal. The cylindrical body and the convex bottoms are both made of stainless steel 316L, thickness 1.5 mm. The hydraulic connections are made of stainless steel with a diameter of 20/27 and a threaded end. The connections are welded to the curved bottoms.

The thermal insulation of the storage tank is achieved by injecting polyurethane foam between the outer wall of the tank and the jacket. The injection is carried out at high pressure in a conformator with automatic mixing and dosing of the two components constituting the polyurethane foam (polyol + diphenylmethane diisocyanate). The minimum thickness of the insulation is 50 mm. The thermal conductivity of the insulation is 0.022 W.m^{-1}.K^{-1}.

The ports outlined previously are shown in Figure III- 5, Inlet/Outlet 1 correspond to the ports connected with the solar panels and Inlet/Outlet 2 are the ports connected to the radiators.
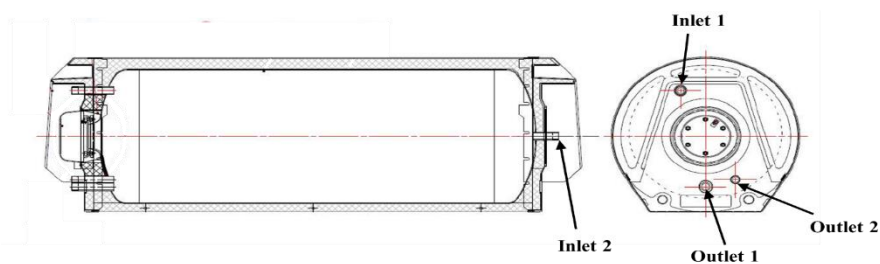
Figure III- 5: Design scheme of the storage tank.

3.2.4.3 Gas boiler

The commercial gas boiler Saunier Duval F25 Themaclassic has a nominal power of 24 kW, with an efficiency of 92.7 % under Low Heating Value (LHV). The maximum water supply temperature is 87 °C. Its power input is 158 W and operates on a minimum gas flowrate of 1.19 m^3/h.

Figure III- 6: Gas boiler Saunier Duval F25 Themaclassic

3.2.4.4 Circulation pumps

Two circulating pumps are used for the water circulation in both solar and distribution loops. The first circulator (Salmson NXL 13-25P) installed on the solar loop and the second (Grundfos UPS 25-60) is installed on the heat distribution loop with 45 W and 60 W, respectively. Both circulators have three variable speeds.

Figure III- 7: Circulating pumps.

3.3. System monitoring & collected data

The objective of the system monitoring implemented in the HSGHS is to collect the set of data required to conceive and develop models of the installation. Furthermore, it must permit, afterwards, to guarantee an optimal functioning by generating output signals to the different actuators.

In this section, we will, on one side, present and define the variables required (temperatures, flow rates …etc.) on each component of the system, then we will define the types of sensors utilized for the collection of data. We will then present some examples of experimental readings, the way all this information is stored and processed and finally we will draw up an energy balance of the HSGH installation.

3.3.1. Instrumentation

The choice of the variables to be measured on the HSGHS, comes from our will to know the key variables of each subsystem of the installation. Thus, the energy balance can be presented globally, but also by subsystem. In addition, the modeling can be done by subsystem as well, which, of course, will allow a more accurate control.

In order to monitor and evaluate the performance of the HSGHS. The unit has been instrumented including 5 points of temperature measurement and two points of flow rate measurement. The selected variables and their positioning on the system are presented in the diagram in Figure III- 8 and Table III- 5 gives the definition of each of them.
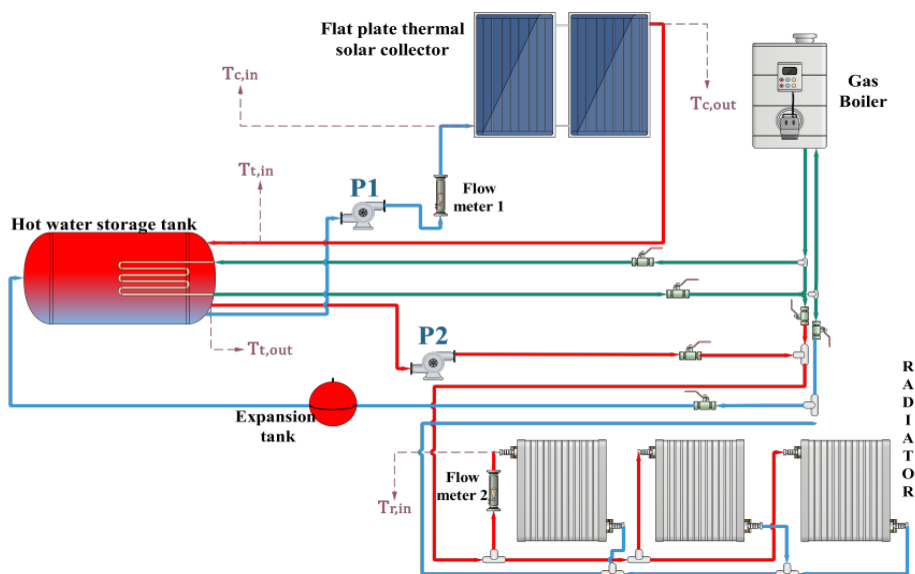
Figure III- 8: Positions of the thermal sensors.

Table III- 5: Specifications of the sensors.

Parameter measured	Reference	Sensor type (number of sensors)	Measurement range	Measurement uncertainty
Collector inlet temperature Collector outlet temperature Tank inlet temperature Tank outlet Temperature Radiator inlet temperature	National Instruments (745690-J001)	Thermocouple J (5)	[0 – 482] °C	±2.2°C
Collector inlet flow rate Radiator inlet flow rate	Platon (PGB4)	Flow meter (2)	[0 -10] L/min	±5%

Temperature measurements are extremely important for the evaluation of the system and modelling and validation of models. Therefore, temperature probes were installed rather than surface mounted sensors, for higher accuracy (see Figure III- 9). Custom probes were purchased to fit the J-Type thermocouples then were plumbed into the inlets and outlets of the main system components.
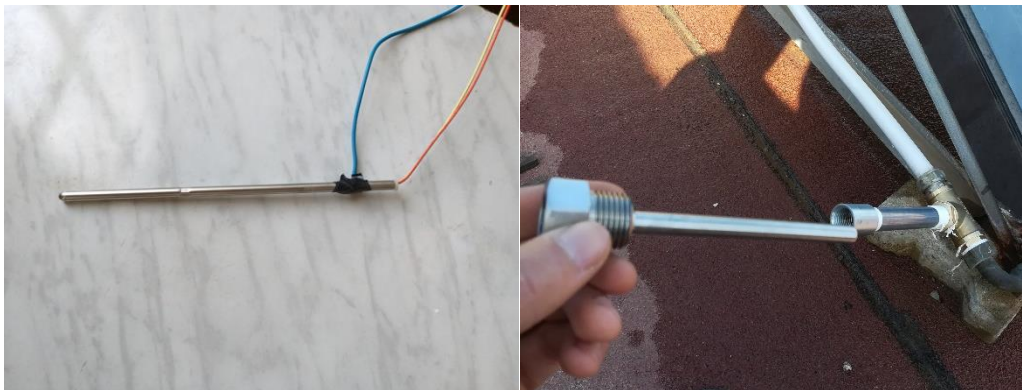
Figure III- 9: Thermocouple Type J and custom thermowell.

For the purpose of control and estimation heat transfer rates within the HSGHS, flow measurements are vital. Two flow rates (model PGB4) were installed for the solar loop at the collector inlet pipe and for the distribution loop at the inlet of the first radiator. The flow rates are read manually. However, since the circulation pumps works on a constant speed, the flow rate is relatively constant for each loop. The positions of the different sensors on the installation are depicted in Figure III- 10.

Figure III- 10: Positions of thermocouples on the different components.

3.3.2. Data acquisition

For the monitoring and characterization of the HSGHS, the installation is equipped with NI-6211 Data acquisition card capable of acquiring and storing data but also of issuing control orders to possible actuators. In our case, we rather focused on the acquisition part. Data is communicated through the DAQ to a virtual instrument (VI) through the DAQ assistant in LabVIEW. The NI-6211 DAQ features up to 16 analog input, among which 10 are connected to the 05 thermocouples, since each thermocouple has 2 wires. As depicted in Figure III- 11. The module is capable of reading ± 200 mV, ± 1V, ± 5V and ± 10V signals with a 16 bits resolution.
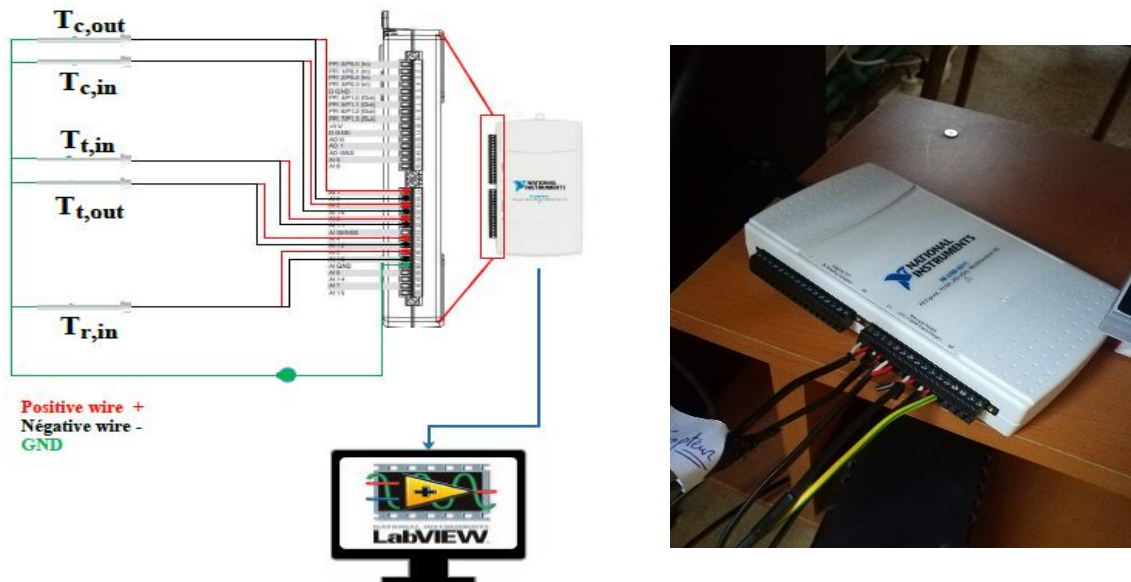
Figure III- 11: thermal sensors wiring to the NI 6211.

3.3.3. LabVIEW controls

Data acquisition is managed through several custom virtual instruments developed in LabVIEW[120]. Three main VIs are used for the acquisition and filtering the data, see Figure III- 12. In fact, the thermocouples behave as an antenna, which renders it very susceptible to noise from 50/60 Hz power sources. Therefore, a 2-4 Hz filter is required to the thermocouples signal to eliminate power line noise. The output voltage of the thermocouples is not directly proportional to the temperature, thus, an integrated linearization in LabVIEW is selected to adapt with the J-Type thermocouples.

The DaQ assistant VI helps to create and configure the tasks, temperature readings, signal type, scales, and sampling rates. After the assignment of each physical channel to the specified measured data, continuous sampling is selected with a sampling rate of 100 and a frequency of 10 Hz. Next, the acquired signals are wired to the Filter VI, where a 2 Hz low pass filter is applied. Finally, the filtered signals are smoothed using a moving average to get 1 min average temperature for each single data to match with the simulation time step that will be discussed in numerical modeling section.
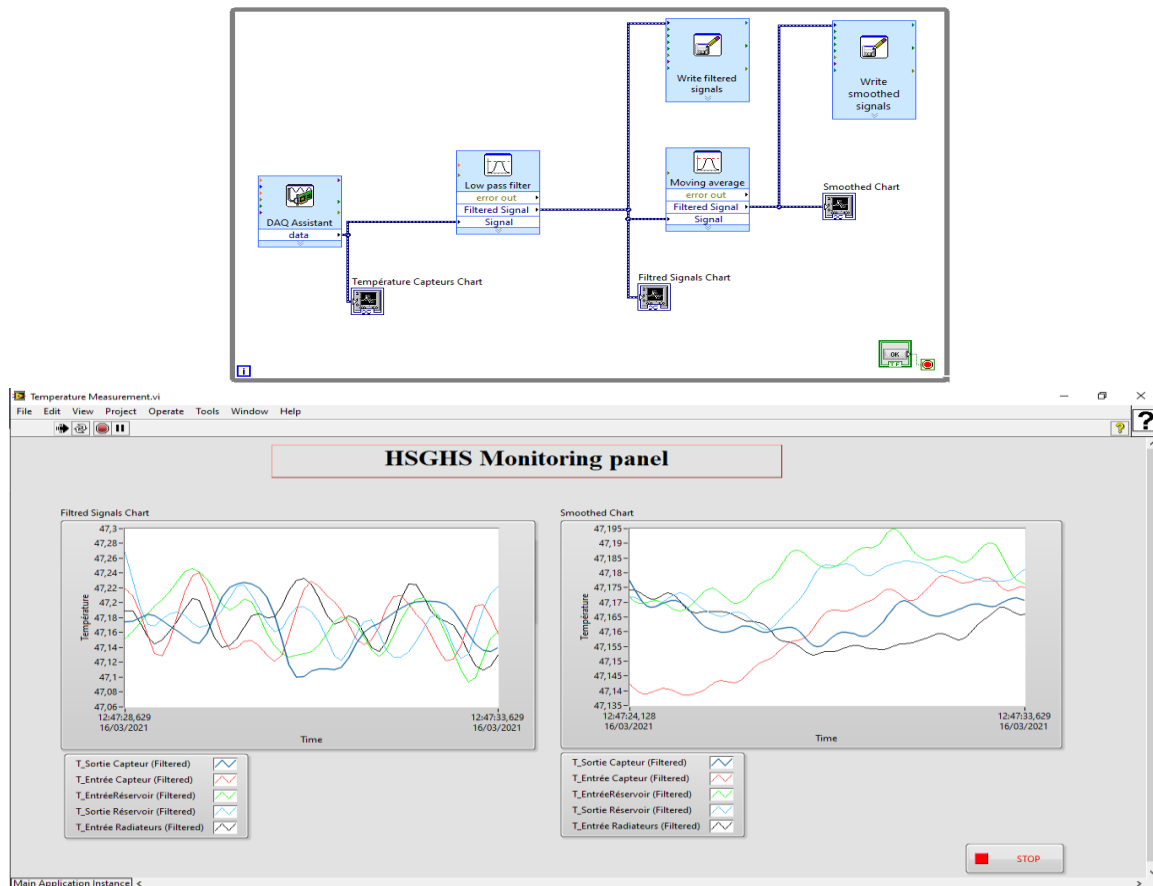
Figure III- 12: Block diagram and front panel of the LabVIEW program.

3.4. Daily performance analysis of the HSGHS

An analysis of the daily energy performances is carried out for the period between January and March 2020, the weather conditions being favorable to the operation of the studied system. Indeed, as observed in Figure III- 13, outdoor temperatures are not very high, heating being necessary, and the solar resource is available for the targeted period. The selected days are thus a suitable example for the study of the solar heating system. The system operated in solar mode only during the experiments.

This section first explains the calculation method of the exchanged energies and the considered uncertainties to finally obtain the daily performance indicators, thanks to the values measured by the sensors represented previously.

3.4.1. System thermal calculations

3.4.1.1 Available solar radiation

Using the radiation data collected from CAMS, the available solar radiation on the collectors can be estimated, first by calculating the solar irradiance, denoted I_t, on the tilted surface, the collectors' array, then multiplying it by the surface. The solar irradiance I_t, can be calculated using Liu and Jordan model [121] because the model n takes into account the measures of the solar irradiance (diffuse and global radiations received on horizontal plane). Also the model takes into account not only the clarity of the sky but also the isotropy of the sky .

$$I_t = I_b R_b + I_d \left(\frac{1 + \cos \alpha}{2}\right) + I \rho_g \left(\frac{1 - \cos \alpha}{2}\right)$$

(III. 1)

Where I_b, I_d and I are respectively the bear, diffuse and total radiation, ρ_g is the ground reflectance, α is the slope of the collectors and R_b is the ratio of the beam radiation it depends on the incidence angle R_b and the zenith angle θ_z which varies for each day and location.

$$R_b = \frac{\cos \theta}{\cos \theta_z}$$

(III. 2)

The available solar radiation on the solar panel Q_a is then:

$$Q_a = I_t * A_c$$

(III. 3)

3.4.1.2 Useful heat rates from collector

Knowing the inlet and outlet temperature measurements of the solar panels and the thermal properties of the fluid, we can then calculate the thermal powers involved in the solar field. The useful heat rate from the solar collector is estimated using Eq (III. 4), from the flow rate readings and the acquired temperatures. The useful power Qu is expressed as follows:

$$Q_u = \dot{m}C_p \left(T_{c,out} - T_{c,\text{in}}\right) \tag{III. 4}$$

3.4.1.3 Error analysis

The uncertainty associated to each of the measured quantity has been estimated. The uncertainty of the sensors, presented in section III.3.1, are considered in order to estimate the precision of the calculated heat rates for obtaining the performance indicators.

The uncertainty on the available solar radiation on the collector is calculated as follows:

$$\frac{\delta Q_a}{Q_a} = \frac{\delta I_t}{I_t} + \frac{\delta A_c}{A_c} \tag{III. 5}$$

The uncertainty on the available solar radiation is approximated to 10 W/m² according to CAMS radiation service user's guide. The uncertainty on the collector area is considered null.

The uncertainty on the useful heat rate is calculated from Eq (III. 6).

$$\frac{\delta Q_u}{|Q_u|} = \frac{\delta \dot{m}}{|\dot{m}|} + \frac{\delta C_p}{|C_p|} + \frac{2\delta T}{\left|(T_{c,out} - T_{c,\text{in}})\right|} \tag{III. 6}$$

The absolute uncertainty on the flow rate arises $\delta \dot{m}$ from the error of measurement in the flow meter PLATON (PGB4). Since it presents oscillations (probably due to the presence of air bubbles). However, the value is already given as a percentage, ±5%, by the manufacturer as presented in Table III- 5.

The uncertainty in measurements of the thermocouples is given ±0.75%, thus the value of the specific heat of water is considered to be 4190 J.kg^{-1}.K^{-1} ±0.75%.

3.4.2. Representation of experimental measurements

Figure III- 13 presents 6 days of measurement that we have selected for their different types of exposure to solar irradiation that characterize them and for their continuity. The first day, the GHI is not very high, and the outdoor temperature is very low. The following days, the solar irradiation is relatively higher (without significant cloudy disturbance). With different outdoor

temperature profiles. The overall GHI during the considered days is around 700 W/m². Days 14th of January and 23rd of February are both interesting days since both had low temperature inferior to 18 °C; thus, heating is needed. And both days presented significant GHI ≥ 500 W/m².

In Figure III- 14, we notice that the higher the temperature and the solar irradiation, the higher the temperature of the fluid leaving the solar field. During these 6 days, the maximum temperature of 32.64°C, at the collectors' field outlet, is reached at 14h03 of February 25th. The collector does not reach higher temperatures because the same water is being circulated from the tank to the radiators to heat the office. Installing a suitable heat exchanger with solar loop might increase the temperature at the collector's outlet. The discrepancy between collectors' outlet and tank's inlet temperatures indicates a significant heat loss along the hydraulic circuit due to the absence of insulation on the pipework, which have considerable length, approximately 9 m for each of the supply and return pipes from and towards collectors. This loss is proportional to the difference between the temperature of the circulating fluid and the outside temperature in addition to the wind velocity.
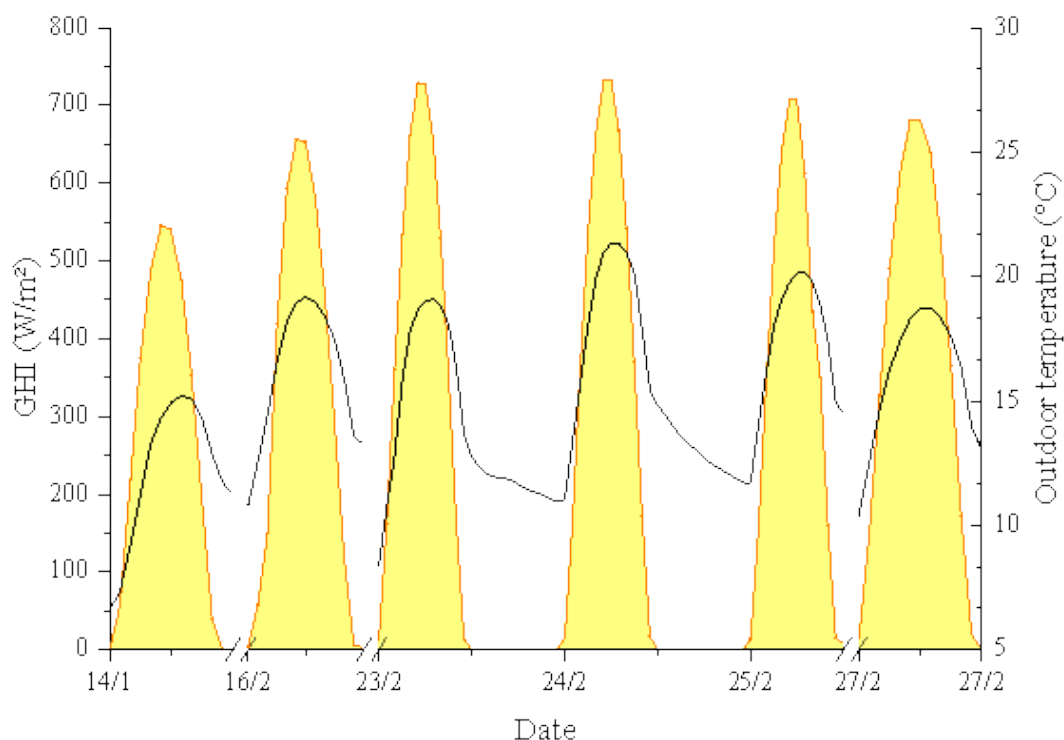
Figure III- 13: Global horizontal irradiation and outdoor temperature of the experiment days.
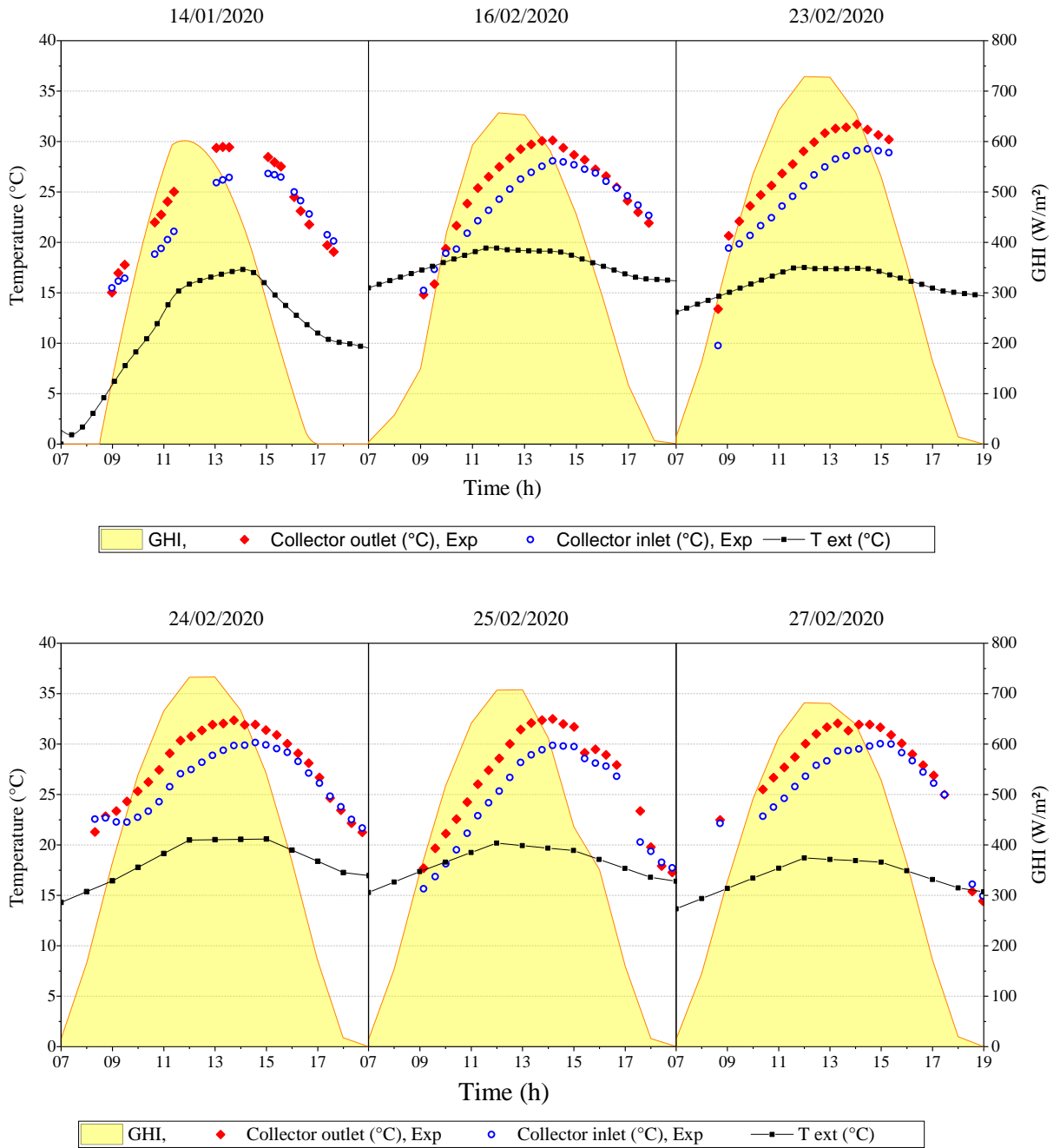
Figure III- 14: Collectors' Outlet/Inlet water temperatures.

We have just presented a brief qualitative study on the behavior of the experimental process as a function of meteorological parameters such as outdoor temperature and solar irradiation, the remaining measured data will be presented in detail further in next chapter for the purpose of validation.

3.4.3. Useful solar energy

Figure III- 15 presents the available solar radiation on the collector and the useful power from the collector. The highest useful power was observed on the 14th of January with a peak of 1100 W while the received solar irradiation on the collector was around 2900 W. The useful power in the remaining days is slightly of the same order of magnitude. In the 23rd, 24th and 25th of February, comparable Q_a is observed. However, higher Q_u is recorded in the 23rd even when the outdoor temperature was lower than the other comparable days, maximum of 17.5°C. we conclude that the solar collector has better performance when operating in low exterior temperatures. Because the higher the temperature the more heat losses are manifested. The discrepancy between the Q_a and Q_u profiles represent the losses in the thermal collector.
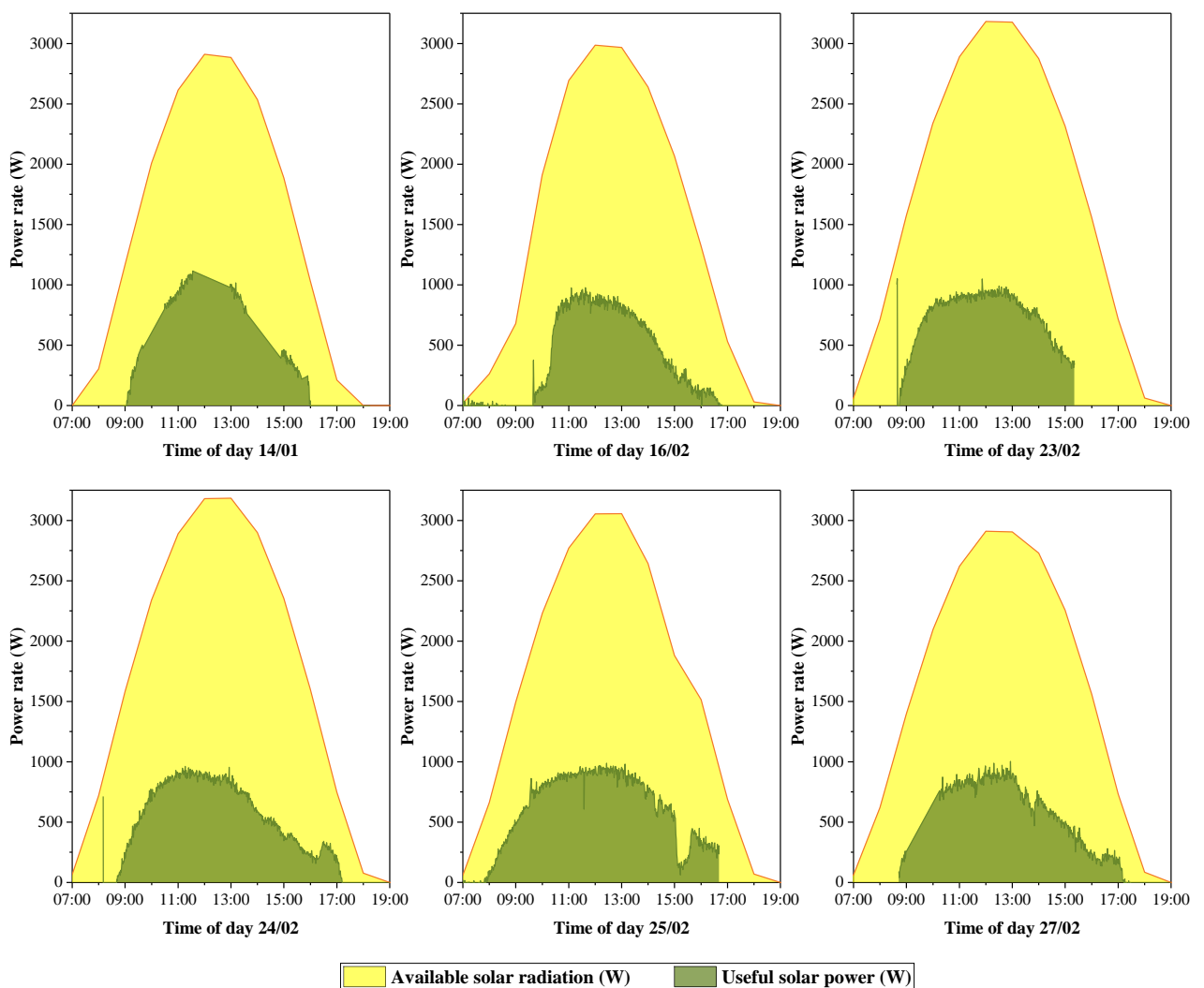
Figure III- 15 : Useful solar power and available solar radiation on the collectors.

The efficiency of the collector η is defined as the ratio of the useful energy to the received irradiation. the efficiency can be estimated using the integrated areas under the curves during the day and can be expressed as follows:

$$\eta = \frac{\int Q_u \, dt}{A_c \int I_t \, dt}$$

(III. 7)

A summary of the daily results of the collectors' efficiency is shown in Table III- 6. Using uncertainty propagation discussed above.

Table III- 6: Daily efficiency of the solar collectors.

Day	Efficiency (%)	Error (%)
14/01/2020	27.56	± 1.88
16/02/2020	20.92	± 1.46
23/02/2020	22.75	± 1.55
24/02/2020	22.81	± 1.56
25/02/2020	27.96	± 1.92
27/02/2020	24.44	± 1.69

3.4.4. Solar collectors' dynamic characterization

Figure III- 16 shows the solar radiation on the tilted surface, thermal efficiency and the temperature difference ΔT between the water inlet and outlet temperature of the solar collector for the considered days. The average solar radiation for the period of the experiment was 1000 W/m². The average temperature difference between the inlet and outlet of the collector was 3.70 °C. During the first few minutes of the tests, the efficiency increases until it reaches the steady state and it sort of stabilize. According to Eq (III. 7) , the collector efficiency depends on the available solar irradiance I_t, difference of temperature ΔT and water flow rate. Since the flow rate is held constant only the solar radiation and the temperature difference influence the efficiency. The effect of the temperature difference on the collectors' efficiency can be seen in the figure below. As ΔT increases the efficiency also increases.
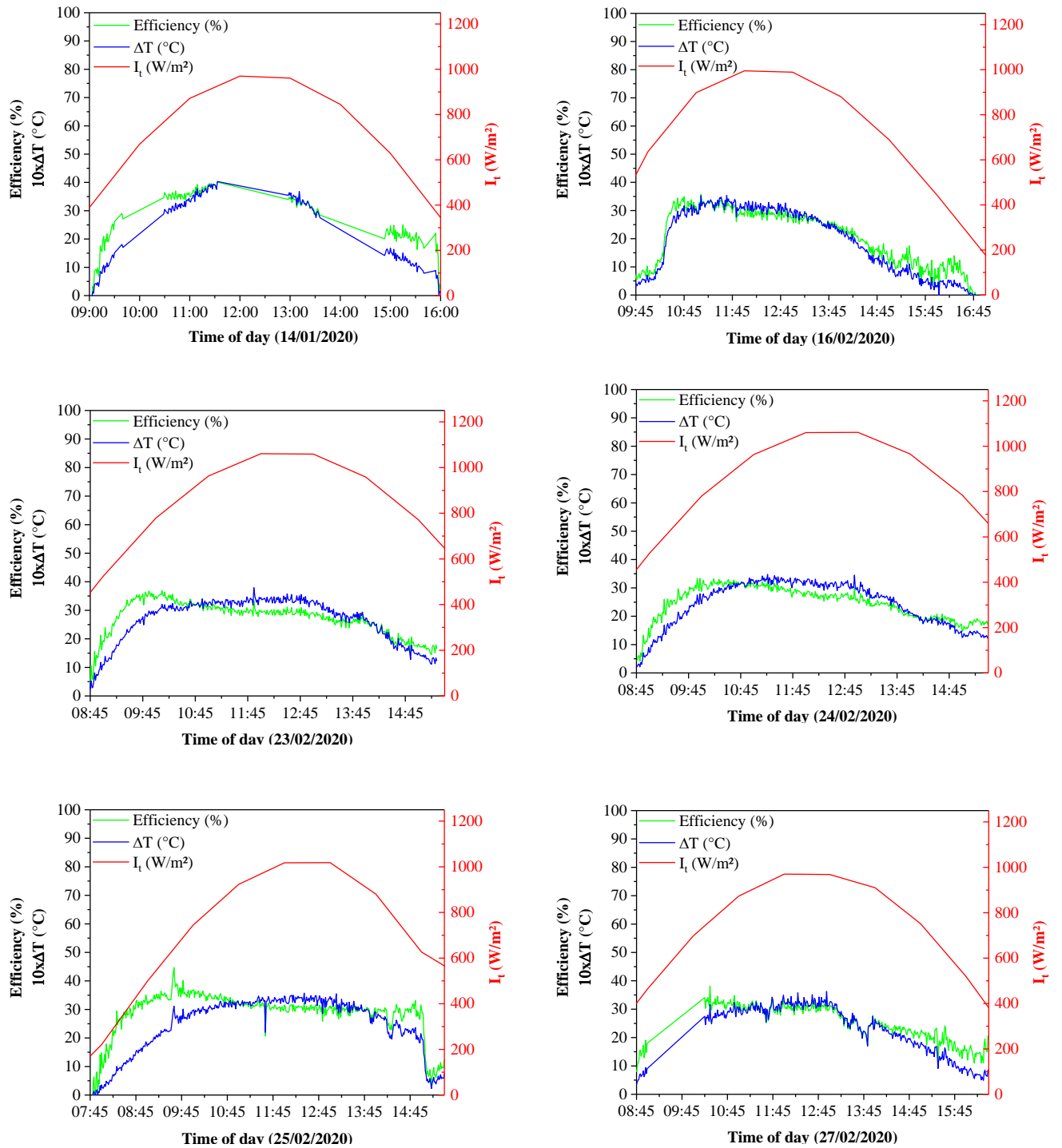
Figure III- 16: Collectors' efficiency and solar irradiance on the tilted surface during experiments.

3.4.5. Steady state characterization

The collector efficiency is highly correlated to the solar radiation I_t and the temperature difference between the outdoor temperature and the absorber temperature (ΔT_a).

$$\Delta T_a = T_{avg} - T_{ext} \tag{III. 8}$$

With the average temperature of the absorber T_{avg} defined as the mean temperature between the collector's inlet and outlet.

$$T_{avg} = \frac{T_{c,in} + T_{c,out}}{2} \tag{III. 9}$$

The performance of the solar field η is given according to the characteristics of efficiency η_0, a_1 and a_2. η_0 being the optical coefficient of the collector, a_1 the coefficient related to losses by conduction and convection (W/m².K) and a_2 the coefficient related to losses by radiation (W/m².K²). These two coefficients have been determined by the manufacturer, see Table III- 4. The higher these heat transfer coefficients are, the more the efficiency of the collectors decreases when the temperature increases.

From these coefficients, it is therefore possible to know the yield of solar panels at any time.

Thus, the efficiency η of the collector, representing the ratio between the energy (heat) extracted at the output of the collector and the energy at the input (solar radiation), is at all times related to I_t and (ΔT_a). The most frequently used mathematical model Eq (III. 10) included among the standard "EN 12975" on solar thermal systems and their components, gives the value of the efficiency of a solar collector.

$$\eta = \eta_0 - a_1 \frac{\Delta T_a}{It} - a_2 \frac{\Delta T_a^2}{It} \tag{III. 10}$$

The efficiency curve displayed in Figure III- 17 characterizes the solar collector regardless of the measured insolation. The steady-state efficiency parameters are obtained by testing the collector over a range of inlet temperatures at the incidence angle ≤ 20° and at global irradiance ≥800 W/m² as specified in EN 12975-2.

The instantaneous efficiency of the solar collector was calculated from the measured data at noon of each day to be around maximum insolation, therefore closer to the irradiance required in EN 12975-2. The efficiency is depicted in Figure III- 17. the discrepancy between the measured efficiency and the efficiency curve is expected since the operating conditions are not similar to the standard requirement. Besides, one collector is partially covered of dust particles from inside which could have reduced the optical efficiency η_0, thus reducing the performance of the collector. Therefore, the routine maintenance of the solar collectors and periodic

inspections are required to keep them operating efficiently. In addition, the aging of the solar panels is a nontrivial factor that may reduce the performance of the solar collectors. The efficiency values are quite close; however, 14th January presented higher efficiency which ascertains that thermal collector performs better in low inlet temperatures and/or higher solar radiation. In fact, as per Eq (III. 11) the useful power from the collector would increase if the difference $(T_{c,in} - T_{ext})$ is minimum. However, the collectors' inlet temperature is not a design parameter that can be controlled.

$$Q_u = F_R A_c [\, I_t(\tau\alpha) - U_L(T_{c,in} - T_{ext})]$$
(III. 11)
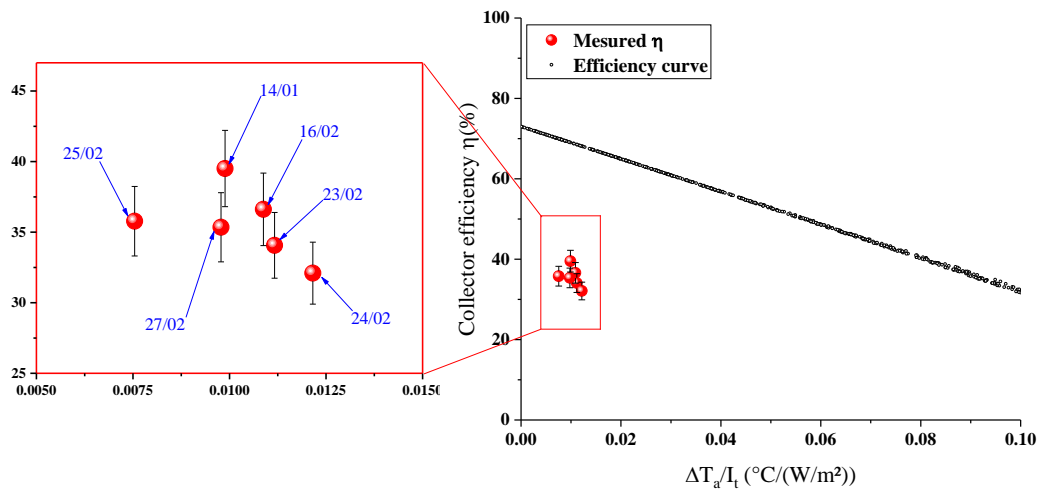
Figure III- 17: Efficiency curve and measured steady-state efficiency.

3.4.6. Daily solar fraction

The solar fraction is a commonly used indicator in solar thermal systems to describe the proportion of energy (heat) needs supplied by the solar part of a system. It is defined as the ratio of the useful solar load produced by the solar system to the heat load. The global heat transfer coefficient of the building was estimated based on the Algerian thermal regulation document, to calculate the daily heat load. The useful power rate from the collectors was then employed to estimate the daily solar fraction.
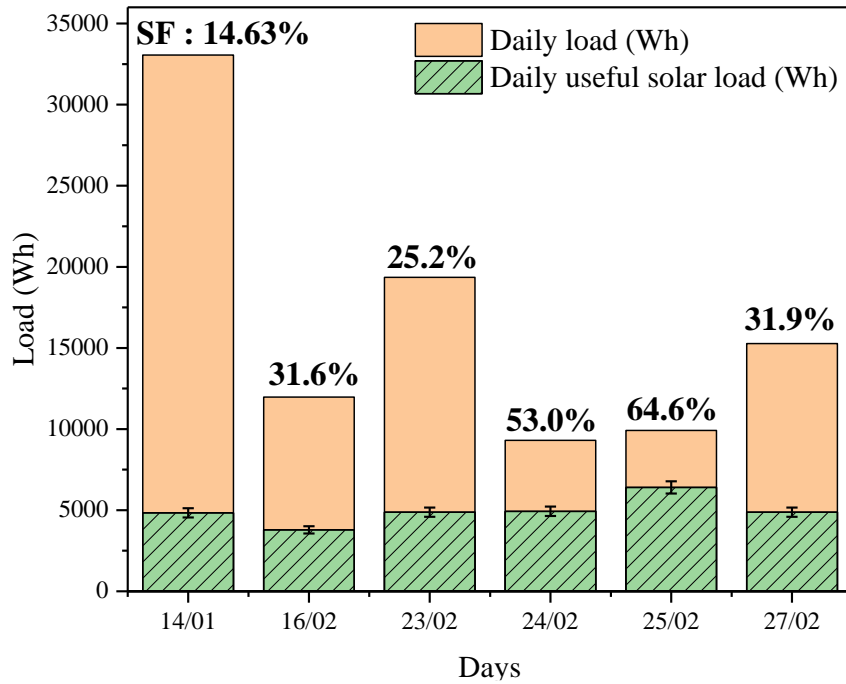
Figure III- 18: Daily solar fraction during experiment days.

Figure III- 18 shows the daily energy loads, the useful solar loads and the solar fraction during the experiment days, since the system is intended to heat the office during working hours, from 7am to 6pm, the daily loads were therefore estimated for that period. The daily solar fraction during the experiments varied between 14.63% and 64.6%. It is noteworthy that the useful solar load is approximately the same. However, it is the daily heat load that varies the most since it highly depends on the outdoor temperature, which was very low (<18°C) on the 14th of January and the 23rd of February as indicated before. The remaining difference in energy is to be provided by the gas boiler to ensure the heat demand inside the building. The solar fraction recorded during the experiments is relatively low, especially when we consider cold days where temperatures are below 18°C. the solar fraction would be around 14% to 25%. Therefore, thorough investigations will be discussed in coming chapters on the system's control strategy and the hybrid operation mode.

3.5. Conclusion

In this chapter, the hybrid solar/gas heating system is designed, built and installed in an office room. The unit instrumentation is outlined with the different materials used to monitor the system. Measurement data is recovered over experiments and will serve as a basis of validation of a numerical model. The experiment is carried out to investigate the thermal performance of the solar collectors and the solar fraction of the system. The experimental results show that the solar collector yield is very low and requires periodic maintenance. The daily solar fraction is relatively low, probably because of the low efficiency of the collectors and the control strategy that should be further investigated.

The carried-out analysis and allowed us to highlight different points of the installation requiring a substantial improvement. These findings will be useful during the modeling phase, which we will discuss in the next chapter.

The performed investigations indicate that the performance of the hybrid solar system in solar mode only is unsatisfactory. In this case to overcome this problem, we will focus on reformulating the design of the system. For this, we need to build knowledge on the relationship between design parameters and the thermal performance of the system. This knowledge consists in identifying the critical parameters that affect thermal performance in order to be able to regulate the desired performance. In this consequence, numerical model and sensitivity analysis based on the DoE technique will be employed.

Chapter 4

Hybrid solar gas heating system Mono-source analysis

4.1. Introduction

In the first part of this work, we have dealt with the experimental study of the installation with tests carried out in winter. Moreover, the results highlighted the necessity of a better understanding of the relationship between the system's performance and the design parameters, as well as a numerical model to predict the long-term performance and to assess the solar heating system operation. Therefore, a numerical model of the installation is developed in TRNSYS with the aim of evaluating the performance of the solar heating system integrated to a building. The numerical model is also used to assist in the sensitivity analysis to study the effect of the different design parameters on the solar fraction.

In this chapter, the developed model is, first, described along with the different tools used during the modeling and the identification of the different TRNSYS types used to model the subsystems. Then, we outline the statistical methodology DoE adopted to identify the relationship between the solar fraction and the design parameters and to conduct the sensitivity study.

The second part details the validation of the numerical model, the latter is executed on solar mode only as in experiments. Then, the effects of the design parameter on the solar fraction are explored through the sensitivity analysis. And meta-models are developed. Finally, we focus on the single objective optimization of the solar fraction using the resulted metamodels and the desirability function approach.

4.2. Solar heating system modeling description

The modelling of the solar heating system and its integration to the building is achievable, first by knowing the heat load of the building. Then the heat production of the system that should be known. The heat is highly dependent of weather conditions and the building characteristics (Performance of the building envelop, setpoint temperature) which will be estimated from dynamic thermal simulations of the deemed building.

In this section, a TRNSYS simulation model of the considered solar system is developed. The hierarchy of the model adopted is presented in Figure IV- 1: Hierarchy of the TRNSYS modeling.. a detailed description for the TRNSYS model can be found in the sections below. The basic principles of the TRNSYS software are described with a graphical overview of the process principle of the program.
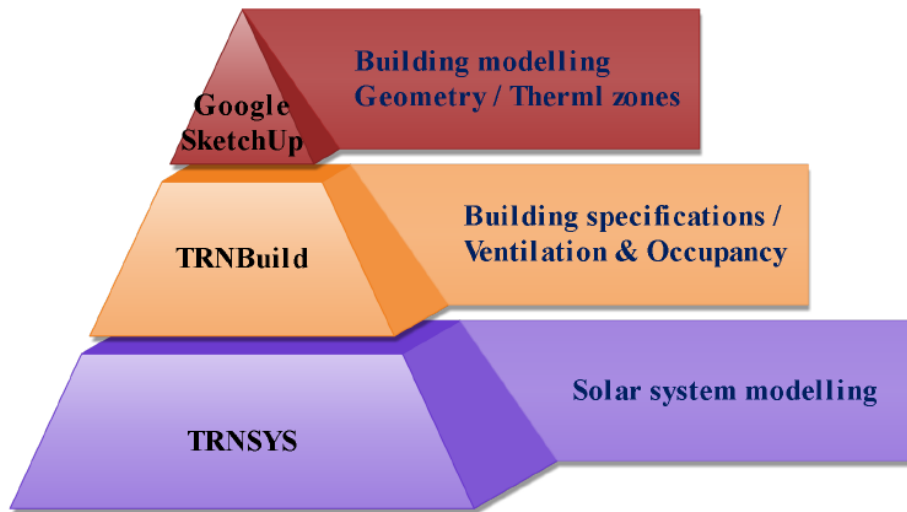
Figure IV- 1: Hierarchy of the TRNSYS modeling.

We present in this section the structure of the TRNSYS model. The present study relies on the modelling of the solar heating system and its hydraulic integration in the building. The solar and hydronic loops are treated separately. The control strategy modes for each loop will be presented. Finally, the modelling of the building is achieved by means of Type 56.

The model will be a simple empty office inside a building. The adjacent zones are also modelled for a detailed study. The geometry of the whole building and the window positions for the office are identical as the real office. The wall layers are added, the ventilation and air infiltration are considered. the internal gains (Lights and equipment) are setup in schedules, the same is done for the occupant patterns. The subsystems for the heating equipment (Solar collectors, storage tank, pumps) are implemented. The radiators are added to the office as internal gains.

To regulate the on/off signals to the different pumps in the system (solar and hydronic loops), temperature controllers are utilized. Instability can occur in many models of controllers when system temperatures are near to their setpoint values. Therefore, dead bands (hysteresis) are added to avoid instabilities, such that the controller on/off signal does not change until the temperatures at collector's outlet, bottom of tank or the air zone temperature have reached their setpoints plus a small difference temperature. The storage tank is used to provide heat for the office via the radiators. The tank is heated during the operation period to 60°C, in the first part of this study.

4.2.1. TRNSYS model solver settings

The TRNSYS software algorithms allow the user to solve complex differential equations. The user sets the tolerance integration and convergence to get accurate results while speeding up the computational time. The solver settings selected in the present study are depicted in Table IV- 1 below:

Table IV- 1: TRNSYS solver settings.

Solver settings	
Simulation start time	7296 (hr)
Simulation stop time	10920 (hr)
Time step	1 (min)
Tolerance integration	0.001
Tolerance convergence	0.02

4.2.2. Description of the building

4.2.2.1 Geometry

To model the thermal behavior of a multizone building, Type 56 is used. First, a separate pre-processing program must be executed. The TRNBuild program reads a file containing building description, then generates two files that will be processed by Type 56 during the TRNSYS simulations. The building geometry can be setup interactively in TRNBuild. However, for complex geometries late versions of TRNSYS offers the possibility to import three dimensional files into TRNBUILD via TRNSYS 3d-plugin.

The geometry of the building was modeled in Google SketchUp. The building was divided into three thermal zones, Office, First floor and Second floor. The heat transfer between the thermal zones is considered through the common walls, moreover, each zone can be treated separately on TRNSYS. Figure IV- 2 shows the building geometry and the thermal zones on SketchUp.
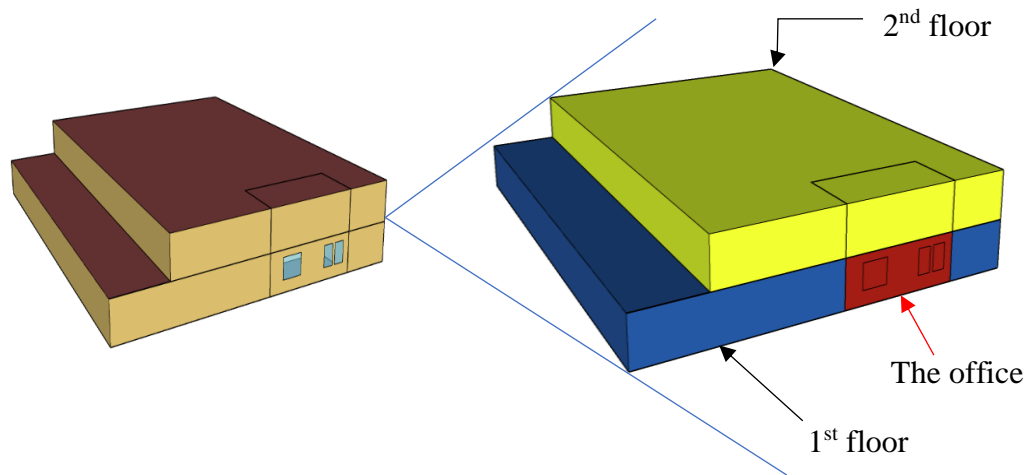
Figure IV- 2: Thermal zones of the building (TRNSYS3d).

4.2.2.2 Building specifications

After the import of the geometry file to TRNBuild, the user sets the wall constructions and fenestrations. The internal walls of the building consist of three layers, inner and outer layers 20 mm of gypsum plaster separated by hollow brick masonry with a thickness of 150 mm with a global U-value of 1.715 W/m².K. The external wall is made of 500 mm reinforced concrete, the outer layer made of cement mortar 20 mm and the inner layer 20 mm of gypsum plaster. Its global U-value is 1.924 W/m².K. The windows of the office are single glazing windows with a U-value of 5.69 W/m².K. From the building specifications we can observe that the building envelope has week insulation and thus important heat losses.

4.2.3. Baseline integrated solar heating system

The integrated solar heating system consisted of flat plate collectors, a horizontal storage tank and a variable speed pump to transfer heat from collectors' array to the tank. The storage tank is used to meet the space heating demands of the building through the hydronic radiators. The system is intended to operate during weekdays from 7am to 6pm. Therefore, a schedule was designated in the model coupled with the pumps controllers to control their operation, which will be detailed hereafter. Hourly weather data of the city El-Harrach in Algiers was considered using the typical mean year (TMY) file, it was therefore used in the sensitivity study. TRNSYS Type 15 allows the interpolation of the weather parameters required for the simulation time step (1 min) (i.e. Dry bulb temperature, solar radiation components, wind velocity).

The developed model used standard components available on TRNSYS library to describe the behavior of the aforementioned equipment, as well as custom types to introduce particular calculations such as the estimation of the solar contribution. The components employed for the deemed model are listed in Table IV- 2 and a detailed mathematical description can be found in the TRNSYS help (mathematical reference)[122]. A discussion of the main components is given in the following sections. Figure IV- 3 displays the arrangement of the TRNSYS types in the simulation model.
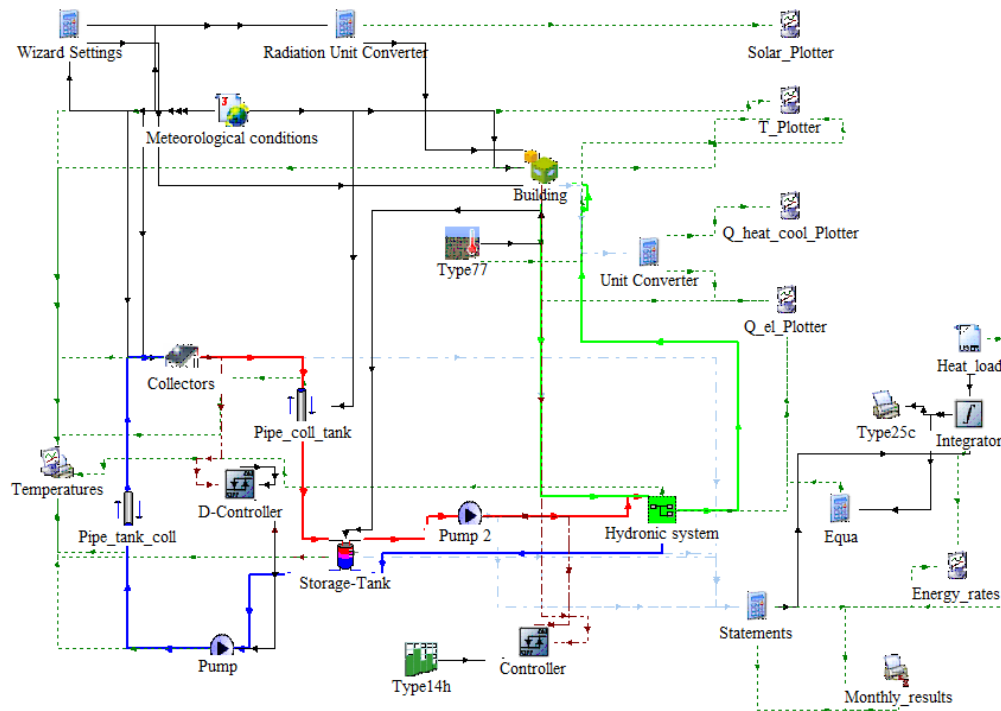
Figure IV- 3: TRNSYS model architecture of the solar heating system.

Table IV- 2: TRNSYS types of the different components.

Component	TRNSYS Type Number
Weather file	15
Building	56
Collector	1
Storage tank (Horizontal)	533
Pump	114
Radiator	1231
Flow diverter	11f
Tee piece	11h
Pipe work	604
Differential controller	2b
Forcing function	14h

4.2.3.1 Flat plate thermal collector

Type 1 was used to model the thermal performance of the collector's array, it is based on a standard quadratic efficiency equation. A general equation for the collector thermal efficiency can be obtained from the Hottel-Whillier equation:

$$\eta = \frac{Q_u}{A_c I_t} = \frac{\dot{m} C_p (T_{c,out} - T_{c,in})}{A_c I_t} = F_R(\tau\alpha)_n - F_R U_L \frac{(T_{c,in} - T_{ext})}{I_t} \tag{IV. 1}$$

The loss coefficient U_L is not exactly constant with respect to temperature, therefore a better expression is obtained by taking into account a linear dependency of U_L versus $(T_i - T_a)$:

$$\eta = \frac{Q_u}{A I_t} = F_R(\tau\alpha)_n - F_R U_L \frac{(T_{c,in} - T_{ext})}{I_t} - F_R U_{L/T} \frac{(T_{c,in} - T_{ext})^2}{I_t} \tag{IV. 2}$$

The equation above can be rewritten as :

$$\eta = a_0 - a_1 \frac{(\Delta T)}{I_T} - a_2 \frac{(\Delta T)^2}{I_T} \tag{IV. 3}$$

The three parameters a_0, a_1 and a_2 define the thermal efficiency of a solar collector, and are given by the manufacturer when the collector is tested according to European Standards (EN 12975-2) [123] as well as ASHRAE Standards ([93-2003)°[124].

4.2.3.2 Storage Tank

The storage tank was modeled using Type 533, which considers a constant volume storage tank with immersed heat exchanger, the fluid in the storage tank interacts with the environment through thermal losses from the edges of the tank, with fluid in the heat exchanger and the flow streams that pass into and out of the tank. The storage tank is divided into five isothermal nodes, as shown in Figure IV- 4, to model stratification inside the tank. Each node is assumed to be isothermal and interact thermally with the adjacent nodes through several mechanisms; conduction between nodes and forced fluid movement from inlets streams or natural destratification mixing.
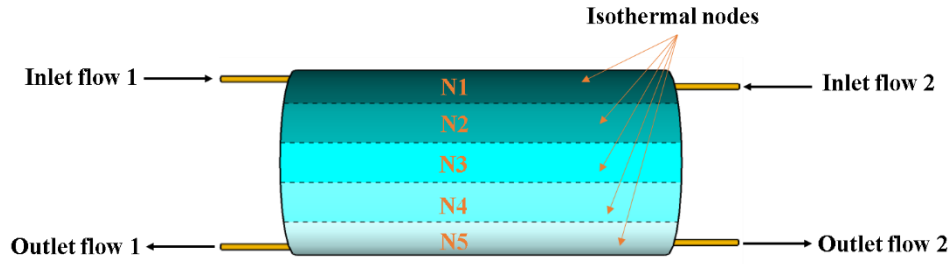
Figure IV- 4: Representation of the storage tank model with the isothermal nodes.

The heat losses (or gains) from the tank's envelope to the environment, for each node are expressed as follows, assuming the same heat loss coefficient and environment temperature :

$$Q_{loss,top,j} = \left(A_{top,j} * U\right) * \left(T_{tank,j} - T_{env}\right) \tag{IV. 4}$$

$$Q_{loss,bottom,j} = \left(A_{bottom,j} * U\right) * \left(T_{tank,j} - T_{env}\right) \tag{IV. 5}$$

$$Q_{loss,edges,j} = \left(A_{edges,j} * U\right) * \left(T_{tank,j} - T_{env}\right) \tag{IV. 6}$$

Where :

$A_{top,j}$: Top surface area attributed to node 1.

$A_{bottom,j}$: Bottom surface area attributed to node N.

$A_{edges,j}$: Edge surface area distributed equally amongst all edges.

U represent the heat loss coefficients for top, bottom and edge areas of the tank, respectively.

$T_{tank,j}$: temperature of the tank node.

T_{env} are environment temperatures for losses.

The conduction between the nodes is considered using the following formulation:

$$Q_{cond,j} = k_j * A_j * (T_j - T_{j+1})/L_{cond,j} + k_{j-1} * A_{j-1} * (T_j - T_{j-1})/L_{cond,j-1} \tag{IV. 7}$$

Where the index j represents the node, j+1 the node directly below j and j-1 the node above the node j, k is the thermal conductivity of the fluid, A is the conduction interface area between the nodes and L_{cond} is the vertical distance between the centroids of the adjacent nodes.

4.2.3.3 Control strategy

In order to control the operation of the pumps, two distinct differential controllers were assigned to each pump. Type 114, representing the pump, works according to a control signal. Type 2b was used to generate the control signal.

The first control concerns the solar loop. To ensure the good operation of the solar system a common control scheme was adopted. It requires the knowing of the temperatures at the bottom of the tank T_5 and at the collector's outlet $T_{c,out}$. When the temperature $T_{c,out}$ exceeds T_5 by a specific amount ΔT_{ON} the pump is turned on. Once the pump is ON, when the measured temperature difference falls below a specified amount ΔT_{OFF}, the controller turns the pump off to avoid the cycle ON and OFF. The choice of ΔT_{ON} and ΔT_{OFF} is determined using Eq (IV. 8). Figure IV- 5displays the control scheme of the solar pump.

$$\Delta T_{OFF} \leq \frac{A_c F_R U_L}{\dot{m} C_p} \Delta T_{ON} \qquad\qquad (IV. 8)$$

Where A_c is the collector area (m²), F_R is the heat removal factor; U_L is the overall heat loss coefficient (W/(m².K)); $\dot{m}$ is the mass flow rate of the fluid (kg/s) and C_p is the specific heat (kJ/(kg.K)).
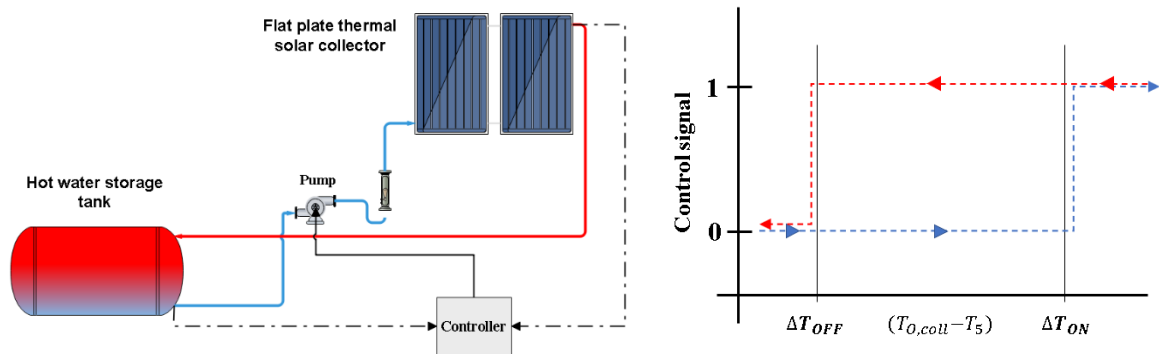
Figure IV- 5: Control scheme of the solar pump.

The second control is about the distribution loop to the radiators, the pump draws off hot water from the storage tank towards the radiators to diffuse heat into the office. The pump operates until the air temperature reaches the setpoint temperature 21°C and. To avoid recurrent ON/OFF cycle, the controller works in a dead band of 1°C (Hysteresis effect). Figure IV- 6 shows the operation scheme of the radiator's pump.
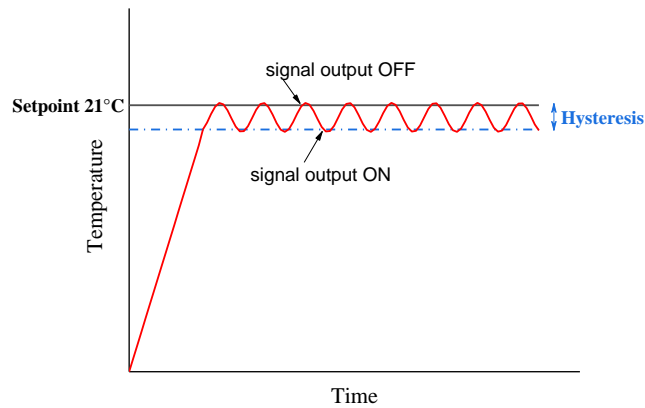
Figure IV- 6 : Control scheme of the radiators pump.

4.3. Methodology and DoE statistical modelling

In this section, a proposed methodology was adopted to conduct the sensitivity study in order to optimize the solar heating system. The methodology is a combination between statistical modelling and dynamic simulations through TRNSYS model. This approach offers the possibility to assess comprehensively the system's performance due to the dynamic-based model. Moreover, the statistical modelling using DoE methods allows to study the influence of the design parameters on the system's performance and the interaction between them. Finally, metamodels can be constructed using this approach, the latter serve as a basis for the optimization of the response of interest [125].

First, the numerical model must be validated with experiments. Then, a response of interest is to be selected. Also, the design parameters to be examined and their levels to delimit the region of study. Next, a design method is to be chosen regarding the studied factors and the aims of the study. Subsequently, metamodels of the response of interest will be constructed, they must be validated with the TRNSYS results and the adequacy of the model must be verified through a residual analysis. Finally, using the constructed metamodels, the optimization of the response of interest is performed and optimum solutions are drawn.

A DoE is implemented based on the following steps:

1. Selection of the response of interest

The response factor SF is selected as a response of interest because it is a commonly used indicator to describe the thermal performance of SHSs. It is defined as the fraction of heating load that can be met by solar energy on an annual basis [126]. Therefore, this indicator has been chosen as the principal response for this study.

2. Factor screening, determining levels and ranges

First, a screening experiment has been established to identify the most important factors among others. The selected factors are the collector area, the storage volume, the water mass flow rate, the pipe diameter, the insulation thickness of the pipes, and the pump control as a categorical factor. Fourteen simulations have been performed on the developed model. It has been observed that the pipe diameter and its insulation thickness effects are not significant and therefore not considered in further sensitivity analysis. At the end, four factors have been considered: the collector area (A), the storage volume (B), the flow rate (C) as continuous predictors and the pump control (D) as a categorical predictor. The analysis has been performed for two collector area intervals, namely, [2-10]m² and [10-20]m² with respect to the technical considerations regarding the flow rate and the storage volume. Each of the continuous predictors has been evaluated at the low and high levels of each interval and their corresponding storage volume and flow rate. Table IV- 3 shows the levels of predictors.

Table IV- 3: Range of variation of the design parameters.

		Factors				
		Collector area (m²)		Normalized storage volume (m³/m²)	Normalized mass flow rate (kg.s^{-1}/m²)	Pump control
Level	Low	2	10	0.05	0.01	Control
	High	10	20	0.18	0.02	No control

The collector area levels are selected in a range from 2 m² (single collector area) to 20 m² which corresponds to the area calculated with the f-Chart method [49] that allows attaining SF of 100% for the considered system. Storage volume levels are between 0.2 m³ corresponding to the current configuration of the SWHS and 5.4 m³ that is a higher value of the recommended range of storage volume-collector area ratio [127]. The area -weighted mass flow rate levels are chosen to try to cover as wide a range as possible, between 0.01 kg.s^{-1}.m^{-2} for the lowest mass

flow rate and 0.02 kg.s^{-1}.m^{-2} for the commonly applied standard collector test mass flow rate [128].

3. Performing the experiments

Using the validated TRNSYS model as a representation of the real system, 120 simulations have been executed with respect to the design matrix. Forty simulations for each collector area interval. The SF values have been calculated and used in the sensitivity analysis to study its variance regarding the chosen factors.

4. Statistical analysis and metamodeling

The objective of the metamodel is to approximate the response SF by a set of independent variables (the four design parameters defined previously) and to determine the relationship between the response and the corresponding factors. From the screening experiment, it has been found that some terms present quadratic variation. Thus, to estimate both interaction and quadratic effect, a full quadratic regression model has been adopted to model the SF, and is given as follows:

$$y = \beta_0 + \sum_{i=1}^{k} \beta_i x_i + \sum_{i=1}^{k} \beta_{ii} x_i^2 + \sum \sum_{i<j} \beta_{ij} x_i x_j \tag{IV. 9}$$

where, y is the predicted response, x_i is the independent variable, β_i are the coefficients that must be computed, and k is the number of factors.

Eq. (IV. 9) can be expressed in matrix notation for simpler solving, as follows:

$$y = b_0 + x'b + x'Bx \tag{IV. 10}$$

where, b_0, b, and B are the estimates of the intercept, linear, and second-order coefficients, respectively. In fact, $x' = [x_1, x_2, \ldots, x_k]$ is the transpose vector of x, $b = [b_1, b_2, \ldots, b_k]$ and B is a symmetric matrix.

$$B = \begin{bmatrix} b_{11} & b_{12}/2 & \cdots & b_{1k}/2 \\ & b_{22} & \cdots & b_{2k}/2 \\ & & \ddots & \vdots \\ sym. & & & b_{kk} \end{bmatrix} \tag{IV. 11}$$

The analysis of variance (ANOVA) has been used in combination with the P-value approach for a level of significance $\alpha = 0.05$ to test the significance of the metamodel alongside the terms

in the model. Thus, if P-value $\leq \alpha$, the association between the response and the term is statistically significant.

5. Response optimization

In order to optimize the solar fraction, the desirability approach was adopted. Desirability function approach is an optimization method utilized for multiple response processes to identify operating conditions x that provide the most desirable response value Y. Moreover, it can be evenly used for single response optimization.

The individual desirability function for maximizing a response is generally defined as:

$$d_i(Y_i) = \begin{cases} 0 & if\ Y_i(x) < L_i \\ \left(\dfrac{Y_i(x) - L_i}{T_i - L_i}\right)^s & if\ L_i \leq Y_i(x) \leq T_i \\ 1.0 & if\ Y_i(x) > T_i \end{cases} \qquad (\text{IV. 12})$$

Where Y_i is the response to be optimized, L_i and T_i are the lower, upper and target values. The exponent s determines the importance to hit a target value.

4.4. TRNSYS model validation

In this section the experimental data presented in chapter III are confronted to the simulation results from the model. The temperature measurements of main components which are solar collectors, storage tank and radiators are compared to the numerical results. The main objective is to develop a complete model of solar heating system to be able to correctly reproduce the short-term and long-term behavior of the installation. Additionally, the model will serve as a basis for the assessment and the optimization of the system's parameters.

Experiments were conducted during winter of 2020; typical representative days were selected with respect to the weather conditions to assess the heat production of the solar heating system under various conditions, cold days with high insolation, cold days with low insolation, warm days with high insolation…etc.

To be able to compare the two data sets, the different input parameters for all the components were established taking into account the real values existing at the experimental installation such as the initial tank temperature. Subsequently, weather data were recovered from online services, CAMS radiation service [129] provides time series global horizontal radiation for actual weather conditions and Infoclimat [130] provides hourly data of the dry bulb temperature

and wind velocity. The closest station (Alger centre, Algiers, Algeria) was selected for that matter.

The sampling period of the DAQ system was 1 second. Therefore, a moving average was utilized to smoothen the data set to 1 minute period to correspond with the simulation time step. Figure IV- 7 displays the comparison of the numerical and experimental data for the considered days.

The model results presented a similar pattern for the three compared components, solar collectors, storage tank and radiator. In the first column of Figure IV- 7 the numerical temperatures at the collector's level follow thoroughly the experimental measurements, the patterns are highly dependent of the weather conditions and the initial water temperature inside the tank. It is worth mentioning that the wind velocity plays an important role, as the pipe work between the collectors and the tank is not insulated and has a significant length, it is subject to external conditions. Therefore, the introduction of the wind velocity data into the developed model presented more accuracy approaching the real behavior of the solar collector.

At the tank's level, the trend of the TRNSYS model is reasonably in concordance the measured data. However, the model slightly overestimates the temperature values due to several possible reasons. For instance, the behavior of the occupant, uncontrolled ventilation (opening of the fenestration), air infiltration, also the thermal capacitance of the building. Subsequently, the temperature profile of the radiator's inlet follows that of the storage tank. Nevertheless, the numerical temperature profiles of the main components match the experimental measurements and showed good agreement between the compared data sets. The RMSE was calculated to evaluate the accuracy of the developed model. The results are depicted in Table IV- 4. The mean RMSE is 1.07 °C, this difference can be evaluated non-significant for heating applications in the building sector.
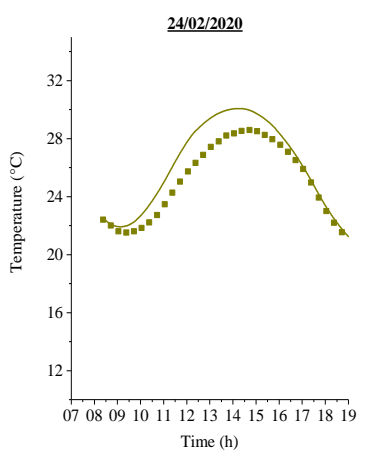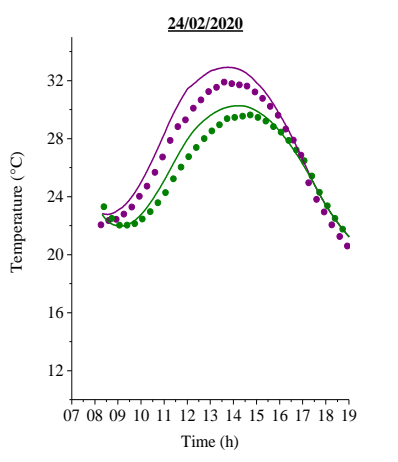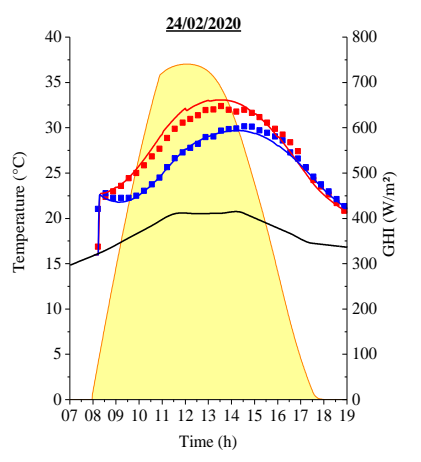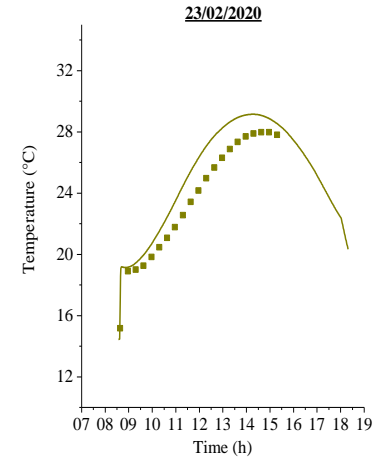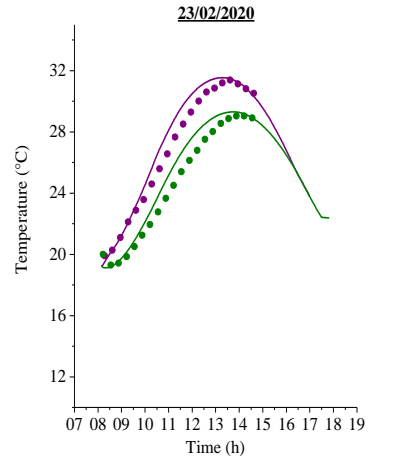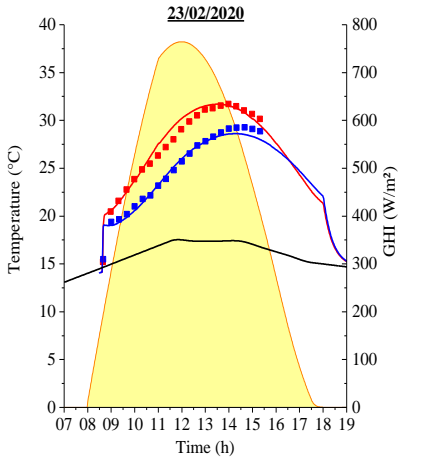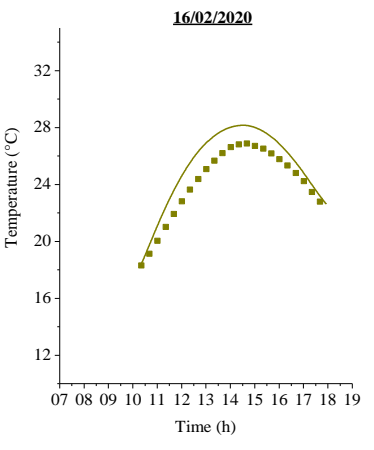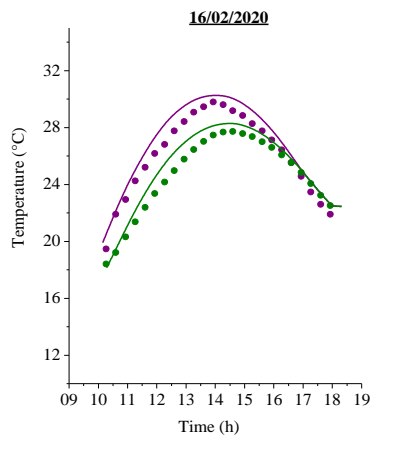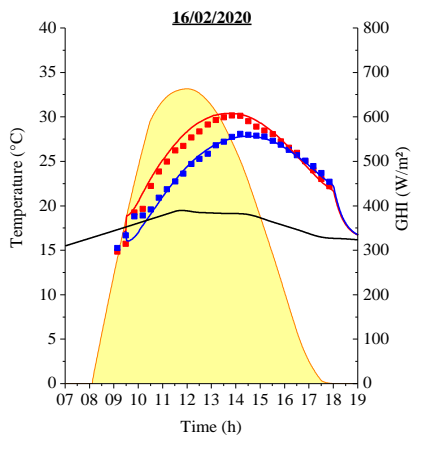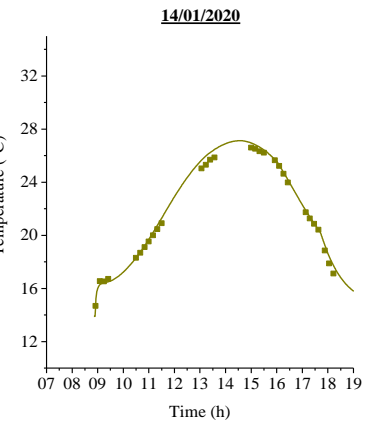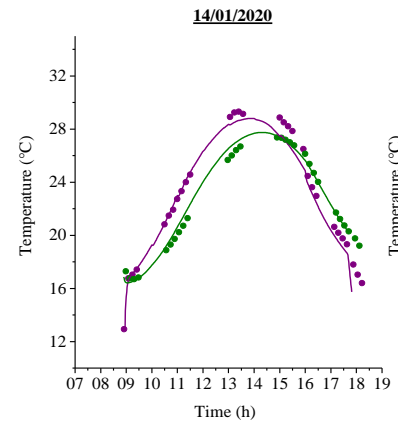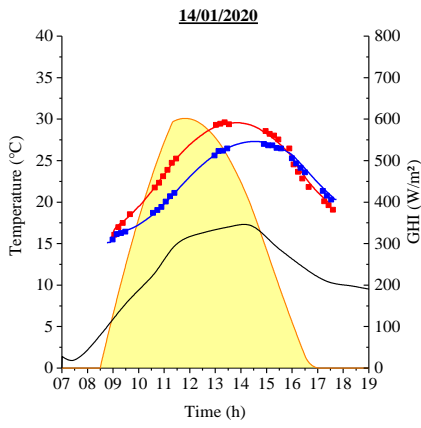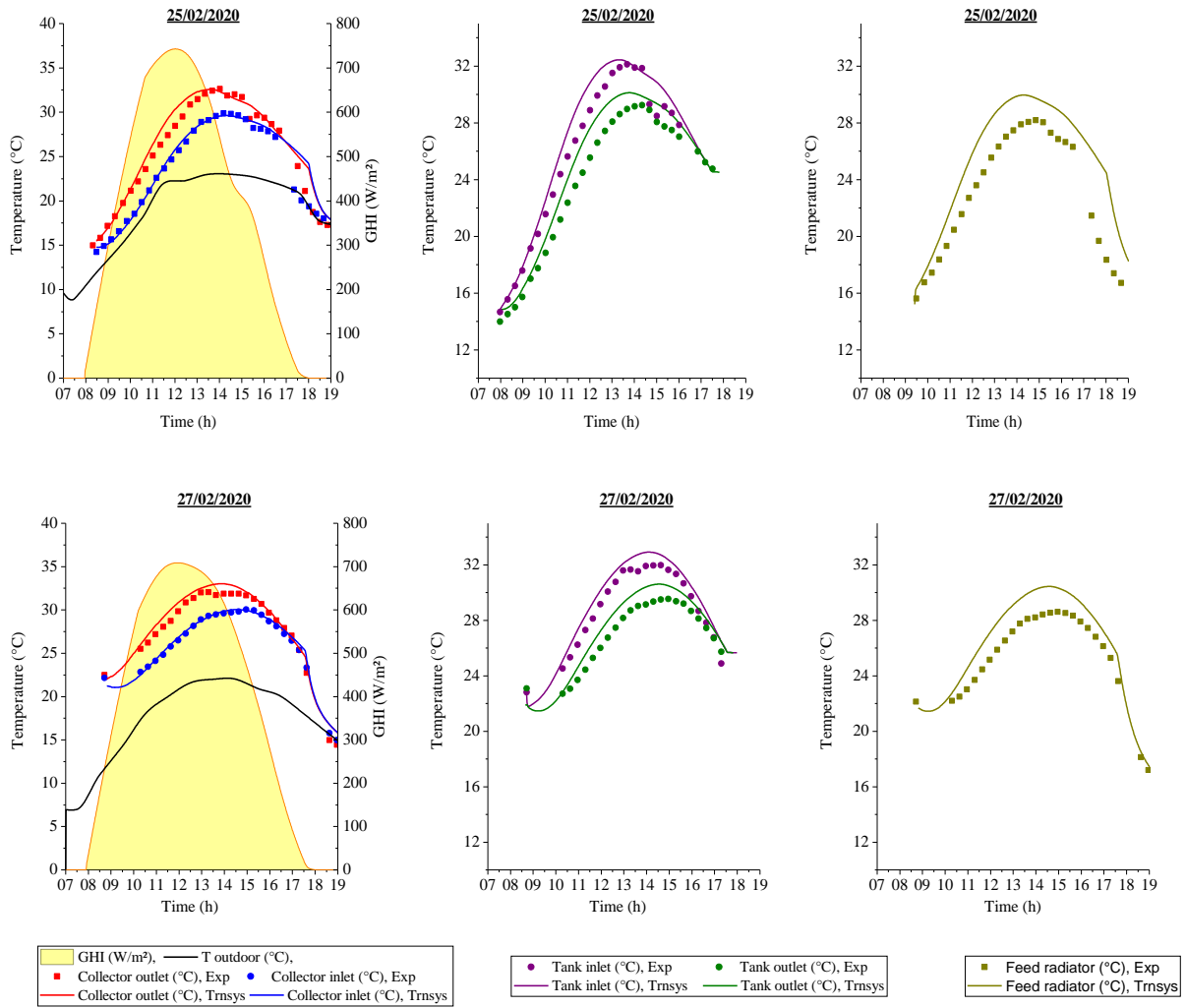
Figure IV- 7: Comparison between experimental and numerical temperatures (Collector, Storage tank and radiator).

Table IV- 4: RMSE between experimental measurements and numerical values.

	RMSE (°C)				
Day	Collector outlet	Collector inlet	Tank inlet	Tank outlet	Radiator
14/01/2020	0,70	0,71	1,32	0,44	0,33
16/02/2020	0,85	0,72	0,81	0,93	1,35
23/02/2020	0,72	0,66	0,81	0,78	1,48
24/02/2020	0,85	0,58	1,13	0,71	1,38
25/02/2020	1,23	1,46	2,33	1,19	2,61
27/02/2020	0,89	0,41	1,97	1,23	1,54

4.5. Sensitivity study

The validated numerical model is used in this section to further analyze the performance of the SWHS and to conduct a sensitivity analysis under different operating conditions using a DoE method. As outlined above, DoE is a method that allows to study situations with a response that varies when varying one or more independent factors. Unlike the parametric studies that analyze the impact of each single design parameter in a one or multiple responses, the aim of the sensitivity analysis, based on the DoE method, is to study and analyze the influence of each key parameter by considering the simultaneous interactions between all design parameters on the response factors. Therefore, an optimization process based on that full-sensitivity analysis could be easily assessed with a high level of confidence.

A total of 80 simulation runs has been performed, each at different factor level permitted to obtain the response SF. The design matrix containing the combinations are presented in Appendix A. The analysis of variance (ANOVA) on the simulation results is performed to examine the interaction between the factors and the influence of the different terms on the response of interest if existing. The ANOVA is executed for a level of confidence of 95% and P-value is selected as the indicator to identify the significance of the different terms, thus P-values<0.05 were considered to be significant.

4.5.1. Development of metamodels

Using the least-squares approach in section IV.3, the resulting coefficients of the different regressions have been determined. Based on the categorical predictor "pump control", two equations have been derived for every single interval. The terms of Eq (IV. 9)are presented in Table IV- 5. Uncoded units were considered for establishing the metamodels because it allows the designer to remove insignificant terms without changing the metamodel.

Table IV- 5: Coefficients of the established metamodels.

y	1st interval [2-10]m²		2nd interval [10-20]m²	
	SF-control	SF-No control	SF-control	SF-No control
β_0	-0.024	0.0202	0.090	0.153
β_1	0.0842	0.0738	0.0757	0.0623
β_2	-0.0276	-0.0388	-0.0619	-0.0648
β_3	0.391	0.524	-0.464	-0.163
β_{11}	-0.002986	-0.002986	-0.001419	-0.001419
β_{22}	0.0007	0.0007	-0.00145	-0.00145
β_{33}	-4.66	-4.66	-0.988	-0.988
β_{12}	-0.00504	-0.00504	-0.00133	-0.00133
β_{13}	0.1451	0.1451	0.0376	0.0376
β_{23}	0.03	0.03	0.1003	0.1003

Where x_1, x_2 and x_3 represent the collector area (m²), storage volume (m³) and mass flow rate (kg.s^{-1}) values, respectively in Eq.(1).

4.5.2. Model adequacy checking

Before the use of the fitted model, it must be verified to what extent the model fits the data. For the deemed model, concerning the variation of the response, R^2 is 97.84%, 95.12%, and for the 1st and 2nd intervals, respectively. These values indicate an adequate fitted model. However, despite the high value of R^2, a residual analysis is performed to check the satisfaction of the model assumptions, then a normal probability plot is generated (Figure IV- 8) presenting the normal percentiles versus the residuals. As it can be seen, the residuals are normally distributed since they follow approximately a straight line, and they do not indicate any serious violation of the model assumptions.
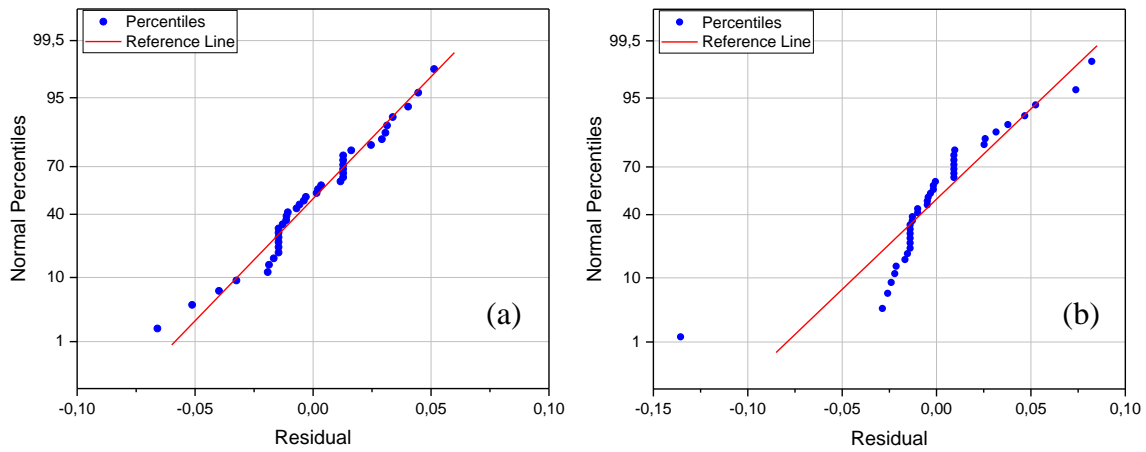
Figure IV- 8: Normal probability plot (a) 1st interval [2-10] m² (b) 2nd interval [10-20] m².

4.5.3. Sensitivity analysis

The pareto chart of the standardized effect is used to compare the relative magnitude and the statistical significance of the main, 2-way, and square interaction effects for a significance level $\alpha = 0.05$. Based on the results of the ANOVA, the Pareto chart depicted in Figure IV- 9 displays the standardized effects with respect to each interval. The bars on the right side of the reference line represent the significant terms, while the bars on the left side indicate the insignificant terms. As it can be seen, the results show that the largest effect is attributed to the collector area (A) then the storage volume (B). The pump control (D) effect becomes more important with higher ranges. Square Terms (AA) and (CC) are significant which means that the response SF follows a curved line. The interactions (AC) and (AD) are recurrent meaning that the interaction between the collector area and the SF depends on the flow rate and the pump control. With larger systems (CD) and (BC) tend to be more significant, then the relationship between solar SF and (C) depends on the control and the storage volume. Also, (BD) and (AB) which emphasize the importance of the storage volume in large systems. Hence, the main effects should not be interpreted without taking into consideration the interaction effect.
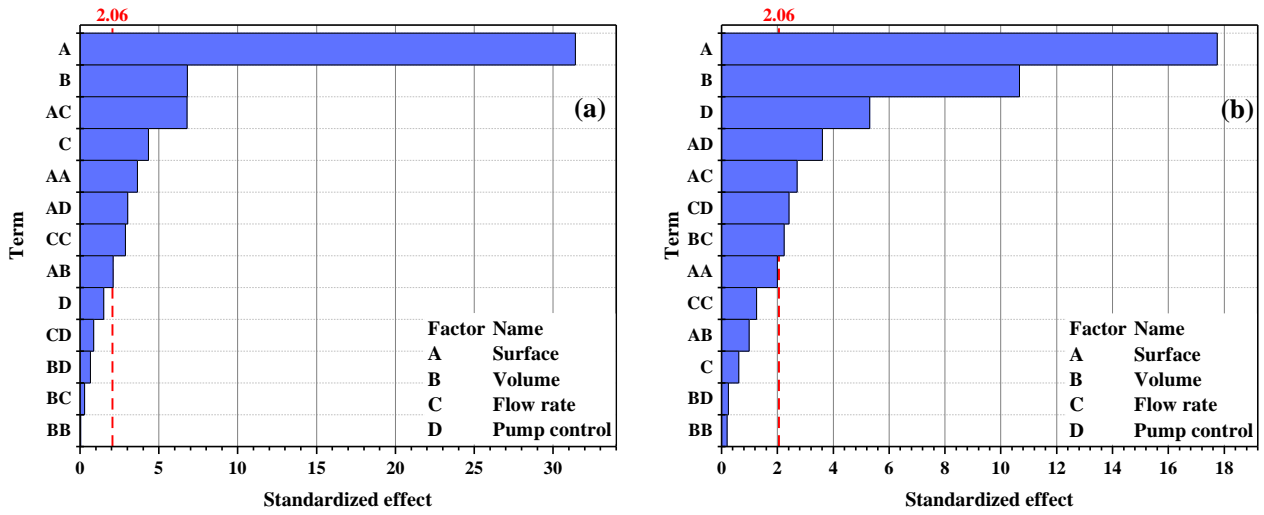
Figure IV- 9: Pareto charts of the standardized effects (a) [2-10]m² (b) [10-20]m².

The Pareto charts displays only the significant terms. Therefore, the normal plot of the standardized effect is utilized to observe the direction of the effect. In a normal plot the terms located to the left side of the reference line have negative impact on the response while the terms to the right have positive impact. As seen in Figure IV- 10, the terms (A), (AC) and (AD) have positive impact in both intervals, obviously to the high influence of the collectors' area. The term (B) has a negative impact on the SF, therefore the choice of the volume of the storage tank is to be handled with care. The control strategy, term (D) plays an important role in increasing the SF and its importance increase with large systems.
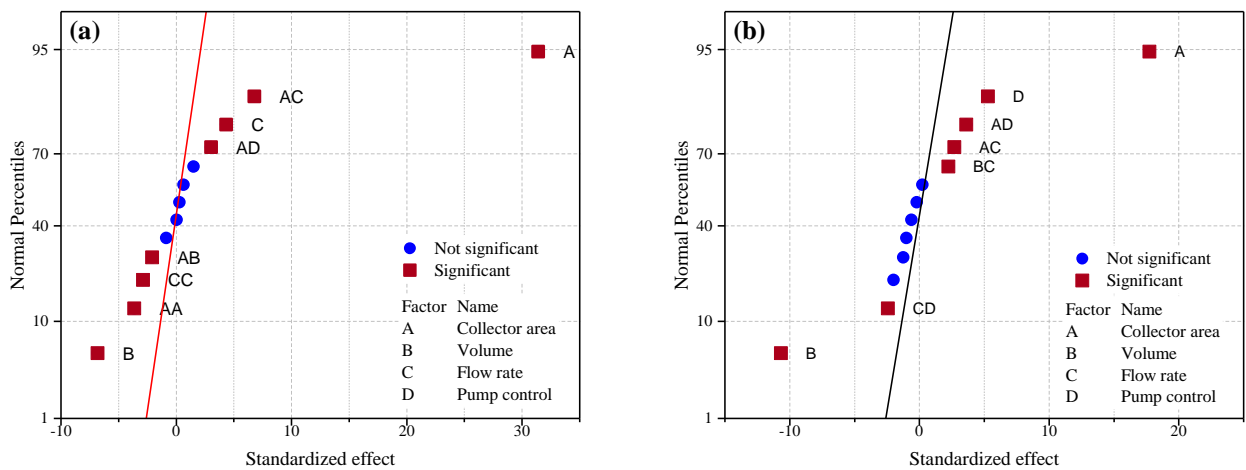
Figure IV- 10: Normal plot of the standardized effects (a) [2-10]m² (b) [10-20]m².

The magnitude of the estimated effects in Figure IV- 11 (a) and (b) shows that the "collector area" (A) is by far the most important factor followed by the "storage volume" (B). "Pump control" plays the next most significant role. "Flow rate" has a significant role in several interaction terms, but it is the least important factor on its own. It is noteworthy that when the interactions are large it can obscure the main effects. From the ANOVA, the interaction between terms was significant, consequently, the main effects cannot be interpreted without considering the interaction effects.
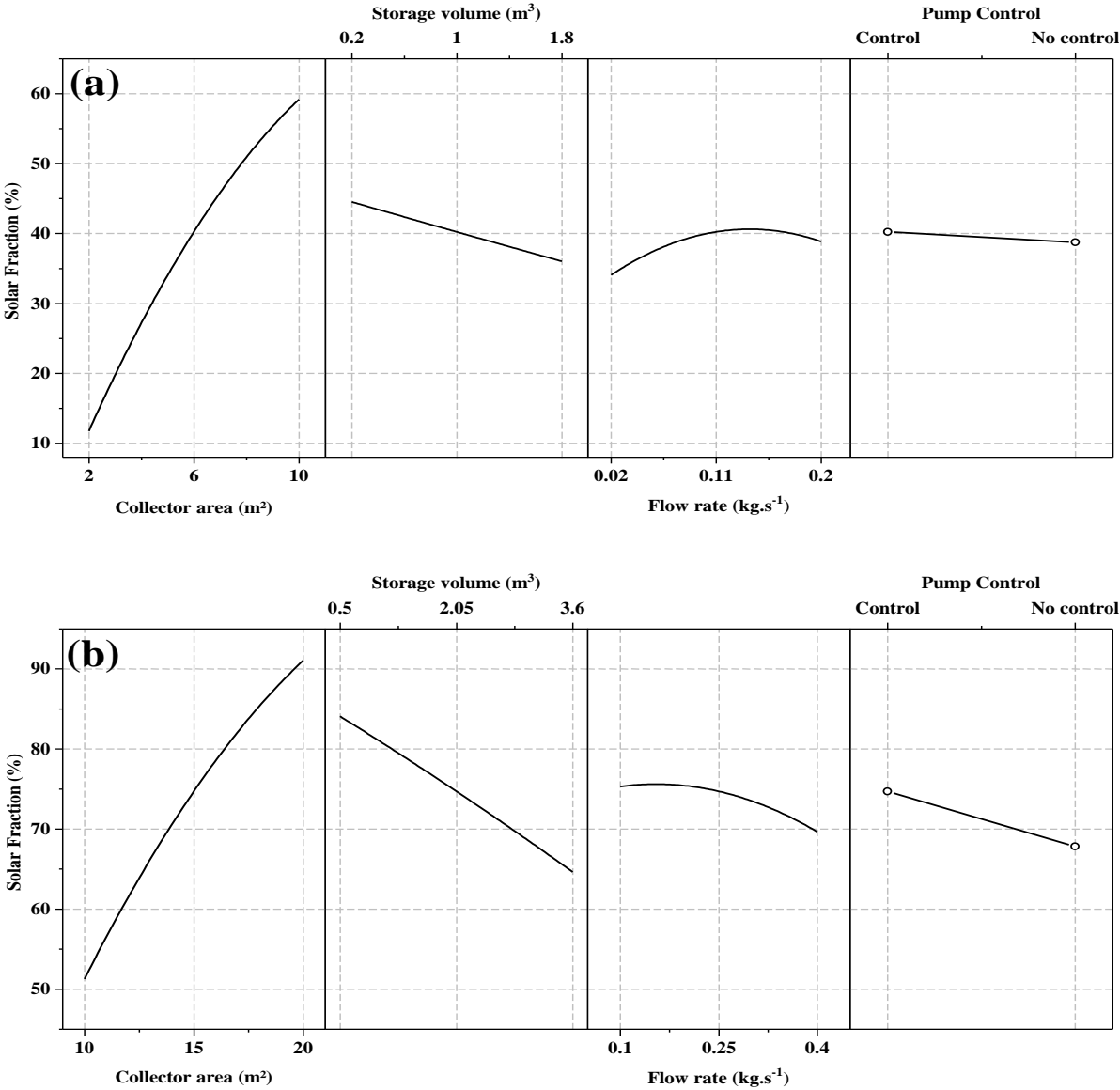
Figure IV- 11: Main effects plot for SF obtained at the different ranges of collector area: (a) [2-10] m² (b) [10-20] m².

The interaction between the different factors has been investigated for the two considered intervals of the collector area. Similar trends were noticed with different magnitudes. Figure IV- 12 shows the results obtained. In which, a half-matrix representing the means of SF is displayed for all combinations of two factors at their different levels. Each x-axis of a column represents the levels of a particular factor. The labels to the right of the columns indicate the factor defining the lines in each row. Nonparallel lines mean that an interaction occurs between two factors. For instance, the relationship between the collector area and the SF depends on the value of the flow rate and the pump control, similarly for the flow rate and SF, the relationship between the two depends on the storage volume and the pump control, while the parallel lines mean no interaction or insignificant association between the factors on the response. As shown in Figure IV- 12, an insignificant interaction between collector area and volume in that interval is observed, which is explained by the choice of the V/S ratio mentioned before, the respect of the interval of the V/S ratio is recommended. Also, no interaction occurs between the storage volume and the pump control on the SF, however, it has an important role interacting with the flow rate and the collectors' area. The terms with the interaction including flow rate are all significant, which explains the importance of the flow rate.

95
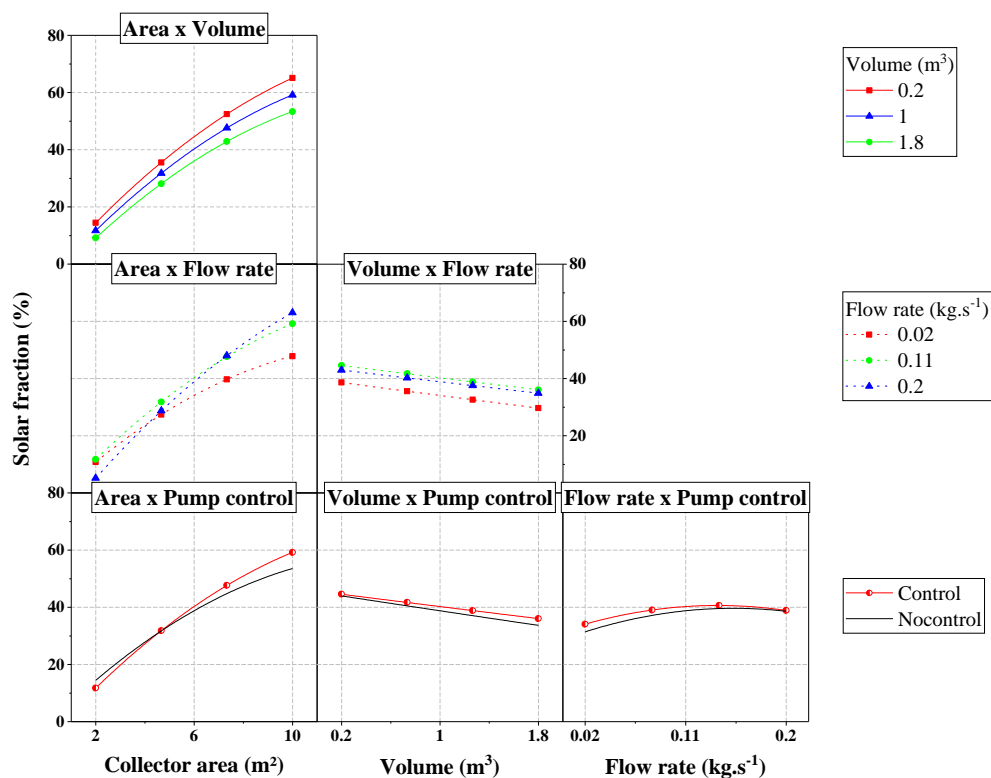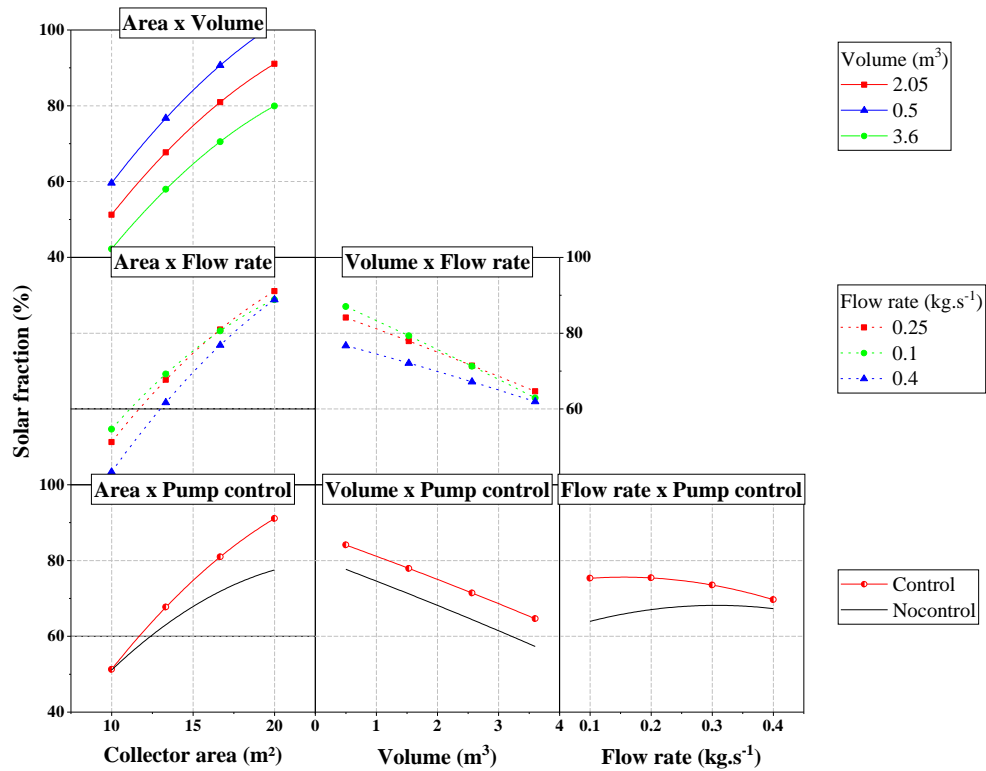
Figure IV- 12: SF curves showing interaction between different design parameters, obtained for [2-10]m² and [10-20]m² intervals.

4.6. Optimization

Once the impact of the design parameters on the response and their interaction effect is quantified, a set of operating conditions that permit to obtain an optimal response were identified. This process was based on the mathematical model by plotting the contour plots to identify an optimum with satisfactory accuracy. Figure IV- 13 illustrates the contour plots of the fitted SF for [10-20]m² interval. Given that the model includes more than two factors, the surface responses were plotted in pairwise holding the third factor at its optimum level from the main and interaction effects. The contour plots represent the value of the response SF. Only plots with respect to "control" level have been displayed.

In Figure IV- 13(a), the SF is plotted against the collector area and the flow rate. As the model revealed significant quadratic terms, the contour presented a curved shape. The highest values of the SF are to the bottom right corner, which corresponds to large values of collector area and low flow rate values. The lowest fractions are to the top left which corresponds to high flow rates and small collector area. Storage volume is held at 0.5 m³. From the contour plot, in order to achieve a SF about 90% or higher, collector area in the range [16-20] m² and flow rate between [0.1-0.4] kg.s⁻¹ are needed.

Similarly, for the couple Area-Volume in Figure IV- 13(b), higher fractions are to the bottom right of the plot. From the contour plot, and for a fixed value of the flow rate 0.25 kg.s⁻¹, it is clear that increasing the volume decreases the SF significantly. Consequently, it will be better to choose small storage volume with a relatively larger collector area to achieve higher SFs in one isocurve. For instance, to attain 90% SF at 0.25 kg.s⁻¹ of flow rate, about 17 m² and 0.5 m³ with respect to the collector area and the volume storage, respectively, are suitable.

As for Figure IV- 13(c), the highest SF values are to the bottom left of the plot. It is noticed that the SF decreases with increasing the flow rate while contrarily for larger storage volumes the SF increases with increasing the flow rate. This can be explained by the significance of the terms (BC) and (AC) in the fitted model compared to the pure quadratic terms (BB) and (CC) which are not significant in that interval. The entire range of flow rate for a tank volume of about 2 m³ allows us to attain 90 % of the SF for the considered collector area (20 m²).
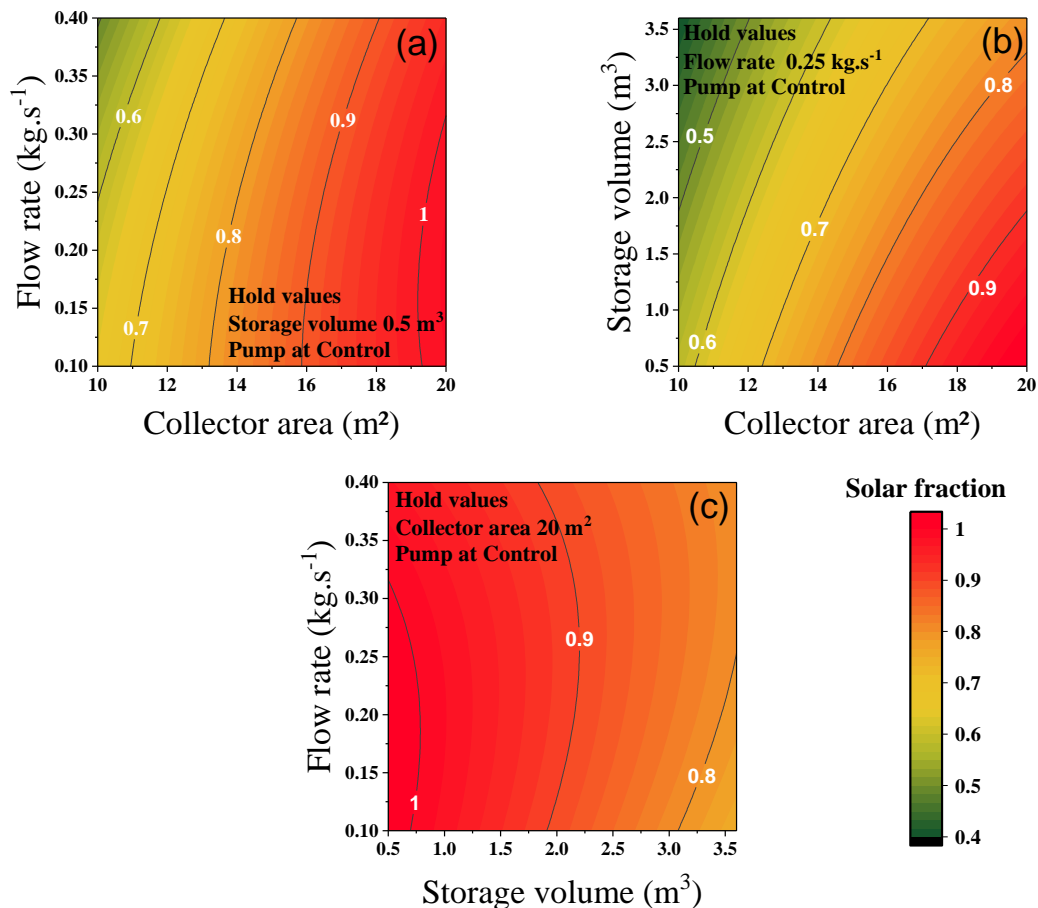
Figure IV- 13: Contour plots of Solar fraction. (a) SF versus flowrate and collector area; (b) SF versus storage volume and collector area; and (c)SF versus storage volume and flowrate.

97

The above set of parameters allows us to reach the outlined SF from a technical point of view. Nevertheless, the economic aspect is of more interest especially to the user, the typical SF is within the range of 25-35% in central/western Europe [131]. The renewable technology platform on renewable heating and cooling (RHC) has set a goal to increase the SF (overall heat demand) from 25% to 60% in active solar buildings [132]. However, since the studied system is located in Algiers, higher SF values could be attained due to the high insolation compared to the central European climate.

Based on these concerns, assuming that an interval of 35-60% is desired, several sets of operating conditions might be determined from the fitted model. However, technical limitations should be considered. The available area for installing solar collectors on the rooftop of the building is 16 m² without having shadow masks, also the affordable space for the storage volume is limited to 1 m³. Working under these constraints multiple solutions were predicted. Two interesting options are displayed in Figure IV- 14 (a) and (b). A set of levels consists of 10 m², 0.61 m³ and 0.1 kg.s^{-1} using the [10-20]m² model ought to provide a SF around 64%. While 8.475 m², 0.2 m³ and 0.2 kg.s^{-1} using [2-10]m² model provides a SF about 60%, although variations are expected regarding the correctness of the fitted model.
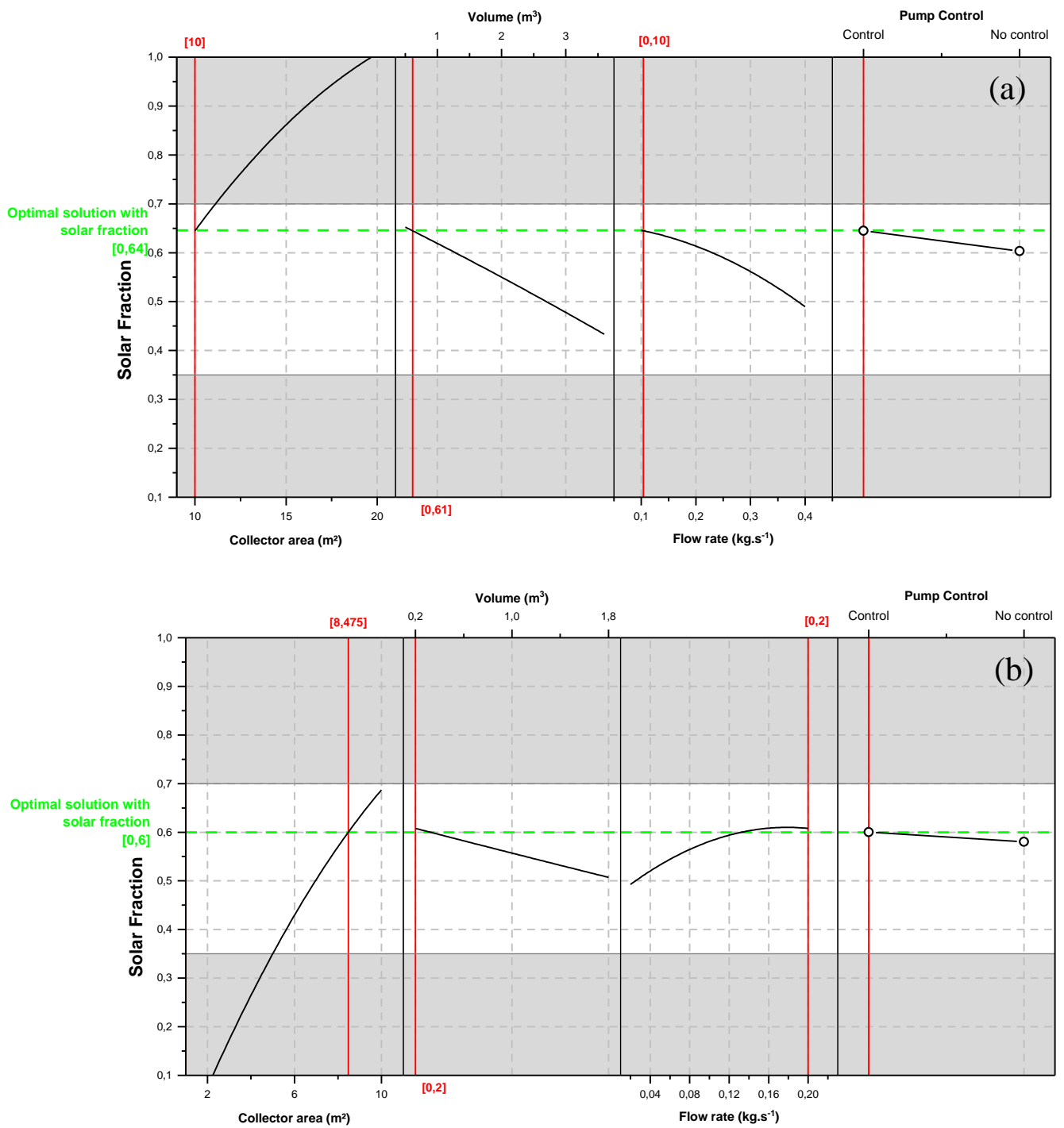
Figure IV- 14: Optimal operating conditions for targeted SF: (a) [10, 20] m²; (b) [2-10] m².

4.7. Conclusion

In this chapter, a developed TRNSYS model was presented then validated against experimental data and was therefore employed to assess and optimize the performance of the system. Then, a methodology based on DoE and Dynamic simulations on TRNSYS was proposed to study the interaction effects between different factors and to optimize the solar fraction. The domain of study was divided into two intervals regarding the collectors' area [2-10] m², [10-20] m² to respect the technical recommendations. Hereafter, the influence of the selected design of parameters on the solar fraction is extensively investigated through a sensitivity analysis. The results showed that SF is highly dependent on the solar collector area and storage volume but cannot be interpreted separately because of the interaction with the remaining factors. Whereas the flow rate is the least significant main effect on its own, but it plays a role in several interaction terms. The pump control strategy influences on the SF and increases with larger systems. Then, metamodels were constructed to formulate a relationship between SF and design parameters. These metamodels were then employed in combination with the desirability function approach to optimize the solar fraction.

The final objective of this work being to propose an optimized system able to improve the management of the two energy sources used (solar and gas), the following chapter will present the development of the various sub-models of a hybrid solar/gas heating system. From the knowledge of each subsystem, we will justify the type of model chosen and we will then present the approach having led to the multi-objective optimization of our system.

Chapter 5

Hybrid solar gas heating system Multi-source analysis

5.1. Introduction

As reported in the above chapter the system was operated in solar mode only and a single objective optimization method was proposed to maximize the SF. In this chapter, the system will operate in solar/gas mode. Subsequently, the TRNSYS model was upgraded, and a gas boiler was implemented along with the control system. The PESR and the levelized cost of heat have been added as objective functions. Therefore, a multi-objective optimization methodology was proposed based on a combination between DoE, GA, and Dynamic simulations.

The chapter first describes the improvement in the TRNSYS model along with the parameters used in the economic evaluation. Then, the proposed methodology for the multiobjective optimization is explained. The second part of the chapter presents the results of the comparison between the control strategy modes, the effect of the design parameters on the three objective functions and the solutions of the multiobjective optimization. A multi-criteria decision-making technique is also illustrated in the present chapter. Finally, a financial subsidy scenario is discussed to analyze the profitability of the hybrid solar system.

5.2. TRNSYS Hybrid solar/gas heating system

5.2.1. System modeling

The TRNSYS model has been improved, integrating the gas boiler to realize the hybridization of the system. Focusing on the control strategy to profit from the synergy between the two energy sources and to reduce the energy consumption of the system while preserving the occupants' comfort. Figure V- 1 depicts the developed TRNSYS model of the hybrid system.

As indicated in the Figure V- 1, the parameters of the additional components of the system are described as well as the equipment costs and fuel prices used for the economic evaluation. The TRNSYS types used for that matter are described in the following.

For the commercial gas boiler considered in this study. The nominal heating capacity is 24 kW. The boiler efficiency is 80% and the setpoint temperature is 80°C while the water mass flow rate through the serpentine heat exchanger is equivalent to 0.1 kg/s. Therefore, Type 122 was used to model the gas boiler, this component will attempt to meet the specified setpoint temperature but may be restrained by the specified heating capacity. The starting and stopping of the boiler is controlled with regards to both outdoor and indoor temperatures.

Given the importance of the control strategy from the sensitivity study conducted in chapter IV. The system was examined under three different control strategy modes in order to identify

the most suited mode for the current system. Type 2b was used to model the control modes. Mode 1 consists of defining a fixed setpoint for the radiators supply water, in our case 60°C is to be maintained in the storage tank, to ensure the availability of hot water when heating is required. On the other hand, Mode 2 consists of defining a setpoint for the room air temperature, 21 °C, the gas boiler will operate unless the temperature inside the office exceeds 21°C with a hysteresis of 1°C±. Meanwhile, Mode 3 is based on a heating curve that considers the radiators water supply temperature as a function of the outdoor temperature.
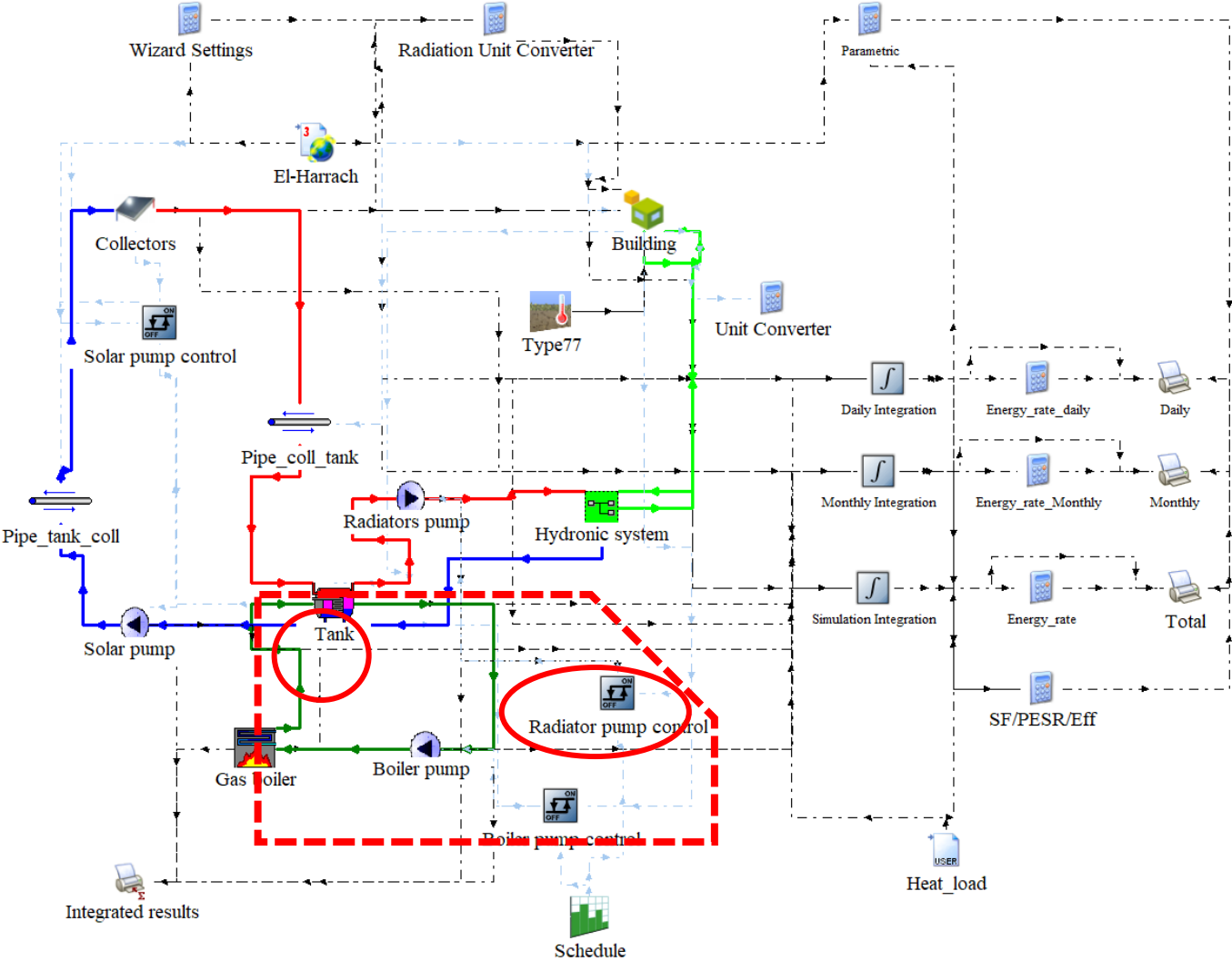
Figure V- 1: TRNSYS model of the HSGHS.

According to the heating curve used in the present work, the gas boiler keeps operating until the water inside the tank is equal to T_{supply}. The supply water temperature is expressed as follows:

$$T_{supply} = -2.22(T_{ext} - 21) + 33.34 \tag{V. 1}$$

For the economic analysis, Table V- 1 summarizes the economic considerations and the equipment costs used in the simulations. The prices of the different equipment were surveyed from the local suppliers of solar equipment and heating devices.

It is worth mentioning that the price of the storage tank is included in the solar collectors' price brought to area unit, which can be expressed in DA (Algerian dinar) as a function of the collector area:

$$C_{sol,coll}(DA) = 55000 * A_{coll}$$

Table V- 1: Economic parameters.

Parameter	Value
Period of economic analysis, Ne	20 years
Discount rate, d	2%
Electricity tariff, Cf,ele	5.47 DA/kWh
Gas Tariff, Cf,gas	0.45 DA/therm
Solar field cost, Cinv,sol	55000 DA/m²
Maintenance costs, M	1% of the Investment cost
Gas boiler cost, Cinvest, GB	80000 DA

*1DA= $ 0.0075 (as established on 11/02/2021)

5.3. Methodology

The main objective is the optimization of the HSGHS performance. In this regard, the adopted methodology is a combination of tools and approaches, where TRNSYS is used to evaluate the thermal performance of the system by means of a seasonal simulation, considering a 1-min time step and an hourly meteorological data (TMY). The TRNSYS developed model compute the chosen objective functions also called responses. In addition, TRNSYS is employed to automate the runs and save the results. The response surface method is used to plan the experiments to be conducted, after defining the responses of interest and the most influential factors. Its objective is to establish mathematical models, metamodels, of second degree that describe the relationship between each response and the independent variables. Then the adequacy of response surface models must be verified and validated against the

simulation results. Finally, the metamodels are loaded into MATLAB, where the three objective functions are assessed (SF, PESR and LCOH). Then a genetic algorithm (GA) is applied to determine the optimal solutions (pareto frontiers) of the objective functions.

Figure V- 2 summarizes the main procedures for the retrieval of optimal solutions following the proposed methodology steps below.

1. Identify the decision variables and objective functions.
2. Select the response surface design (Central composite, Box-Behneken or define custom response surface design.
3. Run the simulations on the validated TRNSYS model.
4. Construct the metamodels for the deemed responses of interest.
5. Check the adequacy of the metamodels, if the metamodels are not fit, use an alternative analysis to fit a regression model or reselect a different response surface design and repeat from step 1.
6. Verify the validity of the metamodels results with TRNSYS model results.
7. Use GA on MATLAB to optimize the objective functions and define pareto fronts.
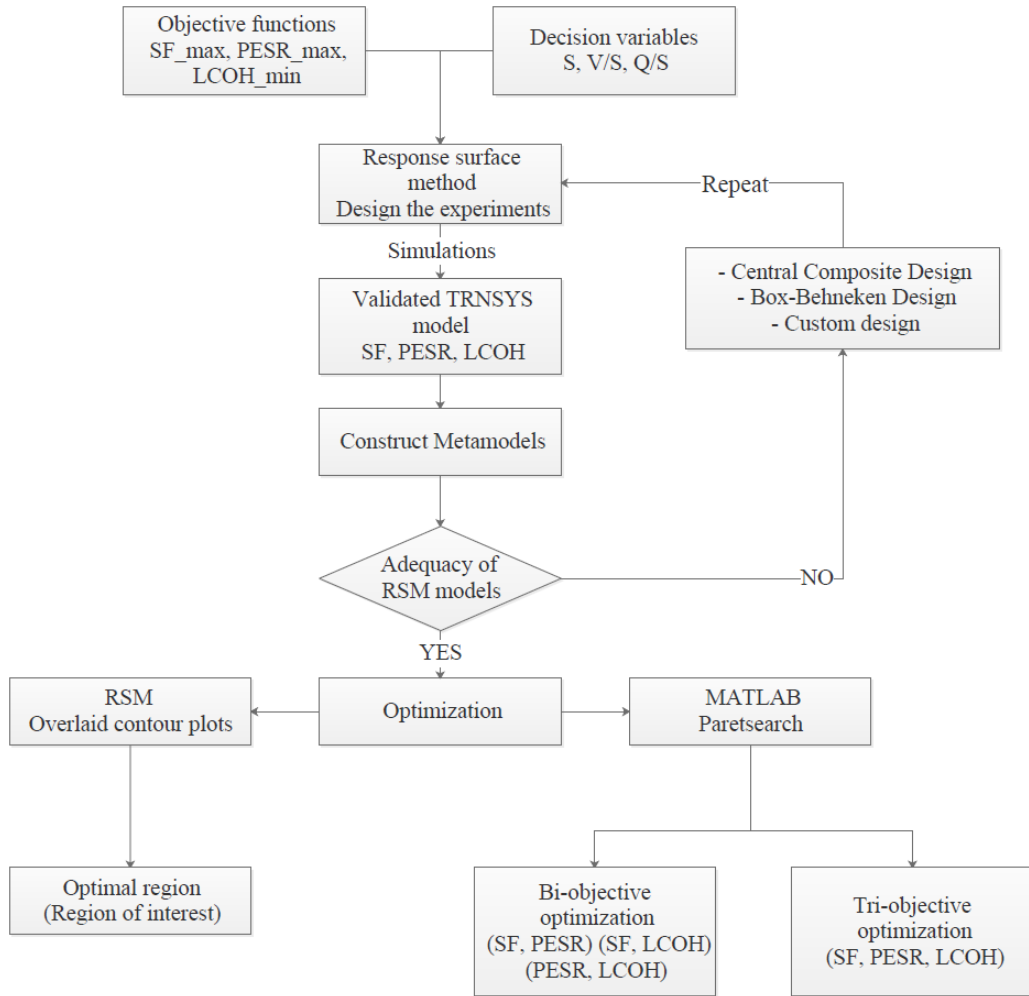
Figure V- 2: The flow chart of multi-objective optimization methodology.

5.3.1. Optimization variables

In a HSGHS, several design variables might determine the performance of the system. To identify these variables, screening experiments were conducted on the investigated system to find the few significant factors from a list of many potential ones. The solar collector area, the storage volume and the flow rate into collectors were the three significant factors. To respect the technical considerations for the good operation of the system, the storage volume variation range was set by the ratio $0.05 \leq V/S \leq 0.18$ (m^3/m^2) [127] and the flow rate $0.01 \leq Q/S \leq 0.02$ (kg.s^{-1}/m^2) which correspond to a minimum flow rate and the highest flow rate used in the collectors' test conditions [128]. Considering that the DoE method utilizes different levels of the factors in each combination, to avoid inconsistency between the deemed variables, the storage volume (V) and the flow rate (Q) were brought to the collector area. Thus, the three decision variables selected for the present study are collector area (S) volume to collector area ratio (V/S) and flow rate to collector area ratio (Q/S).

Table V- 2: Decision variables levels.

Levels	$S(m^2)$	V/S (m^3/m^2)	Q/S $(kg.s^{-1}/m^2)$
Low	2	0.05	0.01
High	20	0.18	0.02

5.3.2. Objective functions

The model falls within the scope of a multi-objective optimization problem, since three objective functions were considered in the present study which are: the maximization of the solar fraction and the primary energy saving ratio (energy), and the minimization of the levelized cost of heat (economical).

As a metric to measure the productivity of a solar system, the SF is commonly used to compare the performance of solar systems. This indicator provides information about the proportion of total heat load supplied by solar energy. The SF can be expressed as follows:

$$SF\ (max) = \frac{\sum f_i L_i}{\sum L_i} \qquad (V.\ 2)$$

Where f_i and L_i represents monthly SF and monthly load, respectively.

The knowledge of the SF alone is insufficient to correctly characterize a hybrid solar system. It is substantial to determine the energy savings realized by the HSGHS compared to a conventional reference system without the solar part. In that regard, the PESR is used to estimate the energy savings. It is the ratio of the energy saved to the energy consumption of the reference system, The PESR can be calculated as: [60].

$$PESR(max) = \frac{PEC_{ref} - PEC_{HSGHS}}{PEC_{ref}} \qquad (V.\ 3)$$

Where PEC_{ref} and PEC_{HSGHS} are the primary energy consumptions of the reference system and the HSGHS, respectively.

When it comes to the economic performance of the HSGHS, Levelized Cost of Heat (LCOH) is used as an economic indicator. LCOH is derived from the levelized cost of energy, it is used to assess the costs of heat production over the lifetime of a solar thermal system and to compare different technological solutions. The LCOH can be estimated from the following formula [133]:

$$LCOH\ (min) = \frac{I_0 - S_0 + \sum_{t=1}^{T} \dfrac{C_t}{(1+r)^t}}{\sum_{t=1}^{T} \dfrac{E_t}{(1+r)^t}} \qquad \text{(V. 4)}$$

Where I_0: Initial investment in DA, S_0: Subsidies and incentives in DA, E_t: Final energy demand per year in kWh, t period of analysis in years and C_t: the total yearly operation and maintenance costs in DA. With $C_t = O + M$. where O represents the operation costs corresponding to the power consumption of the pumps which depends on electricity price and of consumption of natural gas for the boiler gas and its price; M represents the maintenance costs and is usually $0.01\ I_0 < M < 0.02\ I_0$ [134].

5.3.3. Optimization procedure

Two different but/and complementary methods were used to achieve a comprehensive multi-objective optimization. Hereafter the followed procedure.

5.3.3.1 Response Surface Method (RSM)

Earlier, the RSM goal was described to establish mathematical models for the considered objective functions. The RSM is very useful when working with continuous variables. Its eventual objective is to determine the optimum operating conditions or a region of the variables space that satisfies the operating requirements. The central composite design was adopted in the present work for its efficiency in fitting second-order models. Figure V- 3 shows the response surface design, where the points represent the combinations used for the simulations in TRNSYS. Then the metamodels were established after the estimation of the different coefficients using the least-squares method. The general full quadratic regression model is given as follows:

$$y = \beta_0 + \sum_{i=1}^{k} \beta_i x_i + \sum_{i=1}^{k} \beta_{ii} x_i^2 + \sum_{i<j} \sum \beta_{ij} x_i x_j \qquad \text{(V. 5)}$$

where, y is the predicted response, x_i is the independent variable, β_i are the coefficients that must be computed, and k is the number of factors.

After building appropriate response surface model for the responses, a rather relatively straightforward approach "overlaid contour plot" has been used to simultaneously optimize multiple responses. or at least keep them in desired ranges because of the difficulty of optimizing several responses without degrading others.
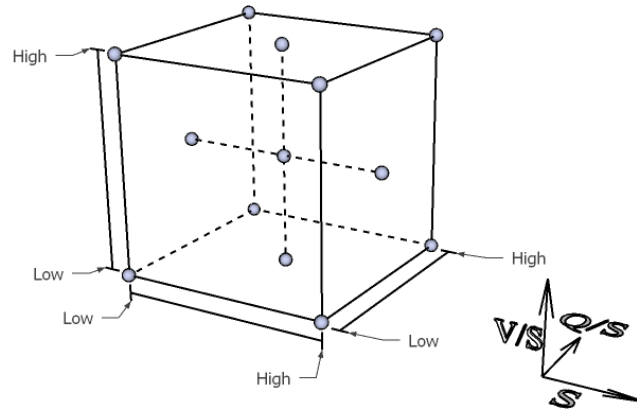
Figure V- 3: Central composit design.

5.3.3.2 Pareto fronts

Multi-objective optimization arises from problems with several objective functions to be optimized. In practical applications, the goal is to find a trade-off between two or more conflicting objective functions subject to optimization. Pareto fronts, help to find nondominated solutions, that is solutions in which the enhancement of one objective involve the degradation of another. For that matter, the paretosearch algorithm in MATLAB was used. This algorithm uses an iterative pattern search to find nondominated solutions converging to points near the true pareto front.

In the present work, the evaluation of the different objective functions considered to be deserving, first through bi-objective optimization to identify the optimal values of each couple of the responses, afterwards a tri-objective optimization was performed to find a trade-off between the optimized responses.

Since most optimization algorithms tend to look for the minimum of a function, for the functions to be maximized, PESR and SF in the present case, the algorithm was set to find the minimum of the negative of these functions. The objective functions were expressed as follows:

$$Min\ F(x_i) = [f_1(x_i), f_2(x_i), f_3(x_i)] \tag{V. 6}$$

$$Subject\ to \qquad x_i^L \le x_i \le x_i^U \tag{V. 7}$$

Where $f(x_i)$ represents the objectives to be minimized simultaneously, x_i^L and x_i^U are the lower and upper limits of the constraints which represent the decision variables.

The objective functions and their constraints are depicted in Table V- 3.

Table V- 3: Objective functions and constraints.

	$[x_i^L \ x_i^U]$			$f(x_i)$	
Surface	V/S ratio	Flow rate	f_1	f_2	f_3
[2 20]	[0.05 0.18]	[0.01 0.02]	$1 - SF$	$1 - PESR$	$LCOH$

5.4. Impact of the control strategy on the performance of the HSGHS

The control strategy plays a major role in the performance of the HSGHS. As mentioned before, a control strategy was adopted to save fuel energy consumed by the gas boiler regarding indoor and indoor environments. The strategy is based on the control of the temperature inside the storage tank to ensure the air setpoint temperature inside the room i.e. 21°C with the minimum required supply temperature to the radiators. Three control modes were investigated, mode 1, with fixed setpoint temperature inside the tank, the boiler maintains 60 °C inside the tank during the operation period. Mode 2, with fixed setpoint temperature inside the room 21°C, the boiler operates at full capacity when the temperature of the room is below the setpoint. And mode 3 that depends on the weather compensation curve, also called heating curve shown in Figure V- 4, where the radiators supply temperature is a function of the outdoor temperature. The three control modes were simulated and compared.

The coldest week, over the Algiers winter season, was selected from the weather analysis as the worst-case scenario to show the impact of the control strategy on the system's performance, the temperature of the bottom of the tank, supply water temperature, for the three modes. The results are depicted in Figure V- 5. the white zones represent the operation period i.e., from 6am to 6pm. In all cases the setpoint temperature inside the office is ensured. However, mode 3 clearly presented the lowest temperatures inside the tank compared to mode 1 and 2. In fact, for mode 3 the supply water temperature decreases with the increase of the outdoor temperature, less heat demand, resulting in reduction of operation time of the boiler and lower temperatures. Therefore, lesser energy consumption.
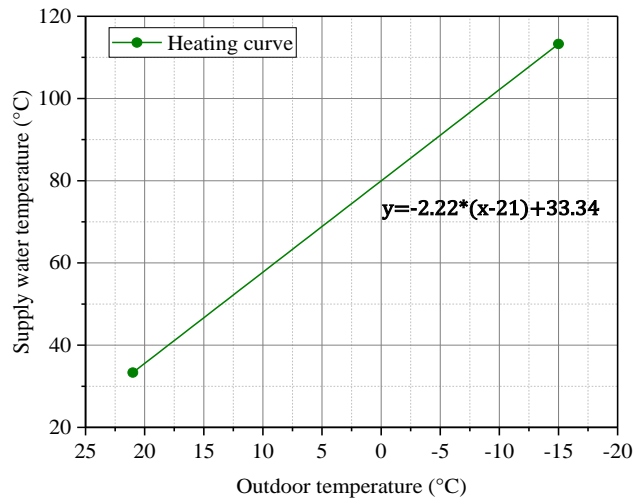
Figure V- 4: Mode 3 Heating curve.
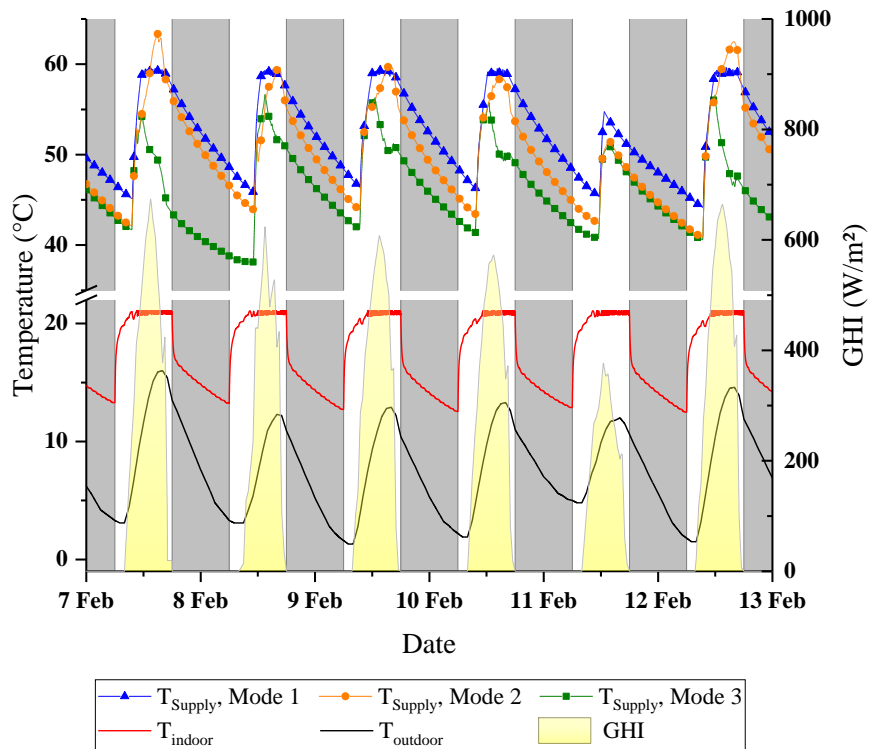
Figure V- 5: Comparison of the water supply temperature Mode 1, Mode 2 and Mode 3.

Table V- 4 shows the monthly results of SF and PESR for the three modes. Both indicators presented better values with the heating curve control mode. For PESR, in mode 1 the boiler prepares the water at 60°C constantly during the operation period, even when heating is not needed. In mode 2 the boiler operates only when the temperature of the office is below the setpoint but operates at higher rates. However, in mode 3 the boiler provides hot water

depending on the outdoor temperature with just the needed temperature to maintain the setpoint inside the office. As for the SF, the solar pump works on condition that the temperature difference between the bottom of the tank and the collector's outlet is between 2°C and 10°C. since the temperature required inside the tank is lower with mode 3, the solar pump tends to operate for a relatively longer period and therefore higher solar contribution.

Table V- 4: SF and PESR monthly values for the three modes.

Months	Mode 1 (Fixed setpoint 60°C)		Mode 2 (Fixed setpoint 21°C)		Mode 3 (Heating curve)	
	SF (%)	PESR (%)	SF (%)	PESR (%)	SF (%)	PESR (%)
Nov	40.96	13.20	48.86	28.60	58.21	38.33
Dec	42.56	15.16	48.83	26.47	59.45	39.47
Jan	21.92	12.24	23.37	16.47	31.21	27.31
Feb	18.34	10.17	19.27	13.68	25.44	22.18
Mar	31.67	11.83	38.10	24.28	48.44	35.22
Total	**28.18**	**12.32**	**31.89**	**20.83**	**40.31**	**31.32**

5.5. Metamodeling and model validation

Using the RSM design, an optimum number of 15 runs only on TRNSYS were executed. The design matrix for the runs is represented in Figure V- 6. The resulted values of the SF, PESR and LCOH were recovered and an analysis of variance (ANOVA) was performed to identify the significant factors. The significance of the terms was decided based on their P-value, P-value less than 0.05 was considered to be statistically significant.
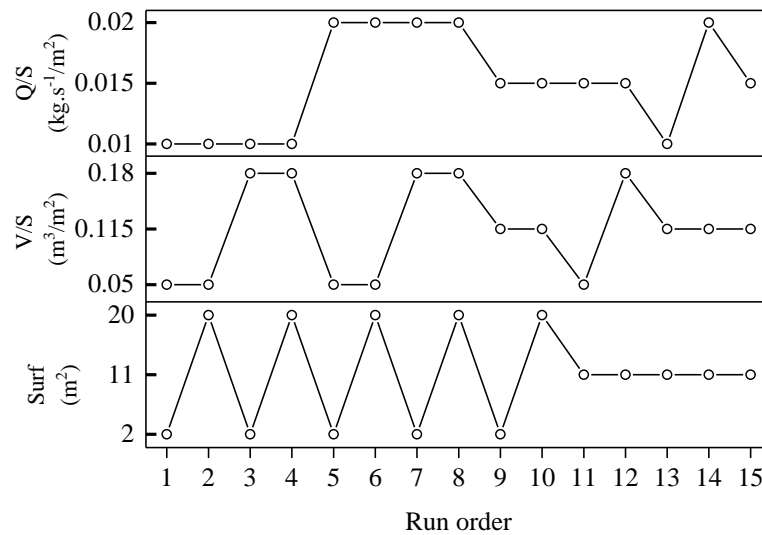
Figure V- 6: Response surface method design matrix.

Figure V- 7 represents the pareto charts for the SF, PESR and LCOH. Pareto charts help illustrate the statistical significance of the main terms and the interaction effects, which are represented by the bars to the right of the reference line in each graph. It is obvious that the collectors' area (S) is by far the most influencing factor, followed by the quadratic term (S*S) in the three responses. The storage volume as the next most significant effect represented by the two-way interaction (S*V/S) for the PESR and the LCOH and the ratio V/S for the SF which emphasize on the respect of the recommended range of the ratio V/S to ensure high SF values. The term (Q/S) appears to be statistically significant for the SF only, certainly because the flow rate in question is that of the solar loop and thus has no influence on the PESR nor the LCOH. Figure V- 8 is complementary to Figure V- 7, it represents the normal plot of the standardized effect, it displays the direction of the impact and the significance of the terms. The collector area has the major impact and represents the main cause of increasing SF, PESR and LCOH values. Since the objective is to reduce the LCOH of the system the solar collectors' area represents the main constraint for the optimization process.
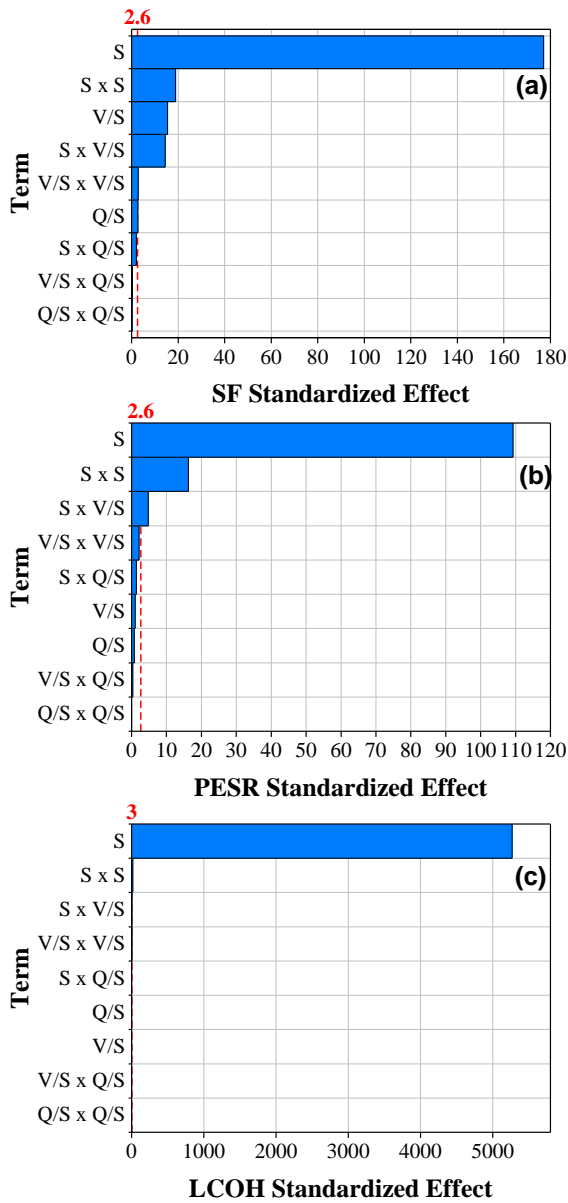
Figure V- 7: Pareto charts of the standardized effects. (a) SF, (b) PESR, (c) LCOH.
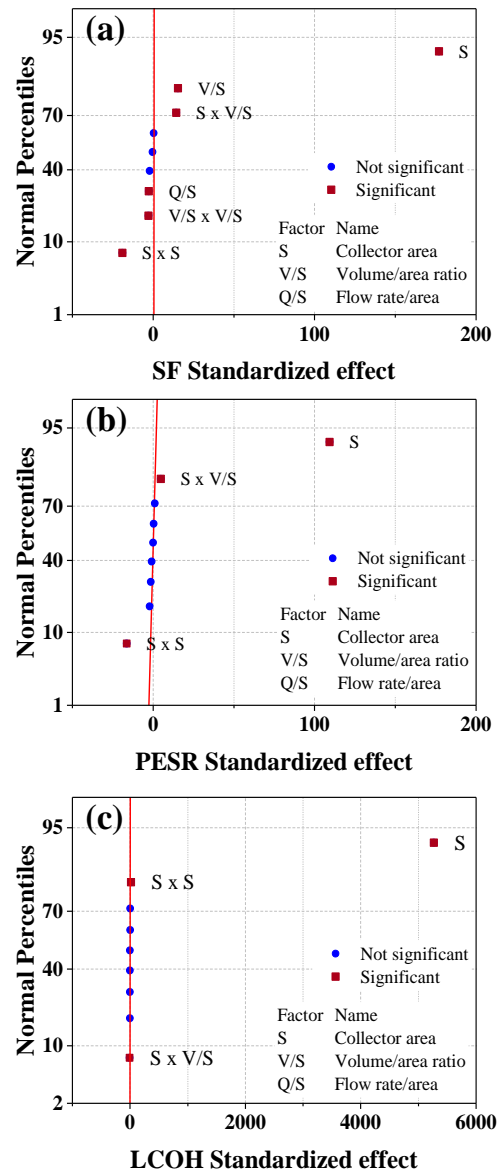
Figure V- 8: Normal plots of the standardized effects. (a) SF, (b) PESR, (c) LCOH.

After estimating the effect of the significant factors, based on the least squares' method, metamodels have been built for each response, the metamodels coefficients are presented in the Table V- 5.

Table V- 5: Metamodels coefficients of the objective functions.

y	SF	PESR	LCOH
β_0	-6.56E-2	1.024E-1	1.777
β_1	1.087E-1	5.155E-2	7.873E-1
β_2	8.36E-1	3.24E-1	-1.77E-1
β_3	1.88	1E-1	-6.6E-1
β_1^2	-1.831E-3	1.004E-3	5.63E-4
β_2^2	-5.10	2.56	1.413
β_3^2	-75	1	1
$\beta_1\beta_2$	1.099E-1	2.312E-2	-1.199E-2
$\beta_1\beta_3$	-2.031E-1	8.42E-2	4.87E-2
$\beta_2\beta_3$	4.7	3.32	-2.07

Afterwards, the adequacy of the built metamodels was verified. The variation R^2 regarding the SF, PESR and LCOH are 99.98%, 99.96% and 100% respectively, which indicates that the model fits well. However, the residual analysis is necessary to check if the model assumptions are satisfactory and to validate the regression model. The residuals indicate the difference between the calculated values from TRNSYS and the predicted values by the regression model. Figure V- 9 represents the normal probability plots of the deemed responses, the normal percentiles follow a straight line which prove the normal distribution of the residuals. Which indicates that the proposed models are adequate.
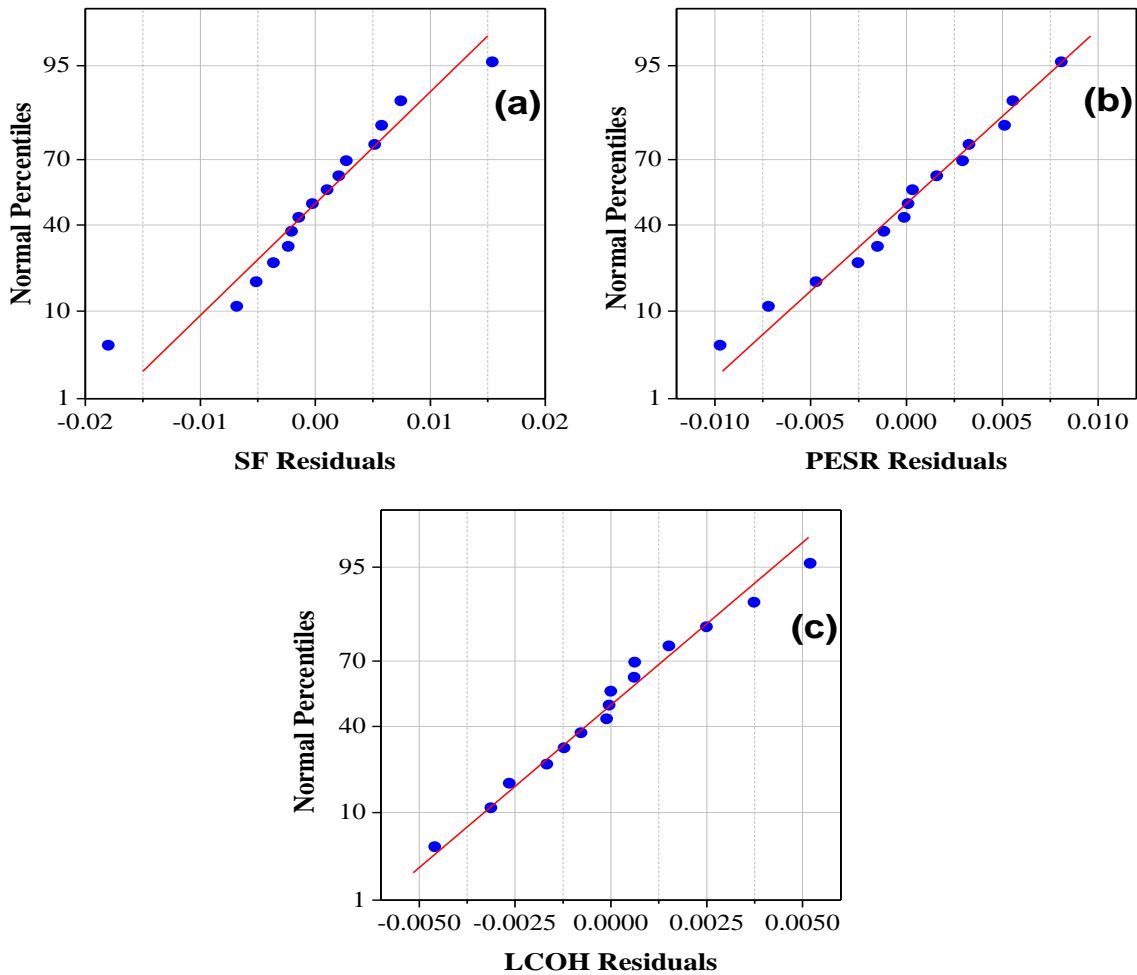
Figure V- 9: Normal probability plots. (a) SF; (b) PESR; (c) LCOH.

5.6. The effect of the decision variables on the system's performance

Based on the ANOVA results presented in the previous section, the ratio Q/S was perceived to be statistically insignificant. For that matter, that factor was held at its medium value to illustrate the responses regarding the collectors' area and the storage/volume ratio. Figure V-10 represents the contour plots for each objective function within a range of solar field [2-12] m². First, the SF certainly increases with the increase of the solar field, obviously V/S ratio has slight influence in smaller areas. Yet more importance in larger areas, higher V/S values generate higher SF for equal collector area. Second, the PESR similarly to the SF tend to rise with the increase of S. However, V/S medium values are preferable since they provide better PESR in each single contour. Finally, the LCOH is mainly influenced by S, compared to V/S ratio, which explains the merely straight lines in Figure V- 10 (c).
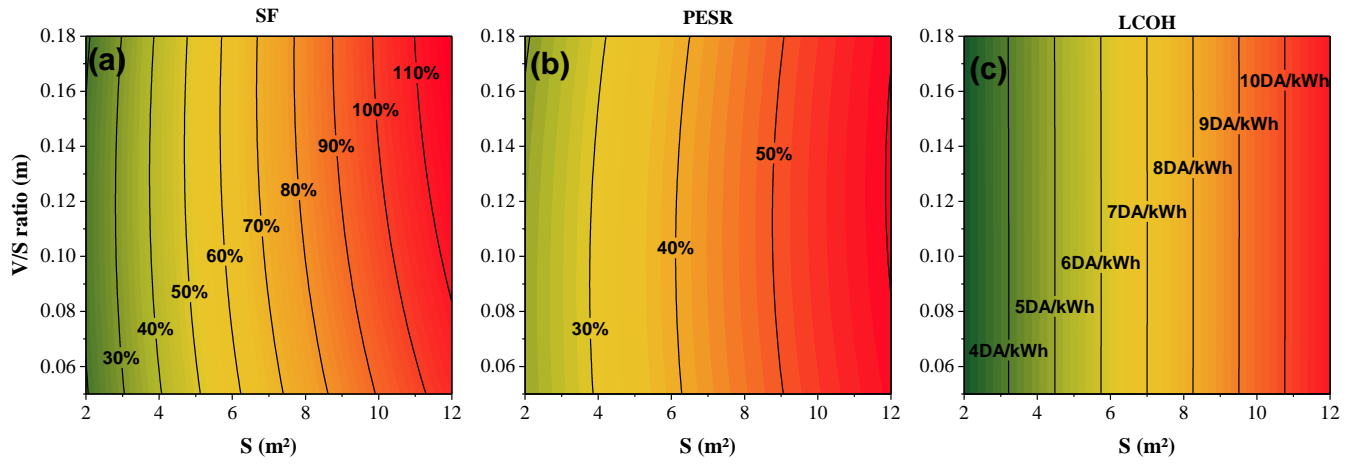
Figure V- 10: Contour plots volume to surface ratio vs collector area.
(a) SF; (b) PESR; (c) LCOH.

5.7. Multi-objective optimization of the HSGHS

5.7.1. Overlaid contour plots

The current system provides a SF and PESR of 40.31 % and 31.32 % indicated in Table V-4. With a LCOH of 4.91 DA/kWh. The LCOH is to be compared to a reference conventional system $LCOH_{ref}$. the present system without the solar part was considered as the reference system. The simulation results yielded a $LCOH_{ref}$ of 2.02 DA/kWh. The aforementioned values were selected as constraints for the definition of the optimal region.

In order to define an optimal region for a maximum SF and PESR while keeping LCOH at minimum possible values, the overlaid contours plot was used. In Figure V- 11. The patterns clearly demonstrate the difficulty of the optimization of the multiple responses, since the maximization of either PESR or SF maximize the LCOH, which opposes to the desired objectives. The LCOH augmentation is due to the elevation of the initial investment cost, the collector field cost mainly. The optimal defined region (white section) could not reach higher ranges than 50% PESR or 100% SF because of the specified constraint of LCOH 8DA/kWh which is four times higher than the value of $LCOH_{ref}$. leaving no chance to the proposed solar system to compete with the reference system. The overlaid contour represents an efficient tool for engineers or designers in the definition of the optimal set range of parameters to facilitate the decisions of the stakeholders.

117
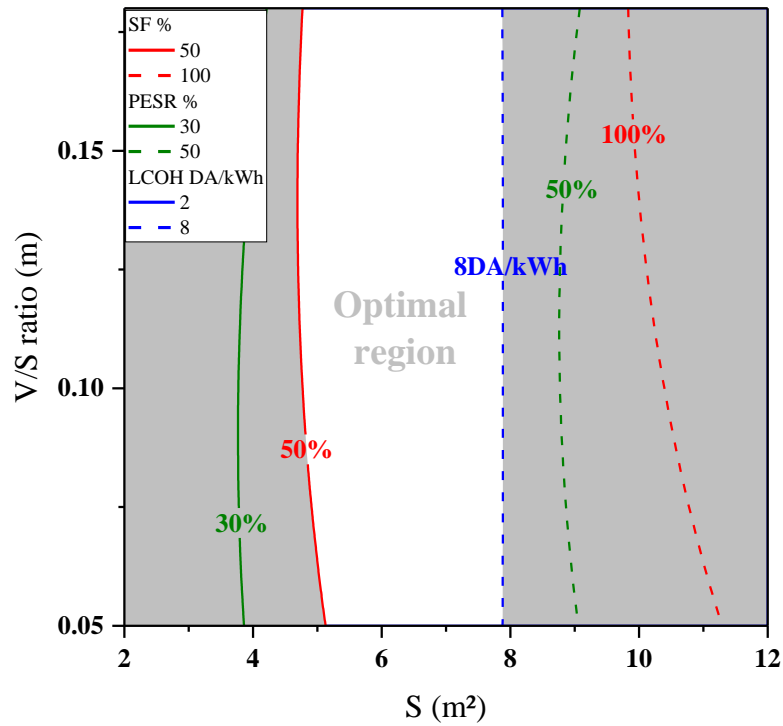
Figure V- 11: Overlayed contours plot, optimal region.

5.7.2. Pareto fronts

The overlayed contour plots define an optimal region for the objective functions. However, the pareto fronts determine the non-dominated solutions, that is the best solutions that provide maximum SF and PESR and minimum LCOH. For that matter, the paretosearch algorithm in MATLAB was used. First, three bi-objective optimizations were considered (SF-PESR), (SF-LCOH) and (PESR-LCOH), to identify the maximum values of SF and PESR and the minimum LCOH achievable for the objective function. Then a tri-objective optimization was executed regarding the three objective functions.

The pareto fronts for the PESR versus SF, LCOH versus SF and LCOH versus PESR obtained through bi-objective optimization process are depicted in Figure V- 12. It can be seen in this figure that the maximum attained PESR is 57.05 % against approximately 100% for solar fraction. This observation is nontrivial, it leads to an interesting reasoning that the solar fraction as a sole performance indicator for hybrid solar systems is not reliable. In fact, a high production of the solar field can conceal the inefficiency of the system. The SF does not give any indication on the overall performance. Known above that LCOH and PESR even LCOH and SF are contradictory objectives and increasing SF or PESR means increasing the initial investment of the solar system. It can be seen in Figure V- 12 (b) and (c) that for the points A and C the SF and PESR are highest and the LCOH is highest (10.69 DA/kWh). For points B and D, the opposite is observed. When the optimization objective is solely the PESR or SF; points A and

118

C are the best solutions. When LCOH only is to be optimized points B and D are the best solutions. The steep slope in Figure V- 12 (b) and (c) indicates that the LCOH increase significantly when SF or PESR increase.

Figure V- 13 shows the pareto frontier of the three objective functions obtained via a tri-objective optimization. The results showed that the optimal solutions, with the constraints in Table V- 3, are located between SF (20%), PESR (22%), LCOH (3.33DA/kWh), lowest point in the pareto front, corresponding to the best solution regarding LCOH and SF (100%), PESR (50%) and LCOH (10.69 DA/kWh).
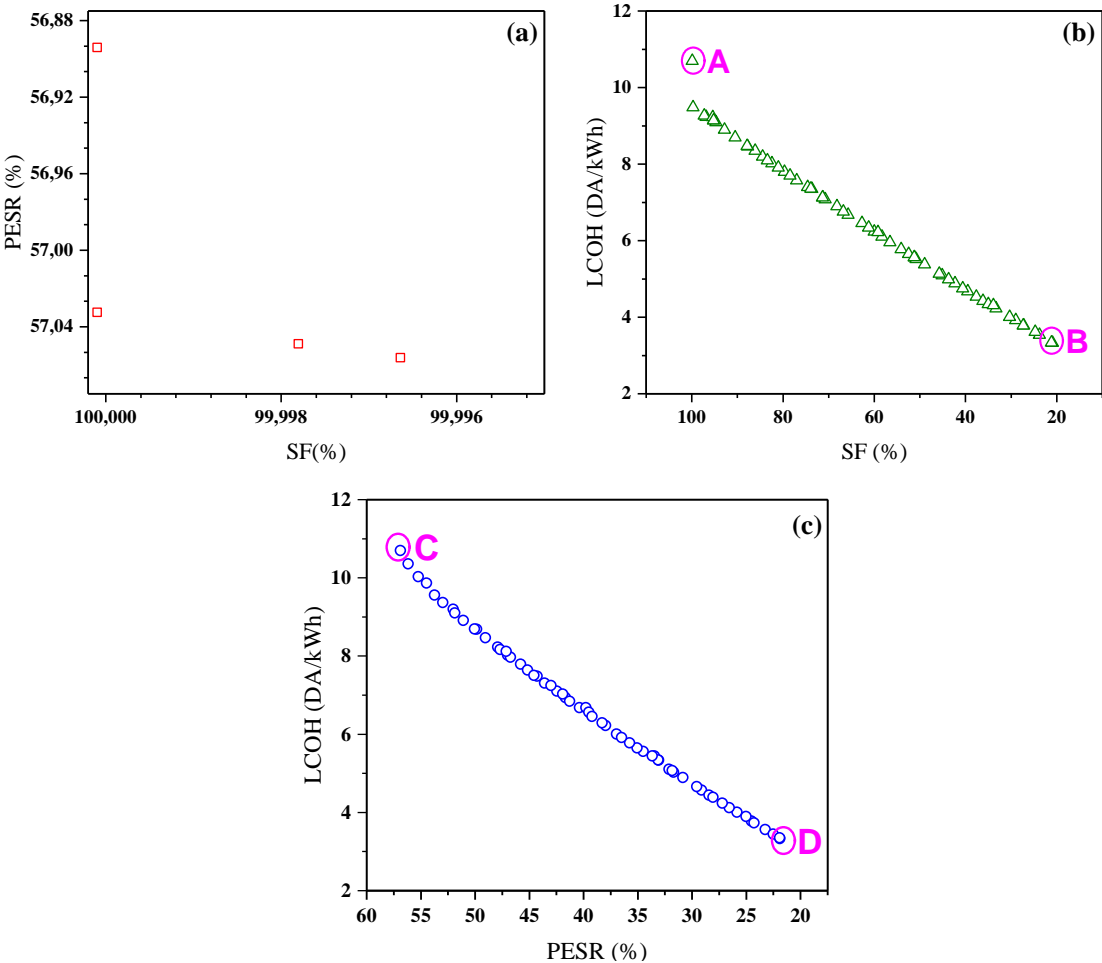
Figure V- 12: Bi-objective optimization pareto fronts. (a) PESR vs SF; (b) LCOH vs SF; (c) LCOH vs PESR.

5.7.3. LINMAP decision making

Every point on the pareto fronts is an optimal solution. To help in the decision making of the most desirable solution, the LINMAP method was utilized. LINMAP is a popular method used for the decision making in multidimensional analysis. Since the objective functions are of different dimensions, the LINMAP method employs the Euclidian non-dimensionalization to

render the objective vectors dimensionless. For both maximizing and minimizing objectives the normalized vectors are defined as follows[135]:

$$F_{ij}^n = \frac{F_{ij}}{\sum_{j=1}^m (F_{ij})^2} \qquad (\text{V. 8})$$

Where F_{ij} represent the solution vector, $(i = 1,2,...,k)$ and $(j = 1,2,...,m)$ are index of alternative solutions and objective function, respectively. m denotes the number of objective functions.

The ideal solution in conflicting objective is usually impossible to attain. For instance, in bi-objective optimization, when one objective reaches its optimum the other would be at its worst. To determine the best solution, the Euclidian distance d_{i+} of each solution from ideal one F_{ideal} is estimated using Eq(V. 9), the shortest distance would represent the best optimal solution from the pareto front. The Euclidian distance is expressed by the following equation [135]:

$$d_{i+} = \sqrt{\sum_{j=1}^m (F_{ij} - F_{ideal})^2} \qquad (\text{V. 9})$$

the best optimal solution would have the minimum distance d_{i+}, consequently i_{final} is given by :

$$i_{final} = i \in \min(d_{i+}) \qquad (\text{V. 10})$$

The best optimal solution for our multi-objective optimization problem is represented by the black dot in Figure V- 13. The values of the objective functions are 72%, 42% and 7.22 DA/kWh, respectively to SF, PESR and LCOH. The decision variables of the three optimal solutions are presented in Table V- 6.

Table V- 6: LINMAP best optimal solution.

	SF	PESR	LCOH	S	V/S	Q/S
Unit	%	%	DA/kWh	m²	m³/m²	kg.s⁻¹/m².
LINMAP	78,46	44,87	7,7	9,87	0,17	0,02
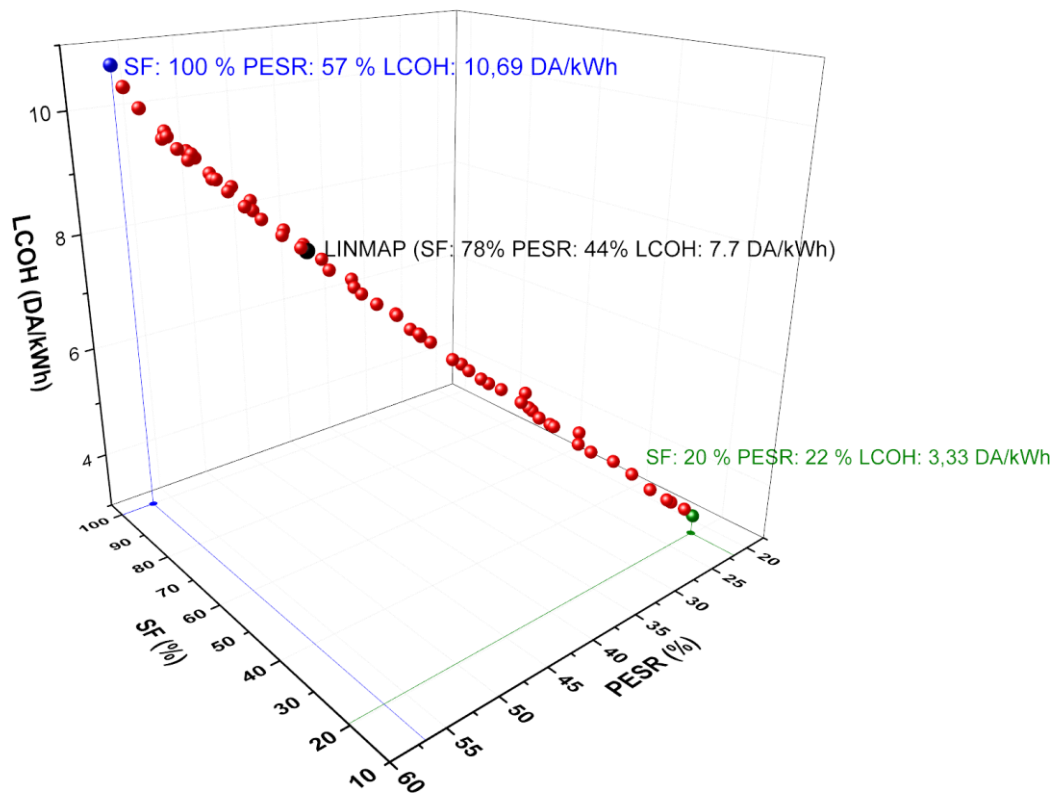
Figure V- 13: Tri-objective optimization pareto front; (LINMAP solution).

Despite the high SF and the moderate PESR presented by the LINMAP solution which is a trade-off between the three objective functions, the economic aspect still represents an obstacle in adopting the HSGHS system. The high LCOH is mainly due to the expensiveness of initial investment cost, because of the import of the different features of the solar heating system namely, the solar collectors and the controller. Furthermore, the low price of the natural gas and the subsidies in Algeria, gas-producing country. These arguments explain the high value of the LCOH. Therefore, subsidizing the purchase and the installation of solar heating systems would set the groundwork for a fairly equitable comparison with conventional systems. Finally, in order to integrate and vulgarize the solar heating systems in the Algerian market, effective policies should be made on a long-term view to promote the local production of certain equipment of the solar heating systems.

5.8. Subsidy scenario

Financial support for the use of solar heating system scenario is considered in this section to examine this possibility and how would this support influence the LCOH. The National Agency for the Promotion and Rationalization of Energy Use (APRUE), has undertaken several actions, including, within the framework of the National Energy Management Program, the program called "ALSOL".

This program aims to promote solar water heaters, to initiate the market, to encourage the creation of new industrial operators, and to develop networks of installers and energy service establishments. Ultimately, it is expected that the solar water heater will be manufactured locally and that a sustainable solar thermal market will be established in Algeria. This program is the first pilot program of its kind in Algeria. It provides direct financial support up to 45% of the cost of the installed individual solar water heater and 35% for a collective solar heating system through the National Fund for Energy Management (FNME) [136].

Therefore, a subsidy of 45% on the investment cost of the solar part of the current system is undertaken to simulate the economic performance of the hybrid solar system under this scenario.

The multi-objective optimization through MATLAB was utilized to retrieve the pareto front of the new LCOH, the SF and the PESR. Using the metamodel constructed before for the LCOH with subsidy, the pareto fronts displayed in Figure V- 14. illustrate the comparison between the two scenarios. It is obvious that the LCOH decreased significantly in the subsidy scenario. In fact, the same solution from energy point of view was defined by the LINMAP technique. However, the new LCOH presents a lower value of 4.87 DA/kWh instead of 7.70 DA/kWh. The standard deviation increases with higher SF and PESR indicating that the subsidy would be even more interesting in larger systems with higher performance.
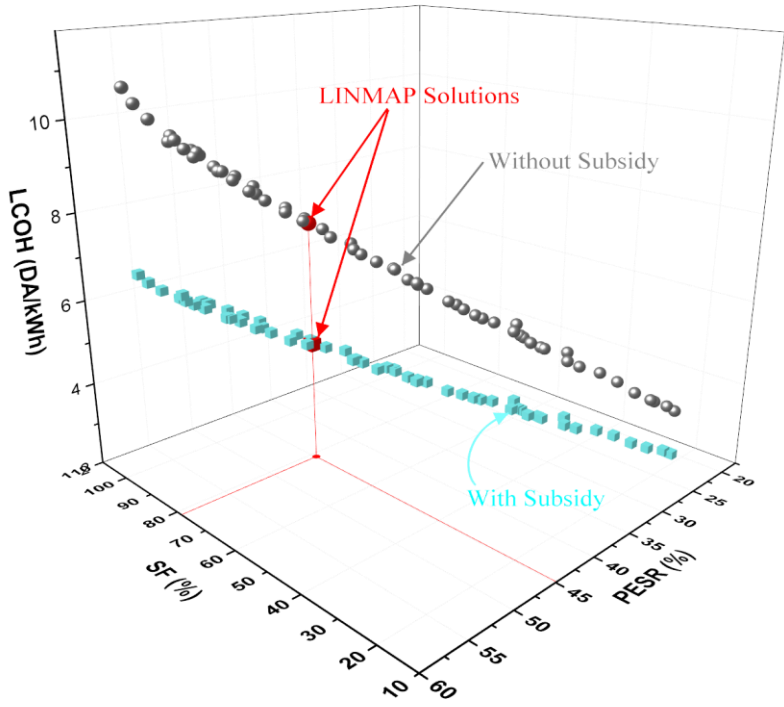
Figure V- 14: Tri-objective optimization comparison between the two scenarios.

5.9. Improving current configuration

The current operational configuration could be improved, by connecting the solar loop to a heat exchanger which is expected to increase the solar fraction, also a three-way valve in the distribution loop would help in reducing the energy consumption while maintaining the thermal comfort of the occupant inside the building. Figure V- 15 shows the schemes of the proposed configuration and the instrumentation.
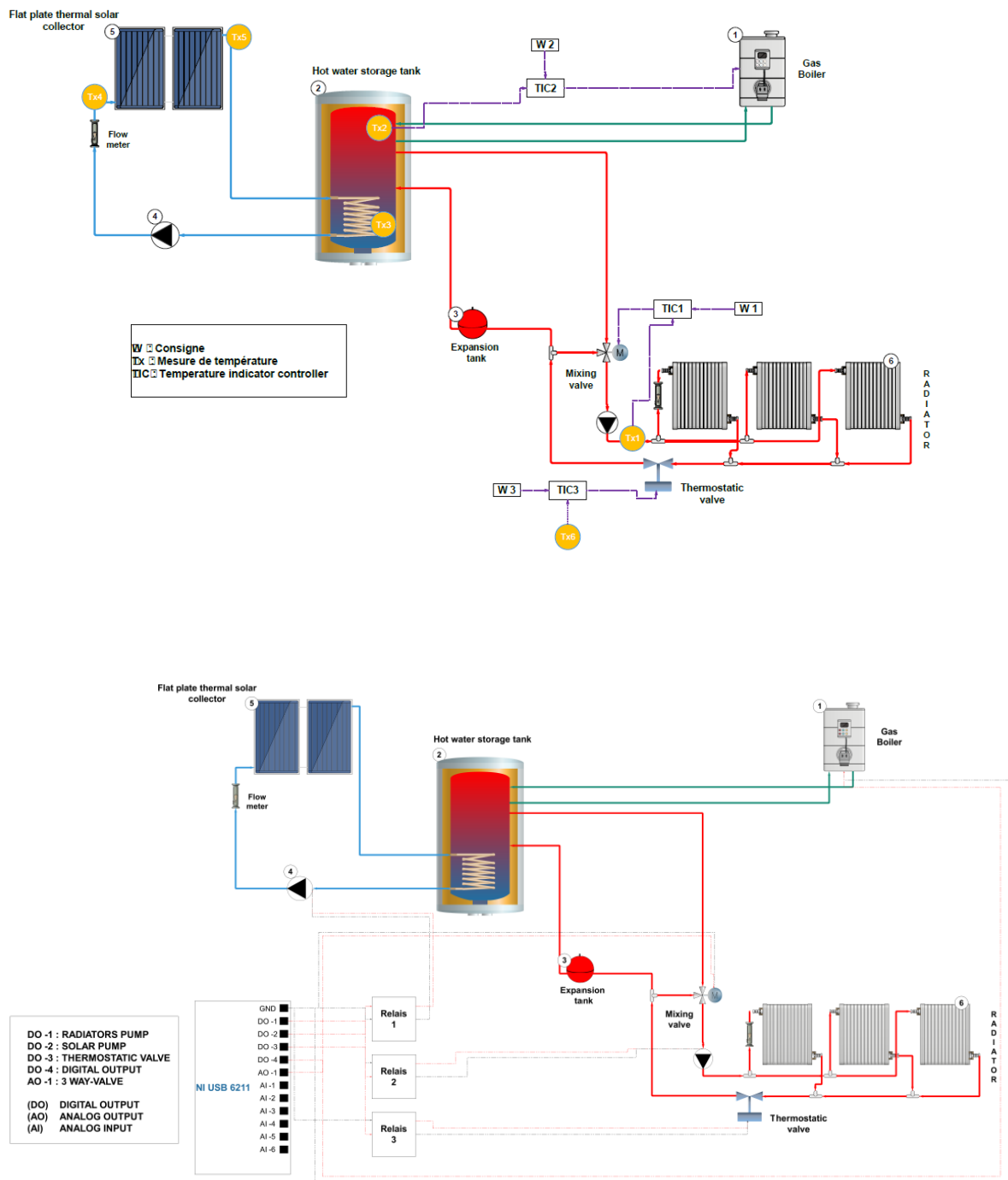
Figure V- 15: Proposed scheme for the HSGHS improvements.

5.10. Conclusion

In this chapter, we presented the upgraded TRNSYS model. The impact of the control strategy was then analyzed regarding SF and PESR. A multi-objective optimization approach was proposed to optimize the configuration of the HSGHS. The method combined RSM and GA with dynamic simulations on TRNSYS. The energy and economic performance of the system was comprehensively evaluated using three indicators, including the SF, PESR and LCOH which were considered as objective functions for the multi-objective optimization. Additionally, the multi-criteria decision-making technique LINMAP was employed to select the best option in the pareto front solutions. According to the study results, the main conclusions are summarized as follows:

(1) The control strategy plays a key role in the enhancement of the system's performance to benefit from the synergy between the two energy sources, the adopted control mode proved an increase from 12% to 31% in PESR and from 28% to 40% in SF.

(2) The results of the bi-objective optimization of SF-PESR showed that for 100% SF the maximum PESR achieved was 57% which proves the necessity of considering a secondary energy indicator with the SF when describing the energy savings and the solar contribution of hybrid solar systems.

(3) The combination of the DoE to the proposed multi-objective optimization methodology reduced significantly the number of simulations to 15 runs only saving remarkably the optimization computing time.

(4) The multi-objective optimization provided a set of optimal solutions, pareto front, the selection of the best option was realized by the LINMAP decision making technique. The best solution obtained was a trade-off between SF, PESR and LCOH with 72%, 42% and 7.22 DA/kWh, respectively.

(5) The HSGHS technology is a viable alternative in terms of energy savings in north African regions and can lead to considerable benefits. However, from economic point of view, the system is still noncompetitive compared to conventional systems in the Algerian context. The high initial investment costs and the low price of the natural gas may act as a financial obstacle that might eventually slow down the implementation of such systems.

The proposed methodology can be applied to any hybrid solar system for whatever objective functions with the same number of simulations/experiments regarding the number of decision variables.

Further investigations on the HSGHS are warranted in future works, the ecological aspect is deserving with the current progress towards clean and sustainable structures, also the building geometry and envelops optimization requires more attention for their significant impact on the energy demand and the environment.

Conclusions and perspectives

General conclusions

The general conclusions of this dissertation are divided into three sections. The first section provides a summary of our scientific contributions along the present dissertation. The second part of the conclusions summarizes the limitations of the present work. The third part exposes the perspectives issued out of this dissertation.

Contributions

In the present research work, we proposed to develop a hybrid solar/gas system capable of providing heat to an office building. The aim is to evaluate the performance of such system in the Algerian context where both energy sources, solar and natural gas, are abundant in order to provide answers about the performance of solar hybrid systems under that climate and about the non-development of solar thermal market in Algeria. This act alongside the shift towards designing and developing efficient solar systems, which lead to further requirements of performance, causes the design and optimization process more and more complex. Adopting a method that is capable of, firstly providing accurate predictions and evaluating the influence of the design parameters on the systems' performance, and secondly optimize the design of the systems to find a trade-off between energy savings and economic profitability.

For this reason, in the present research work, we proposed the combined use of numerical simulations, design of experiments technique and an optimization process based on genetic algorithm. Energy performance simulations are capable of providing adequate results with less time and cost. DoE techniques enables the development of metamodeling relationships between studied variables and design parameters. These metamodels allow the prediction of studied variables in a fast and simple way, as well as to identify the most influential parameters on the studied variables, so that we can know where to extend investigation in the design process. In addition, the metamodels allowed us to search for optimal design of the hybrid solar system in a multi-criterion dimension.

An experimental unit of the hybrid solar/gas heating system have been developed, the unit was equipped with sensors and acquisition system that allow the monitoring and the data collection. Experiments were performed during the winter of 2020 and experimental investigation of the system's performance was carried out. A dynamic numerical model was developed in TRNSYS and experimental measurement were used to validate the developed model. The proposed method was then applied to the numerical model to perform sensitivity analysis and to develop metamodels to approximate the solar fraction as a function of the predefined factors. Using the desirability function approach, the metamodels were used to

integrate the solar fraction in the optimization process of system design. The results showed that the use of the adopted methodology permits to achieve better performance by identifying the optimal design parameters.

The numerical model was improved incorporating a new control strategy to benefit the most from the synergy between the two energy sources. In hybrid operation mode, the primary energy savings and the levelized cost of heat were added to the solar fraction as objective functions to find a reasonable trade-off between the desired objectives. A comparative study between three control strategy modes was performed. The results indicate that a suitable control strategy would significantly improve the solar contribution and increase energy-savings. The best control strategy was then integrated in the numerical model and the effect of the design parameters on the objective functions was investigated through a sensitivity analysis.

Moreover, the DoE technique reduced the number of experiments to an optimal number allowing the designer to develop metamodels for each objective function. These metamodels were employed in a multiobjective optimization process using genetic algorithm to find the Pareto front of the optimal solutions. Furthermore, the metamodels when written in their vectorized form reduce the computing time. The results of the multiobjective optimization indicate that the use of solar fraction as a sole evaluation criterion in hybrid solar systems is not viable, therefore an indicator of energy savings is required. The multiobjective optimization provides a set of optimal solutions, the use of decision-making technique is often required, the LINMAP technique was utilized in the current study to select the best optimal solution. Even though the system showed better performance the energy cost was still high compared to the conventional system because of high investment costs and low fuel price.

Finally, we succeeded in achieving a trade-off between thermal performance energy-savings and energy cost. For this reason, we now propose a generalized framework for the design of energy-efficient hybrid solar systems. This includes the following stages:

1. Adopt an energy performance simulation tool and develop a reliable numerical model.
2. Define response variables, based on the functional requirements (such as thermal performance, energy savings, economic and environmental impacts, etc.) and design parameters. Design parameters ranges could be obtained from standards recommendations.
3. Choose an experimental design plan (full factorial, composite …etc.) depending on the number of design parameters and perform numerical simulation for each experiment.
4. Identify critical parameters using statistical analysis (ANOVA).

128

5. Develop meta-modeling relationships between response variables and design parameters. Meta-models should then be validated using graphical methods or by comparing their predictions to additional random simulations.

6. Launch an optimization process to achieve desired objectives.

Limitations

The limitations of this research work are the following:

- The current system was limited in terms of configuration (orientation of the tank, positions of inlets and outlets)

- It is noteworthy that the results of this study applied to the case of an office building, cannot be considered as guidelines for designers, except for strictly similar buildings in terms of geometry, final use, and climate area. Indeed, each system requires a specific optimization analysis.

- The proposed approach is applied to a very specific case study and the use of the metamodels is restricted to the range of the factors' levels

- Few parameters are considered in this analysis.

Perspectives

To overcome the limitation of the present research work, some possible directions in which future work should be oriented as follows:

- Extend the application of the proposed approach to other configurations.

- Increase the number of parameters and response variables by simultaneously considering several issues (energy, economic, environmental …etc.). DoE technique could help in reducing drastically the number of simulations, when increasing the number of parameters, by applying different types of experimental design.

- The current operational configuration could be improved, by connecting the solar loop to a heat exchanger which is expected to increase the solar fraction, also a three-way valve in the distribution loop would help in reducing the energy consumption while maintaining the thermal comfort of the occupant inside the building. Figure V- 15. shows the schemes of the proposed configuration and the instrumentation.

References

References

[1] M. Colakoglu and A. Durmayaz, "Energy, exergy and environmental-based design and multiobjective optimization of a novel solar-driven multi-generation system," *Energy Conversion and Management*, vol. 227, p. 113603, Jan. 2021, doi: 10.1016/j.enconman.2020.113603.

[2] C. Waibel, R. Evins, and J. Carmeliet, "Co-simulation and optimization of building geometry and multi-energy systems: Interdependencies in energy supply, energy demand and solar potentials," *Applied Energy*, vol. 242, pp. 1661–1682, May 2019, doi: 10.1016/j.apenergy.2019.03.177.

[3] V. Tulus, D. Boer, L. F. Cabeza, L. Jiménez, and G. Guillén-Gosálbez, "Enhanced thermal energy supply via central solar heating plants with seasonal storage: A multi-objective optimization approach," *Applied Energy*, vol. 181, pp. 549–561, Nov. 2016, doi: 10.1016/j.apenergy.2016.08.037.

[4] A. J. Marszal *et al.*, "Zero Energy Building – A review of definitions and calculation methodologies," *Energy and Buildings*, vol. 43, no. 4, pp. 971–979, Apr. 2011, doi: 10.1016/j.enbuild.2010.12.022.

[5] F. Chlela, A. Husaunndee, C. Inard, and P. Riederer, "A new methodology for the design of low energy buildings," *Energy and Buildings*, vol. 41, no. 9, pp. 982–990, Sep. 2009, doi: 10.1016/j.enbuild.2009.05.001.

[6] J. Williams *et al.*, "Less is more: A review of low energy standards and the urgent need for an international universal zero energy standard," *Journal of Building Engineering*, vol. 6, pp. 65–74, Jun. 2016, doi: 10.1016/j.jobe.2016.02.007.

[7] F. Salata, V. Ciancio, J. Dell'Olmo, I. Golasi, O. Palusci, and M. Coppi, "Effects of local conditions on the multi-variable and multi-objective energy optimization of residential buildings using genetic algorithms," *Applied Energy*, vol. 260, p. 114289, Feb. 2020, doi: 10.1016/j.apenergy.2019.114289.

[8] U. Persson and S. Werner, "Heat distribution and the future competitiveness of district heating," *Applied Energy*, vol. 88, no. 3, pp. 568–576, Mar. 2011, doi: 10.1016/j.apenergy.2010.09.020.

[9] R. S. Kamel, A. S. Fung, and P. R. H. Dash, "Solar systems and their integration with heat pumps: A review," *Energy and Buildings*, vol. 87, pp. 395–412, Jan. 2015, doi: 10.1016/j.enbuild.2014.11.030.

[10] University of Wisconsin--Madison. Solar Energy Laboratory, *TRNSYS, a transient simulation program*. Madison, Wis. : The Laboratory, 1975., 1975. [Online]. Available: https://search.library.wisc.edu/catalog/999800551102121

[11] G. Derringer and R. Suich, "Simultaneous Optimization of Several Response Variables," *Journal of Quality Technology*, vol. 12, no. 4, pp. 214–219, Oct. 1980, doi: 10.1080/00224065.1980.11980968.

[12] *MATLAB. (2019). version 7.10.0 (R2019a). Natick, Massachusetts: The MathWorks Inc.*

[13] "Data & Statistics," *IEA*. https://www.iea.org/data-and-statistics (accessed Mar. 23, 2021).

[14] A. Robert and M. Kummert, "Designing net-zero energy buildings for the future climate, not for the past," *Building and Environment*, vol. 55, pp. 150–158, Sep. 2012, doi: 10.1016/j.buildenv.2011.12.014.

[15] D. Ürge-Vorsatz, L. F. Cabeza, S. Serrano, C. Barreneche, and K. Petrichenko, "Heating and cooling energy trends and drivers in buildings," *Renewable and Sustainable Energy Reviews*, vol. 41, pp. 85–98, Jan. 2015, doi: 10.1016/j.rser.2014.08.039.

[16] L. De Boeck, S. Verbeke, A. Audenaert, and L. De Mesmaeker, "Improving the energy performance of residential buildings: A literature review," *Renewable and Sustainable Energy Reviews*, vol. 52, pp. 960–975, Dec. 2015, doi: 10.1016/j.rser.2015.07.037.

[17] M. G. Alpuche, I. González, J. M. Ochoa, I. Marincic, A. Duarte, and E. Valdenebro, "Influence of Absorptance in the Building Envelope of Affordable Housing in Warm Dry Climates," *Energy Procedia*, vol. 57, pp. 1842–1850, 2014, doi: 10.1016/j.egypro.2014.10.048.

[18] N. Aste, A. Angelotti, and M. Buzzetti, "The influence of the external walls thermal inertia on the energy performance of well insulated buildings," *Energy and Buildings*, vol. 41, no. 11, pp. 1181–1187, Nov. 2009, doi: 10.1016/j.enbuild.2009.06.005.

[19] R. M. Lazzarin, "Condensing boilers in buildings and plants refurbishment," *Energy and Buildings*, vol. 47, pp. 61–67, Apr. 2012, doi: 10.1016/j.enbuild.2011.11.029.

[20] N. Kannan and D. Vakeesan, "Solar energy for future world: - A review," *Renewable and Sustainable Energy Reviews*, vol. 62, pp. 1092–1105, Sep. 2016, doi: 10.1016/j.rser.2016.05.022.

[21] T. T. Chow, "A review on photovoltaic/thermal hybrid solar technology," *Applied Energy*, vol. 87, no. 2, pp. 365–379, Feb. 2010, doi: 10.1016/j.apenergy.2009.06.037.

[22] P. M. Cuce and S. Riffat, "A comprehensive review of heat recovery systems for building applications," *Renewable and Sustainable Energy Reviews*, vol. 47, pp. 665–682, Jul. 2015, doi: 10.1016/j.rser.2015.03.087.

[23] "Medical Assistants : Occupational Outlook Handbook: : U.S. Bureau of Labor Statistics." https://www.bls.gov/ooh/healthcare/medical-assistants.htm (accessed Mar. 23, 2021).

[24] D. Kolokotsa, D. Tsiavos, G. S. Stavrakakis, K. Kalaitzakis, and E. Antonidakis, "Advanced fuzzy logic controllers design and evaluation for buildings' occupants thermal–visual comfort and indoor air quality satisfaction," *Energy and Buildings*, vol. 33, no. 6, pp. 531–543, Jul. 2001, doi: 10.1016/S0378-7788(00)00098-0.

[25] S. Kalogirou, *Solar energy engineering: processes and systems*, Second edition. Amsterdam ; Boston: Elsevier, AP, Academic Press is an imprint of Elsevier, 2014.

[26] A. Rey and R. Zmeureanu, "Multi-objective optimization framework for the selection of configuration and equipment sizing of solar thermal combisystems," *Energy*, vol. 145, pp. 182–194, Feb. 2018, doi: 10.1016/j.energy.2017.10.125.

[27] M. Raisul Islam, K. Sumathy, and S. Ullah Khan, "Solar water heating systems and their market trends," *Renewable and Sustainable Energy Reviews*, vol. 17, pp. 1–25, Jan. 2013, doi: 10.1016/j.rser.2012.09.011.

[28] E. Vengadesan and R. Senthil, "A review on recent development of thermal performance enhancement methods of flat plate solar water heater," *Solar Energy*, vol. 206, pp. 935–961, Aug. 2020, doi: 10.1016/j.solener.2020.06.059.

[29] K. K. Matrawy and I. Farkas, "Comparison study for three types of solar collectors for water heating," *Energy Conversion and Management*, vol. 38, no. 9, pp. 861–869, Jun. 1997, doi: 10.1016/S0196-8904(96)00089-1.

[30] H. Hottle and A. Whillier, "Evaluation of flat-plate solar collector performance," *Transaction of conference on the use of Solar Energy*, vol. 02, pp. 74–104, Jan. 1958.

[31] M. Kovarik, "Optimal distribution of heat conducting material in the finned pipe solar energy collector," *Solar Energy*, vol. 21, no. 6, pp. 477–484, 1978, doi: 10.1016/0038-092X(78)90071-3.

[32] K. G. T. Hollands and B. A. Stedman, "Optimization of an absorber plate fin having a step-change in local thickness," *Solar Energy*, vol. 49, no. 6, pp. 493–495, Dec. 1992, doi: 10.1016/0038-092X(92)90157-6.

[33] B. Kundu, "Performance analysis and optimization of absorber plates of different geometry for a flat-plate solar collector: a comparative study," *Applied Thermal Engineering*, vol. 22, no. 9, pp. 999–1012, Jun. 2002, doi: 10.1016/S1359-4311(01)00127-2.

[34] F. C. O'Brien-Bernini and J. G. McGowan, "Performance modeling of non-metallic flat plate solar collectors," *Solar Energy*, vol. 33, no. 3–4, pp. 305–319, 1984, doi: 10.1016/0038-092X(84)90161-0.

[35] K. Sopian, R. Zulkifli, J. Sahari, and M. Y. Othman, "Thermal performance of thermoplastic natural rubber solar collector," *Journal of Materials Processing Technology*, vol. 123, no. 1, pp. 179–184, Apr. 2002, doi: 10.1016/S0924-0136(02)00093-6.

[36] C. Dorfling, C. H. Hornung, B. Hallmark, R. J. J. Beaumont, H. Fovargue, and M. R. Mackley, "The experimental response and modelling of a solar heat collector fabricated from plastic microcapillary films," *Solar Energy Materials and Solar Cells*, vol. 94, no. 7, pp. 1207–1221, Jul. 2010, doi: 10.1016/j.solmat.2010.03.008.

[37] S. Furbo and L. Jivan Shah, "Thermal advantages for solar heating systems with a glass cover with antireflection surfaces," *Solar Energy*, vol. 74, no. 6, pp. 513–523, Jun. 2003, doi: 10.1016/S0038-092X(03)00186-5.

[38] R. Shukla, K. Sumathy, P. Erickson, and J. Gong, "Recent advances in the solar water heating systems: A review," *Renewable and Sustainable Energy Reviews*, vol. 19, pp. 173–190, Mar. 2013, doi: 10.1016/j.rser.2012.10.048.

[39] Y. Kim and T. Seo, "Thermal performances comparisons of the glass evacuated tube solar collectors with shapes of absorber tube," *Renewable Energy*, vol. 32, no. 5, pp. 772–795, Apr. 2007, doi: 10.1016/j.renene.2006.03.016.

[40] M. M. A. Khan, N. I. Ibrahim, I. M. Mahbubul, H. Muhammad. Ali, R. Saidur, and F. A. Al-Sulaiman, "Evaluation of solar collector designs with integrated latent heat thermal energy storage: A review," *Solar Energy*, vol. 166, pp. 334–350, May 2018, doi: 10.1016/j.solener.2018.03.014.

[41] J. Settino *et al.*, "Overview of solar technologies for electricity, heating and cooling production," *Renewable and Sustainable Energy Reviews*, vol. 90, pp. 892–909, Jul. 2018, doi: 10.1016/j.rser.2018.03.112.

[42] N. Altuntop, M. Arslan, V. Ozceyhan, and M. Kanoglu, "Effect of obstacles on thermal stratification in hot water storage tanks," *Applied Thermal Engineering*, vol. 25, no. 14–15, pp. 2285–2298, Oct. 2005, doi: 10.1016/j.applthermaleng.2004.12.013.

[43] J. Rhee, A. Campbell, A. Mariadass, and B. Morhous, "Temperature stratification from thermal diodes in solar hot water storage tank," *Solar Energy*, vol. 84, no. 3, pp. 507–511, Mar. 2010, doi: 10.1016/j.solener.2009.12.007.

[44] A. A. Dehghan and A. Barzegar, "Thermal performance behavior of a domestic hot water solar storage tank during consumption operation," *Energy Conversion and Management*, vol. 52, no. 1, pp. 468–476, Jan. 2011, doi: 10.1016/j.enconman.2010.06.075.

[45] L. M. Ayompe and A. Duffy, "Thermal performance analysis of a solar water heating system with heat pipe evacuated tube collector using data from a field trial," *Solar Energy*, vol. 90, pp. 17–28, Apr. 2013, doi: 10.1016/j.solener.2013.01.001.

[46] J. Shi, K. Lin, Z. Chen, and H. Shi, "Annual dynamic thermal performance of solar water heaters: A case study in China's Jiangsu Province," *Energy and Buildings*, vol. 173, pp. 399–408, Aug. 2018, doi: 10.1016/j.enbuild.2018.04.048.

[47] S. Singh, A. Kumar, and A. Yadav, "Experimental Investigation of Thermal Performance Evaluation of Solar Flat Plate Collector," *Materials Today: Proceedings*, vol. 24, pp. 1533–1540, 2020, doi: 10.1016/j.matpr.2020.04.473.

[48] W. A. Beckman, S. A. Klein, and J. A. Duffie, *Solar heating design, by the f-chart method*. New York: Wiley, 1977.

[49] J. A. Duffie and W. A. Beckman, *Solar Engineering of Thermal Processes.* Somerset: Wiley, 2013. Accessed: Jun. 24, 2020. [Online]. Available: http://public.ebookcentral.proquest.com/choice/publicfullrecord.aspx?p=4434532

[50] J. A. Duffie and W. A. Beckman, *Solar engineering of thermal processes*, 2nd ed. New York: Wiley, 1991.

[51] S. A. Klein and W. A. Beckman, "A general design method for closed-loop solar energy systems," *Solar Energy*, vol. 22, no. 3, pp. 269–282, 1979, doi: 10.1016/0038-092X(79)90142-7.

[52] L. M. Ayompe, A. Duffy, S. J. McCormack, and M. Conlon, "Validated TRNSYS model for forced circulation solar water heating systems with flat plate and heat pipe evacuated tube collectors," *Applied Thermal Engineering*, vol. 31, no. 8–9, pp. 1536–1542, Jun. 2011, doi: 10.1016/j.applthermaleng.2011.01.046.

[53] D. Jonas, M. Lämmle, D. Theis, S. Schneider, and G. Frey, "Performance modeling of PVT collectors: Implementation, validation and parameter identification approach using TRNSYS," *Solar Energy*, vol. 193, pp. 51–64, Nov. 2019, doi: 10.1016/j.solener.2019.09.047.

[54] B. Delač, B. Pavković, and K. Lenić, "Design, monitoring and dynamic model development of a solar heating and cooling system," *Applied Thermal Engineering*, vol. 142, pp. 489–501, Sep. 2018, doi: 10.1016/j.applthermaleng.2018.07.052.

[55] A. Mehmood, A. Waqas, Z. Said, S. M. A. Rahman, and M. Akram, "Performance evaluation of solar water heating system with heat pipe evacuated tubes provided with natural gas backup," *Energy Reports*, vol. 5, pp. 1432–1444, Nov. 2019, doi: 10.1016/j.egyr.2019.10.002.

[56] J. Deng, Z. Tian, J. Fan, M. Yang, S. Furbo, and Z. Wang, "Simulation and optimization study on a solar space heating system combined with a low temperature ASHP for single family rural residential houses in Beijing," *Energy and Buildings*, vol. 126, pp. 2–13, Aug. 2016, doi: 10.1016/j.enbuild.2016.05.019.

[57] S. Bahria, M. Amirat, A. Hamidat, M. El Ganaoui, and M. El Amine Slimani, "Parametric study of solar heating and cooling systems in different climates of Algeria – A comparison between conventional and high-energy-performance buildings," *Energy*, vol. 113, pp. 521–535, Oct. 2016, doi: 10.1016/j.energy.2016.07.022.

[58] C. Bongs *et al.*, "A technical report of subtask C Deliverable C2-B," *Solar Air Conditioning and Refrigeration*, p. 39, 2009.

[59] F. Mehdaoui, M. Hazami, A. Messaouda, and A. Guizani, "Performance analysis of two types of Solar Heating Systems used in buildings under typical North-African climate (Tunisia)," *Applied Thermal Engineering*, vol. 165, p. 114203, Jan. 2020, doi: 10.1016/j.applthermaleng.2019.114203.

[60] J. Wang, Z. Han, and Z. Guan, "Hybrid solar-assisted combined cooling, heating, and power systems: A review," *Renewable and Sustainable Energy Reviews*, vol. 133, p. 110256, Nov. 2020, doi: 10.1016/j.rser.2020.110256.

[61] M. Herrando, A. M. Pantaleo, K. Wang, and C. N. Markides, "Solar combined cooling, heating and power systems based on hybrid PVT, PV or solar-thermal collectors for building applications," *Renewable Energy*, vol. 143, pp. 637–647, Dec. 2019, doi: 10.1016/j.renene.2019.05.004.

[62] J. Wang, Y. Chen, and N. Lior, "Exergo-economic analysis method and optimization of a novel photovoltaic/thermal solar-assisted hybrid combined cooling, heating and power system," *Energy Conversion and Management*, vol. 199, p. 111945, Nov. 2019, doi: 10.1016/j.enconman.2019.111945.

[63] A. Georgiev, R. Popov, and E. Toshkov, "Investigation of a hybrid system with ground source heat pump and solar collectors: Charging of thermal storages and space heating," *Renewable Energy*, vol. 147, pp. 2774–2790, Mar. 2020, doi: 10.1016/j.renene.2018.12.087.

[64] M. Mehrpooya, H. Hemmatabady, and M. H. Ahmadi, "Optimization of performance of Combined Solar Collector-Geothermal Heat Pump Systems to supply thermal load needed for heating greenhouses," *Energy Conversion and Management*, vol. 97, pp. 382–392, Jun. 2015, doi: 10.1016/j.enconman.2015.03.073.

[65] X. Zhang *et al.*, "Experimental and analytic study of a hybrid solar/biomass rural heating system," *Energy*, vol. 190, p. 116392, Jan. 2020, doi: 10.1016/j.energy.2019.116392.

[66] J. Huang, J. Fan, and S. Furbo, "Demonstration and optimization of a solar district heating system with ground source heat pumps," *Solar Energy*, vol. 202, pp. 171–189, May 2020, doi: 10.1016/j.solener.2020.03.097.

[67] E. Bellos, C. Tzivanidis, K. Moschos, and K. A. Antonopoulos, "Energetic and financial evaluation of solar assisted heat pump space heating systems," *Energy Conversion and Management*, vol. 120, pp. 306–319, Jul. 2016, doi: 10.1016/j.enconman.2016.05.004.

[68] S. Karki, K. R. Haapala, and B. M. Fronk, "Investigation of the combined efficiency of a solar/gas hybrid water heating system," *Applied Thermal Engineering*, vol. 149, pp. 1035–1043, Feb. 2019, doi: 10.1016/j.applthermaleng.2018.12.086.

[69] J. Wang, S. Li, G. Zhang, and Y. Yang, "Performance investigation of a solar-assisted hybrid combined cooling, heating and power system based on energy, exergy, exergo-economic and exergo-environmental analyses," *Energy Conversion and Management*, vol. 196, pp. 227–241, Sep. 2019, doi: 10.1016/j.enconman.2019.05.108.

[70] H. Ahn, D. Rim, G. S. Pavlak, and J. D. Freihaut, "Uncertainty analysis of energy and economic performances of hybrid solar photovoltaic and combined cooling, heating, and power (CCHP + PV) systems using a Monte-Carlo method," *Applied Energy*, vol. 255, p. 113753, Dec. 2019, doi: 10.1016/j.apenergy.2019.113753.

[71] M. Leckner and R. Zmeureanu, "Life cycle cost and energy analysis of a Net Zero Energy House with solar combisystem," *Applied Energy*, vol. 88, no. 1, pp. 232–241, Jan. 2011, doi: 10.1016/j.apenergy.2010.07.031.

[72] Y. Chen, J. Wang, and P. D. Lund, "Sustainability evaluation and sensitivity analysis of district heating systems coupled to geothermal and solar resources," *Energy Conversion and Management*, vol. 220, p. 113084, Sep. 2020, doi: 10.1016/j.enconman.2020.113084.

[73] A. Araújo and R. Silva, "Energy modeling of solar water heating systems with on-off control and thermally stratified storage using a fast computation algorithm," *Renewable Energy*, vol. 150, pp. 891–906, May 2020, doi: 10.1016/j.renene.2020.01.026.

[74] A. R. Starke, J. M. Cardemil, and S. Colle, "Multi-objective optimization of a solar-assisted heat pump for swimming pool heating using genetic algorithm," *Applied Thermal Engineering*, vol. 142, pp. 118–126, Sep. 2018, doi: 10.1016/j.applthermaleng.2018.06.067.

[75] R. Li, Y. Dai, and G. Cui, "Multi-objective optimization of solar powered adsorption chiller combined with river water heat pump system for air conditioning and space heating application," *Energy*, vol. 189, p. 116141, Dec. 2019, doi: 10.1016/j.energy.2019.116141.

[76] E. Bellos and C. Tzivanidis, "Multi-objective optimization of a solar assisted heat pump-driven by hybrid PV," *Applied Thermal Engineering*, vol. 149, pp. 528–535, Feb. 2019, doi: 10.1016/j.applthermaleng.2018.12.059.

[77] A. Araújo, R. Silva, and V. Pereira, "Solar thermal modeling for rapid estimation of auxiliary energy requirements in domestic hot water production: On-off versus proportional flow rate control," *Solar Energy*, vol. 177, pp. 68–79, Jan. 2019, doi: 10.1016/j.solener.2018.11.003.

[78] J. M. Cardemil, A. R. Starke, and S. Colle, "Multi-objective optimization for reducing the auxiliary electric energy peak in low cost solar domestic hot-water heating systems in Brazil," *Solar Energy*, vol. 163, pp. 486–496, Mar. 2018, doi: 10.1016/j.solener.2018.01.008.

[79] H. Yousefi, M. H. Ghodusinejad, and A. Kasaeian, "Multi-objective optimal component sizing of a hybrid ICE + PV/T driven CCHP microgrid," *Applied Thermal Engineering*, vol. 122, pp. 126–138, Jul. 2017, doi: 10.1016/j.applthermaleng.2017.05.017.

[80] J. N. Cheng Hin and R. Zmeureanu, "Optimization of a residential solar combisystem for minimum life cycle cost, energy use and exergy destroyed," *Solar Energy*, vol. 100, pp. 102–113, Feb. 2014, doi: 10.1016/j.solener.2013.12.001.

[81] Lingfeng Wang and C. Singh, "Multicriteria Design of Hybrid Power Generation Systems Based on a Modified Particle Swarm Optimization Algorithm," *IEEE Trans. Energy Convers.*, vol. 24, no. 1, pp. 163–172, Mar. 2009, doi: 10.1109/TEC.2008.2005280.

[82] A. R. Starke, J. M. Cardemil, R. Escobar, and S. Colle, "Multi-objective optimization of hybrid CSP+PV system using genetic algorithm," *Energy*, vol. 147, pp. 490–503, Mar. 2018, doi: 10.1016/j.energy.2017.12.116.

[83] M.-H. Kim, D. Kim, J. Heo, and D.-W. Lee, "Techno-economic analysis of hybrid renewable energy system with solar district heating for net zero energy community," *Energy*, vol. 187, p. 115916, Nov. 2019, doi: 10.1016/j.energy.2019.115916.

[84] H. Yousefi, M. H. Ghodusinejad, and Y. Noorollahi, "GA/AHP-based optimal design of a hybrid CCHP system considering economy, energy and emission," *Energy and Buildings*, vol. 138, pp. 309–317, Mar. 2017, doi: 10.1016/j.enbuild.2016.12.048.

[85] S. Miglani, K. Orehounig, and J. Carmeliet, "Design and optimization of a hybrid solar ground source heat pump with seasonal regeneration," *Energy Procedia*, vol. 122, pp. 1015–1020, Sep. 2017, doi: 10.1016/j.egypro.2017.07.468.

[86] Z. Tian, B. Perers, S. Furbo, and J. Fan, "Thermo-economic optimization of a hybrid solar district heating plant with flat plate collectors and parabolic trough collectors in series," *Energy Conversion and Management*, vol. 165, pp. 92–101, Jun. 2018, doi: 10.1016/j.enconman.2018.03.034.

[87] F. Ren, J. Wang, S. Zhu, and Y. Chen, "Multi-objective optimization of combined cooling, heating and power system integrated with solar and geothermal energies," *Energy Conversion and Management*, vol. 197, p. 111866, Oct. 2019, doi: 10.1016/j.enconman.2019.111866.

[88] O. Bany Mousa, R. A. Taylor, and A. Shirazi, "Multi-objective optimization of solar photovoltaic and solar thermal collectors for industrial rooftop applications," *Energy Conversion and Management*, vol. 195, pp. 392–408, Sep. 2019, doi: 10.1016/j.enconman.2019.05.012.

[89] S. K. Shah, L. Aye, and B. Rismanchi, "Multi-objective optimisation of a seasonal solar thermal energy storage system for space heating in cold climate," *Applied Energy*, vol. 268, p. 115047, Jun. 2020, doi: 10.1016/j.apenergy.2020.115047.

[90] F. Ren, Z. Wei, and X. Zhai, "Multi-objective optimization and evaluation of hybrid CCHP systems for different building types," *Energy*, vol. 215, p. 119096, Jan. 2021, doi: 10.1016/j.energy.2020.119096.

[91] A. Rey and R. Zmeureanu, "Multi-objective optimization of a residential solar thermal combisystem," *Solar Energy*, vol. 139, pp. 622–632, Dec. 2016, doi: 10.1016/j.solener.2016.10.008.

[92] M. Anderson, P. Whitcomb, and an O. M. C. Safari, *DOE Simplified, 3rd Edition*. 2015. Accessed: Jun. 30, 2020. [Online]. Available: https://www.safaribooksonline.com/complete/auth0oauth2/&state=/library/view//97814 82218947/?ar

[93] P. G. Mathews, *Design of experiments with MINITAB*. Milwaukee, Wis: ASQ Quality Press, 2005.

[94] D. C. Montgomery, *Design and analysis of experiments*, Ninth edition. Hoboken, NJ: John Wiley & Sons, Inc, 2017.

[95] F. Calise, M. Dentice d'Accadia, R. D. Figaj, and L. Vanoli, "Thermoeconomic optimization of a solar-assisted heat pump based on transient simulations and computer Design of Experiments," *Energy Conversion and Management*, vol. 125, pp. 166–184, Oct. 2016, doi: 10.1016/j.enconman.2016.03.063.

[96] F. Calise, A. Palombo, and L. Vanoli, "Maximization of primary energy savings of solar heating and cooling systems by transient simulations and computer design of experiments," *Applied Energy*, vol. 87, no. 2, pp. 524–540, Feb. 2010, doi: 10.1016/j.apenergy.2009.08.033.

[97] R. Nowzari, N. Mirzaei, and L. B. Y. Aldabbagh, "Finding the best configuration for a solar air heater by design and analysis of experiment," *Energy Conversion and Management*, vol. 100, pp. 131–137, Aug. 2015, doi: 10.1016/j.enconman.2015.04.058.

[98] S. A. Kalogirou, R. Agathokleous, G. Barone, A. Buonomano, C. Forzano, and A. Palombo, "Development and validation of a new TRNSYS Type for thermosiphon flat-plate solar thermal collectors: energy and economic optimization for hot water production in different climates," *Renewable Energy*, vol. 136, pp. 632–644, Jun. 2019, doi: 10.1016/j.renene.2018.12.086.

[99] C. Ghiaus and N. Jabbour, "Optimization of multifunction multi-source solar systems by design of experiments," *Solar Energy*, vol. 86, no. 1, pp. 593–607, Jan. 2012, doi: 10.1016/j.solener.2011.11.002.

[100] Y. Cao, L. W. W. Mihardjo, and T. Parikhani, "Thermal performance, parametric analysis, and multi-objective optimization of a direct-expansion solar-assisted heat pump water heater using NSGA-II and decision makings," *Applied Thermal Engineering*, vol. 181, p. 115892, Nov. 2020, doi: 10.1016/j.applthermaleng.2020.115892.

[101] H. Sun, S. U. Gil, W. Liu, and Z. Liu, "Structure optimization and exergy analysis of a two-stage TEC with two different connections," *Energy*, vol. 180, pp. 175–191, Aug. 2019, doi: 10.1016/j.energy.2019.05.077.

[102] M. S. Al-Homoud, "Computer-aided building energy analysis techniques," *Building and Environment*, vol. 36, no. 4, pp. 421–433, May 2001, doi: 10.1016/S0360-1323(00)00026-3.

[103] A. Foucquier, S. Robert, F. Suard, L. Stéphan, and A. Jay, "State of the art in building modelling and energy performances prediction: A review," *Renewable and Sustainable Energy Reviews*, vol. 23, pp. 272–288, Jul. 2013, doi: 10.1016/j.rser.2013.03.004.

[104] J. A. Clarke, *Energy simulation in building design*, 2nd ed. Oxford: Butterworth-Heinemann, 2001.

[105] F. Haldi and D. Robinson, "The impact of occupants' behaviour on building energy demand," *Journal of Building Performance Simulation*, vol. 4, no. 4, pp. 323–338, Dec. 2011, doi: 10.1080/19401493.2011.558213.

[106] E. Fabrizio and V. Monetti, "Methodologies and Advancements in the Calibration of Building Energy Models," *Energies*, vol. 8, no. 4, pp. 2548–2574, Mar. 2015, doi: 10.3390/en8042548.

[107] A. Saltelli, Ed., *Sensitivity analysis in practice: a guide to assessing scientific models*. Hoboken, NJ: Wiley, 2004.

[108] W. Tian, "A review of sensitivity analysis methods in building energy analysis," *Renewable and Sustainable Energy Reviews*, vol. 20, pp. 411–419, Apr. 2013, doi: 10.1016/j.rser.2012.12.014.

[109] N. Delgarm, B. Sajadi, K. Azarbad, and S. Delgarm, "Sensitivity analysis of building energy performance: A simulation-based approach using OFAT and variance-based sensitivity analysis methods," *Journal of Building Engineering*, vol. 15, pp. 181–193, Jan. 2018, doi: 10.1016/j.jobe.2017.11.020.

[110] K. J. Lomas and H. Eppel, "Sensitivity analysis techniques for building thermal simulation programs," *Energy and Buildings*, vol. 19, no. 1, pp. 21–44, Jan. 1992, doi: 10.1016/0378-7788(92)90033-D.

[111] A. Ioannou and L. C. M. Itard, "Energy performance and comfort in residential buildings: Sensitivity for building parameters and occupancy," *Energy and Buildings*, vol. 92, pp. 216–233, Apr. 2015, doi: 10.1016/j.enbuild.2015.01.055.

[112] D. B. Crawley, "Which Weather Data Should You Use for Energy Simulations of Co," p. 18, 1993.

[113] G. Ruiz and C. Bandera, "Validation of Calibrated Energy Models: Common Errors," *Energies*, vol. 10, no. 10, p. 1587, Oct. 2017, doi: 10.3390/en10101587.

[114] B. M. Behrendt, D. Raimondo, Y. Zhang, S. Schwarz, J. E. Christensen, and B. W. Olesen, "A SYSTEM FOR THE COMPARISON OF TOOLS FOR THE SIMULATION OF WATER-BASED RADIANT HEATING AND COOLING SYSTEMS," p. 8.

[115] D. C. Montgomery, *Introduction to statistical quality control*, 6th ed. Hoboken, N.J: Wiley, 2009.

[116] R. H. Myers, D. C. Montgomery, and C. M. Anderson-Cook, *Response surface methodology: process and product optimization using designed experiments*, Fourth edition. Hoboken, New Jersey: Wiley, 2016.

[117] E. C. Harrington, "Harrington, E.C. (1965) The Desirability Function. Industrial Quality Control, 21, 494-498.," 1965.

[118] G. Zhou, L. Fu, and X. Li, "Optimisation of ultrasound-assisted extraction conditions for maximal recovery of active monacolins and removal of toxic citrinin from red yeast rice by a full factorial design coupled with response surface methodology," *Food Chemistry*, vol. 170, pp. 186–192, Mar. 2015, doi: 10.1016/j.foodchem.2014.08.080.

[119] M. T. M. Emmerich and A. H. Deutz, "A tutorial on multiobjective optimization: fundamentals and evolutionary methods," *Nat Comput*, vol. 17, no. 3, pp. 585–609, Sep. 2018, doi: 10.1007/s11047-018-9685-y.

[120] R. Bitter, T. Mohiuddin, and M. Nawrocki, *LabVIEW: Advanced programming techniques*. Crc Press, 2006.

[121] J. A. Duffie and W. A. Beckman, *Solar engineering of thermal processes / John A. Duffie, William A. Beckman*, 4th ed. Hoboken: John Wiley, 2013.

[122] J. W. Mitchell *et al.*, "Mathematical Reference," p. 705.

[123] S. Fischer, W. Heidemann, H. Müller-Steinhagen, B. Perers, P. Bergquist, and B. Hellström, "Collector test method under quasi-dynamic conditions according to the European Standard EN 12975-2," *Solar Energy*, vol. 76, no. 1, pp. 117–123, Jan. 2004, doi: 10.1016/j.solener.2003.07.021.

[124] "Method of testing to determine the thermal performance of solar collectors. (ASHRAE standard)," 1985, [Online]. Available: https://www.osti.gov/biblio/575023

[125] M. D.-E. Sarmouk, A. Smaili, H. Fellouah, and A. Merabtine, "Experimental and numerical investigations of a solar space heating system based on design of experiments method," *Solar Energy*, vol. 216, pp. 396–410, Mar. 2021, doi: 10.1016/j.solener.2021.01.039.

[126] K. Hudon, "Solar Energy – Water Heating," in *Future Energy*, Elsevier, 2014, pp. 433–451. doi: 10.1016/B978-0-08-099424-6.00020-X.

[127] M. C. Rodríguez-Hidalgo, P. A. Rodríguez-Aumente, A. Lecuona, M. Legrand, and R. Ventas, "Domestic hot water consumption vs. solar thermal energy storage: The optimum size of the storage tank," *Applied Energy*, vol. 97, pp. 897–906, Sep. 2012, doi: 10.1016/j.apenergy.2011.12.088.

[128] F. Bava and S. Furbo, "Correction of collector efficiency depending on variations of collector type, solar collector fluid, volume flow rate and collector tilt." Dec. 22, 2014. [Online]. Available: https://task45.iea-shc.org/fact-sheets

[129] "CAMS radiation service - www.soda-pro.com." http://www.soda-pro.com/web-services/radiation/cams-radiation-service (accessed Jun. 29, 2020).

[130] "Infoclimat - Weather in real time." https://www.infoclimat.fr/ (accessed Jun. 29, 2020).

[131] B. Sørensen, Ed., *Solar energy storage*. Amsterdam Boston Heidelberg London New York Oxford Paris San Diego San Francisco Singapore Sydney Tokyo: AP, Academic Press is an imprint of Elsevier, 2015.

[132] Ivancic, Mugnier, Stryi-Hipp, and Weiss, "Solar Heating and Cooling Technology Roadmap." Renewable Heating & Cooling (RHC), Jun. 2014. Accessed: Jul. 01, 2020. [Online]. Available: https://www.rhc-platform.org/wp_content/uploads/2019/04/Solar_Thermal_Roadmap.pdf

[133] J. Huang, J. Fan, S. Furbo, D. Chen, Y. Dai, and W. Kong, "Economic analysis and optimization of combined solar district heating technologies and systems," *Energy*, vol. 186, p. 115886, Nov. 2019, doi: 10.1016/j.energy.2019.115886.

[134] Y. Louvet *et al.*, "IEA SHC Task 54, Guideline for levelized cost of heat (LCoH) calculations for solar thermal applications. Solar Heating & Cooling programme, Internaional Energy Agency IEA. 2019." Accessed: Feb. 14, 2021. [Online]. Available: https://task54.iea-shc.org/Data/Sites/1/publications/A01-Info-Sheet--LCOH-for-Solar-Thermal-Applications.pdf

[135] M. E. Zayed, J. Zhao, A. H. Elsheikh, W. Li, and M. A. Elaziz, "Optimal design parameters and performance optimization of thermodynamically balanced dish/Stirling concentrated solar power system using multi-objective particle swarm optimization," *Applied Thermal Engineering*, vol. 178, p. 115539, Sep. 2020, doi: 10.1016/j.applthermaleng.2020.115539.

[136] "Agence de promotion et de rationnalisation de l'utilisation de l'énergie, (APRUE)." http://www.aprue.org.dz/ (accessed Sep. 30, 2020).

Appendices

Appendix A : DoE matrices and results

Table A- 1: Result of running simulation experiments of SF [2-10]m² (Solar mode only)

Experiment number	Factors				Response
	A	B	C	D	SF
1	-1	-1	-1	1	0,166
2	1	-1	-1	1	0,473
3	-1	1	-1	1	0,096
4	1	1	-1	1	0,385
5	-1	-1	1	1	0,036
6	1	-1	1	1	0,684
7	-1	1	1	1	0,016
8	1	1	1	1	0,567
9	-1	0	0	1	0,066
10	1	0	0	1	0,643
11	0	-1	0	1	0,479
12	0	1	0	1	0,349
13	0	0	-1	1	0,344
14	0	0	1	1	0,400
15	0	0	0	1	0,415
16	-1	-1	-1	2	0,150
17	1	-1	-1	2	0,511
18	-1	1	-1	2	0,088
19	1	1	-1	2	0,371
20	-1	-1	1	2	0,164
21	1	-1	1	2	0,635
22	-1	1	1	2	0,102
23	1	1	1	2	0,508
24	-1	0	0	2	0,125
25	1	0	0	2	0,560
26	0	-1	0	2	0,441
27	0	1	0	2	0,318
28	0	0	-1	2	0,310
29	0	0	1	2	0,380
30	0	0	0	2	0,373

Table A- 2: ANOVA table for SF between [2-10]m².

Source	DF	Adj SS	Adj MS	F-Value	P-Value	Remarks
Model	13	1,11663	0,085895	90,42	0,000	Significant
Linear	4	1,00069	0,250173	263,35	0,000	Significant
A	1	0,93658	0,936579	985,92	0,000	Significant
B	1	0,04409	0,044086	46,41	0,000	Significant
C	1	0,01788	0,017880	18,82	0,000	Significant
D	1	0,00215	0,002146	2,26	0,145	
Square	3	0,05826	0,019419	20,44	0,000	Significant
A*A	1	0,01255	0,012552	13,21	0,001	Significant
B*B	1	0,00000	0,000001	0,00	0,971	
C*C	1	0,00785	0,007847	8,26	0,008	Significant
2-Way Interaction	6	0,05768	0,009614	10,12	0,000	Significant
A*B	1	0,00416	0,004160	4,38	0,046	Significant
A*C	1	0,04368	0,043681	45,98	0,000	Significant
A*D	1	0,00865	0,008653	9,11	0,006	Significant
B*C	1	0,00007	0,000072	0,08	0,785	
B*D	1	0,00040	0,000396	0,42	0,524	
C*D	1	0,00072	0,000720	0,76	0,392	
Error	26	0,02470	0,000950			
Lack-of-Fit	16	0,02470	0,001544	*	*	
Pure Error	10	0,00000	0,000000			
Total	39					

Table A- 3: Result of running simulation experiments of SF [10-20]m² (Solar mode only)

Experiment number	Factors				Response
	A	B	C	D	SF
1	-1	-1	-1	1	0,692
2	1	-1	-1	1	0,988
3	-1	1	-1	1	0,421
4	1	1	-1	1	0,731
5	-1	-1	1	1	0,359
6	1	-1	1	1	0,995
7	-1	1	1	1	0,399
8	1	1	1	1	0,780
9	-1	0	0	1	0,539
10	1	0	0	1	0,907
11	0	-1	0	1	0,894
12	0	1	0	1	0,625
13	0	0	-1	1	0,728
14	0	0	1	1	0,744
15	0	0	0	1	0,757
16	-1	-1	-1	2	0,601
17	1	-1	-1	2	0,834
18	-1	1	-1	2	0,381
19	1	1	-1	2	0,642
20	-1	-1	1	2	0,624
21	1	-1	1	2	0,867
22	-1	1	1	2	0,404
23	1	1	1	2	0,695
24	-1	0	0	2	0,494
25	1	0	0	2	0,784
26	0	-1	0	2	0,773
27	0	1	0	2	0,560
28	0	0	-1	2	0,634
29	0	0	1	2	0,671
30	0	0	0	2	0,664

Table A- 4: ANOVA table for SF between [10-20]m².

Source	DF	Adj SS	Adj MS	F-Value	P-Value	Remarks
Model	13	0,880241	0,067711	38,97	0,000	Significant
Linear	4	0,794650	0,198663	114,35	0,000	Significant
A	1	0,547474	0,547474	315,12	0,000	Significant
B	1	0,197806	0,197806	113,86	0,000	Significant
C	1	0,000650	0,000650	0,37	0,546	
D	1	0,048720	0,048720	28,04	0,000	Significant
Square	3	0,029518	0,009839	5,66	0,004	Significant
A*A	1	0,006923	0,006923	3,98	0,056	
B*B	1	0,000067	0,000067	0,04	0,846	
C*C	1	0,002717	0,002717	1,56	0,222	
2-Way Interaction	6	0,056073	0,009345	5,38	0,001	Significant
A*B	1	0,001702	0,001702	0,98	0,331	
A*C	1	0,012713	0,012713	7,32	0,012	Significant
A*D	1	0,022646	0,022646	13,04	0,001	Significant
B*C	1	0,008696	0,008696	5,01	0,034	Significant
B*D	1	0,000101	0,000101	0,06	0,811	
C*D	1	0,010215	0,010215	5,88	0,023	Significant
Error	26	0,045171	0,001737			
Lack-of-Fit	16	0,045171	0,002823	*	*	
Pure Error	10	0,000000	0,000000			
Total	39	0,925412				

Table A- 5: Result of running simulation experiments of SF, PESR, LCOH and LCOh$_{sub}$

Experiment number	Factors			Response			
	S	V/S	Q/S	SF	PESR	LCOH	LCOH_sub
1	-1	-1	-1	0,20	0,22	3,34	2,25
2	1	-1	-1	1,49	0,75	17,73	10,95
3	-1	1	-1	0,19	0,19	3,35	2,26
4	1	1	-1	1,73	0,78	17,72	10,94
5	-1	-1	1	0,20	0,22	3,33	2,24
6	1	-1	1	1,44	0,74	17,74	10,96
7	-1	1	1	0,19	0,20	3,35	2,25
8	1	1	1	1,70	0,77	17,72	10,94
9	-1	0	0	0,19	0,21	3,34	2,25
10	1	0	0	1,63	0,78	17,72	10,94
11	0	-1	0	0,98	0,55	10,49	6,56
12	0	1	0	1,10	0,57	10,49	6,55
13	0	0	-1	1,07	0,58	10,49	6,55
14	0	0	1	1,05	0,57	10,48	6,55
15	0	0	0	1,07	0,58	10,48	6,55

Table A- 6: ANOVA table for SF (Hybrid mode)

Source	DF	Adj SS	Adj MS	F-Value	P-Value	Remarks
Model	9	5,09189	0,56577	3592,71	0,000	Significant
Linear	3	4,97391	1,65797	10528,40	0,000	Significant
S	1	4,93525	4,93525	31339,71	0,000	Significant
V/S	1	0,03757	0,03757	238,58	0,000	Significant
Q/S	1	0,00109	0,00109	6,90	0,047	Significant
Square	3	0,08423	0,02808	178,28	0,000	Significant
S*S	1	0,05655	0,05655	359,07	0,000	Significant
V/S*V/S	1	0,00119	0,00119	7,57	0,040	Significant
Q/S*Q/S	1	0,00001	0,00001	0,06	0,819	
2-Way Interaction	3	0,03375	0,01125	71,45	0,000	Significant
S*V/S	1	0,03307	0,03307	209,99	0,000	Significant
S*Q/S	1	0,00067	0,00067	4,24	0,094	
V/S*Q/S	1	0,00002	0,00002	0,12	0,746	
Error	5	0,00079	0,00016			
Total	14	5,09268				

Table A- 7: ANOVA table for PESR (Hybrid mode)

Source	DF	Adj SS	Adj MS	F-Value	P-Value	Remarks
Model	9	0,797615	0,088624	1373,19	0,000	Significant
Linear	3	0,771240	0,257080	3983,34	0,000	Significant
S	1	0,771133	0,771133	11948,35	0,000	Significant
V/S	1	0,000067	0,000067	1,04	0,356	
Q/S	1	0,000040	0,000040	0,63	0,465	
Square	3	0,024788	0,008263	128,03	0,000	Significant
S*S	1	0,017018	0,017018	263,69	0,000	Significant
V/S*V/S	1	0,000301	0,000301	4,66	0,083	
Q/S*Q/S	1	0,000000	0,000000	0,00	0,995	
2-Way Interaction	3	0,001587	0,000529	8,20	0,022	Significant
S*V/S	1	0,001463	0,001463	22,67	0,005	Significant
S*Q/S	1	0,000115	0,000115	1,78	0,240	
V/S*Q/S	1	0,000009	0,000009	0,14	0,719	
Error	5	0,000323	0,000065			
Total	14	0,797938				

Table A- 8: ANOVA table for LCOH (Hybrid mode)

Source	DF	Adj SS	Adj MS	F-Value	P-Value	Remarks
Model	9	517,208	57,468	3085117,70	0,000	Significant
Linear	3	517,200	172,400	9255206,09	0,000	Significant
S	1	517,200	517,200	27765616,12	0,000	Significant
V/S	1	0,000	0,000	0,55	0,490	
Q/S	1	0,000	0,000	1,62	0,260	
Square	3	0,008	0,003	139,19	0,000	Significant
S*S	1	0,005	0,005	287,07	0,000	Significant
V/S*V/S	1	0,000	0,000	4,92	0,077	
Q/S*Q/S	1	0,000	0,000	0,00	0,995	
2-Way Interaction	3	0,000	0,000	7,80	0,025	Significant
S*V/S	1	0,000	0,000	21,15	0,006	Significant
S*Q/S	1	0,000	0,000	2,06	0,210	
V/S*Q/S	1	0,000	0,000	0,19	0,677	
Error	5	0,000	0,000			
Total	14	517,208				

Table A- 9: ANOVA table for LCOH$_{sub}$ (Hybrid mode)

Source	DF	Adj SS	Adj MS	F-Value	P-Value	Remarks
Model	9	189,009	21,001	1127428,87	0,000	Significant
Linear	3	189,001	63,000	3382139,63	0,000	Significant
S	1	189,001	189,001	10146416,71	0,000	Significant
V/S	1	0,000	0,000	0,55	0,490	
Q/S	1	0,000	0,000	1,62	0,260	
Square	3	0,008	0,003	139,19	0,000	Significant
S*S	1	0,005	0,005	287,07	0,000	Significant
V/S*V/S	1	0,000	0,000	4,92	0,077	
Q/S*Q/S	1	0,000	0,000	0,00	0,995	
2-Way Interaction	3	0,000	0,000	7,80	0,025	Significant
S*V/S	1	0,000	0,000	21,15	0,006	Significant
S*Q/S	1	0,000	0,000	2,06	0,210	
V/S*Q/S	1	0,000	0,000	0,19	0,677	
Error	5	0,000	0,000			
Total	14	189,009				